UNIVERSITY OF Southampton

University of Southampton Research Repository
ePrints Soton

Copyright © and Moral Rights for this thesis are retained by the author and/or other copyright owners. A copy can be downloaded for personal non-commercial research or study, without prior permission or charge. This thesis cannot be reproduced or quoted extensively from without first obtaining permission in writing from the copyright holder/s. The content must not be changed in any way or sold commercially in any format or medium without the formal permission of the copyright holders.

When referring to this work, full bibliographic details including the author, title, awarding institution and date of the thesis must be given e.g.

AUTHOR (year of submission) "Full thesis title", University of Southampton, name of the University School or Department, PhD Thesis, pagination

http://eprints.soton.ac.uk

UNIVERSITY OF SOUTHAMPTON

FACULTY OF PHYSICAL AND APPLIED SCIENCES

School of Physics and Astronomy

Southampton High Energy Physics Group

Chiral Symmetry Breaking Transitions in Holographic Duals

by

Astrid Gebauer

Presented for the degree of

Doctor of Philosophy

November 2011

UNIVERSITY OF SOUTHAMPTON

ABSTRACT

FACULTY OF PHYSICAL AND APPLIED SCIENCES

SCHOOL OF PHYSICS AND ASTRONOMY

SOUTHAMPTON HIGH ENERGY PHYSICS GROUP

DOCTOR OF PHILOSOPHY

CHIRAL SYMMETRY BREAKING TRANSITIONS IN HOLOGRAPHIC DUALS

by Astrid Gebauer

Generalisations of the AdS/CFT Correspondence are used to study chiral symmetry breaking in dual gauge theories. We use the D3/D7 and D3/D5 systems to model both 3+1 and 2+1 dimensional, strongly coupled, gauge theories with quark fields. We show that chiral symmetry breaking is induced by either an imposed running coupling/dilaton profile or a background magnetic field. We explore the low energy effective theory of the pions of these models deriving simple integral equations for low energy parameters in the spirit of constituent quark model results. We also explore the phase structure of these models, with respect to temperature, chemical potential and applied electric field. The phase diagrams contain regions with broken and restored chiral symmetry separated by first order, second order and BKT transitions. There is an extra transition associated with the melting of the meson states into the background plasma. Finally we use the phenomenological dilaton profile to engineer holographic descriptions of theories with QCD-like phase diagrams.

Contents

List of Figures

List of Tables

Declaration of Authorship

I, Astrid Gebauer, declare that this thesis, entitled "Chiral Symmetry Breaking Transitions in Holographic Duals" and the work presented in it are my own. I confirm that

- This work was done wholly or mainly while in candidature for a research degree at this university.
- Where any part of this thesis has previously been submitted for a degree or any other qualification at this university or any other institution, this has been clearly stated.
- Where I have consulted the published work of others, this is always clearly attributed.
- Where I have quoted the work of others, the source is always given. With the exception of such quotations, this thesis is entirely my own work.
- I have acknowledged all main sources of help.
- Where the thesis is based on work done by myself jointly with others, I have made this clear.
- Work contained in this thesis has previously been published as stated in the following list:
  - Chapter 2: In collaboration with R. Alvares, N. Evans and G. J. Weatherill published as "Holographic integral equations and walking technicolour," Phys. Rev. D **81** 025013 (2010) [arXiv:0910.3073 [hep-ph]].

– Chapter 3: In collaboration with N. Evans, K. Y. Kim and M. Magou published as "Holographic Description of the Phase Diagram of a Chiral Symmetry Breaking Gauge Theory," JHEP **1003** 132 (2010) [arXiv:1002.1885 [hep-th]].

– Chapter 4: In collaboration with N. Evans, K. Y. Kim and M. Magou published as "Phase diagram of the D3/D5 system in a magnetic field and a BKT transition," Phys. Lett. **B698** 91-95 (2011) [arXiv:1003.2694 [hep-th]].

– Chapter 5: In collaboration with N. Evans and K.-Y. Kim published as "E, B, μ, T Phase Structure of the D3/D7 Holographic Dual," JHEP **05** 067 (2011) [arXiv:1103.5627 [hep-ph]].

– Chapter 6: In collaboration with N. Evans, and K. -Y. Kim published as "Towards a Holographic Model of the QCD Phase Diagram," arXiv:1109.2633 [hep-th].

No claims for originality are made for the material in chapter 1 which was compiled from a variety of sources.

Signed:

Date:

Acknowledgements

I would like to thank my supervisor Nick Evans for help, advice, guidance and inspiration in physics and other matters. His friendly and patient nature was very much appreciated. Of course, I would also like to thank Raul Alvares, James French, Keun-Young Kim, Maria Magou and George Weatherill for good collaboration and discussions. I could profit especially much from Keun-Young's wide knowledge. Thanks to the whole Theory Group for creating a great atmosphere for study and growth. I would like to thank the University of Southampton for financial support and for the opportunity to teach. The hours spent with my students will always be a precious memory to me. I thank my family and am particularly grateful towards my parents for supporting me in every possible way. I would also like to thank my boyfriend Lennart Fechner for great moral support. I thank my former physics teacher Bernd Raschdorf for showing me how amazing physics is. And last but not least, I would like to thank whoever or whatever made the universe and its theories so unbelievably beautiful.

And here, poor fool! with all my lore
I stand, no wiser than before;

(Da steh ich nun, ich armer Tor!
Und bin so klug als wie zuvor;)

—from Johann Wolfgang von Goethe's Faust

Chapter 1

Introduction

1.1 Overview

The laws of nature and the world of physics have been fascinating humankind for thousands of years. The more scientists find out about physics the more they admire the beauty and simplicity of the physics which surrounds us. There are four different forces in nature: the electromagnetic force, the weak nuclear force, the strong force and gravity. Ever since James Clerk Maxwell identified electricity and magnetism to be different manifestations of the same phenomena it has been the goal of many researchers to unify all forces of nature. Gauge theories included in the Standard Model of Particle Physics (SM) are the commonly accepted theory of how the electromagnetic, the weak and the strong force interact with matter.

A gauge theory is in general a type of field theory which is invariant under a group of local transformations. These transformations are called gauge transformations. One example of a gauge theory is Quantum Electrodynamics (QED). The QED Lagrangian is invariant under local phase rotations of the fermion fields. It is very interesting that one must introduce a gauge field in order to keep the Lagrangian, containing fermion fields, invariant under gauge transformations. This gauge field represents the photon. QED is an Abelian gauge theory, i.e. it does not matter in which order two successive gauge transformations are applied to the fermion fields. The theory of the strong nuclear force is formulated using non-Abelian gauge

theories [1], i.e. the order of the gauge transformations is important. This particular theory is called Quantum Chromodynamics (QCD).

General Relativity is currently the best theoretical description of gravity. It describes gravity on large length scales and it is experimentally well tested. Up to now scientists have not found a way of describing gravity on a quantum level, neither are there tests of gravity on short distance scales, because it is very weak compared to the other forces of nature. It is hard to exclude the other forces, e.g. the electrostatic force, well enough. This makes it hard to build an experimental set-up in which gravity is the only force acting. We are in need of a different theory of gravity on the quantum level as general relativity can not be quantised.

The aim still stands to unify these two theories of nature into one single theory of everything. The best candidate for such a theory of everything is string theory. It naturally incorporates all four forces of nature and is able to give a short scale definition of gravity. It is even more remarkable that there exist gauge/gravity dualities arising from string theory, which propose that some strongly coupled theories describe the same physics as dual gravitational theories. In the following we will discuss QCD and string theory a little further and introduce gauge/gravity dualities.

1.2 QCD

QCD [2, 3, 4], the theory of the strong force, is the current model for the interactions between quarks and the strong force carriers the gluons. The charge associated with the strong force is the colour charge, i.e. red, green and blue. Quarks can never be found on their own. They have only been seen forming bound states, the so called hadrons. If one tries to separate quarks from each other, one can put infinitely much energy into pulling them apart, but still not succeed. In this process more quarks are pair created which pair up with the original quarks to form new bound states. No matter how much energy one puts into separating a quark bound state one can never observe a single quark alone. This property is

called *confinement*. There are two classes of hadrons that have been discovered so far, baryons and mesons. Baryons, e.g. protons and neutrons, consist of three quarks which all have to have a different colour to make the baryon colour neutral and therefore stable under strong interactions. Mesons are bound states of a quark and an anti-quark, they are e.g. pions and kaons. They are colour-neutral as well and therefore the quark and the anti-quark need to have a colour and an anti-colour which cancel each other to make the meson not have a colour charge overall. Quarks come in six different flavours: up, down, charm, strange, top and bottom. Nearly all hadronic matter in everyday life is made up of up and down quarks, as the other flavours are much heavier and decay into up and down quarks quickly.

The QCD Lagrangian is

$$\begin{aligned} \mathcal{L} &= \overline{\psi}\left(i\partial_\mu\gamma^\mu + gA^a_\mu\gamma^\mu t^a - m\right)\psi - \frac{1}{4}F^a_{\mu\nu}F^{\mu\nu a} && (1.1)\\ &= \overline{\psi}\left(i\not{D} - m\right)\psi - \frac{1}{4}F^a_{\mu\nu}F^{\mu\nu a}, && (1.2) \end{aligned}$$

with

$$F^a_{\mu\nu} = \partial_\mu A^a_\nu - \partial_\nu A^a_\mu + g f^{abc} A^b_\mu A^c_\nu, \tag{1.3}$$

from [5], where $\not{D} = \partial_\mu\gamma^\mu - igA^a_\mu\gamma^\mu t^a$ is the covariant derivative. Here ψ is the Dirac fermion field representing the quarks which is in the fundamental representation of the gauge group SU(3). A_μ is the gauge field representing the gluons which are in the adjoint representation of SU(3). The t^a are the eight generators of the gauge group. f^{abc} are the structure constants of the gauge group, g is the gauge coupling constant and m are the masses of the quarks. The Roman indices are gauge group indices and the Greek indices are spacetime indices, they are both summed over. The first part of (1.1) consists of the kinetic term for the quark, the interaction term describing a vertex with two quarks and a gluon and the mass term for the quark. The second part contains the gluon kinetic term and a term representing gluons interacting with each other. When calculating physical observables one can read off so called Feynman rules from the Lagrangian. Then one needs to draw all Feynman diagrams related to the process one is interested in and sum all contributions from each diagram up. The sum can be expressed as a

power series in the coupling constant. For a small coupling constant $g < 1$, one can ignore higher order terms of the coupling constant and approximate the solution with the leading terms. This is called *perturbation theory*. When calculating loop diagrams one will need to use renormalisation. This procedure is well described in [5]. This is a very successful way of doing calculations in QED. We will see shortly that this tool is not applicable to such a large range of calculations in QCD.

1.2.1 The Beta Function of QCD

Perturbation theory can be used when calculating the beta function $\beta(g)$ of QCD. The beta function is a measure of the running of the renormalised, dimensionless coupling constant g with the energy scale, μ, of a physical process. It is defined as

$$\beta(g) = \frac{\partial}{\partial \ln \mu} g = \mu \frac{\partial}{\partial \mu} g. \tag{1.4}$$

The beta function tells us a great deal about the properties of a gauge theory. There are three different behaviours the beta function can have. Either $\beta > 0$, $\beta = 0$, or $\beta < 0$. In the first case the coupling constant is small at low energies, which we call the infrared regime, growing larger at high energies, the ultraviolet regime. That means that particles are more attracted to each other the smaller the distance is between them. This is the case for QED. In the second case of $\beta = 0$, there is no running of the coupling. This is the case for *conformal theories* and for other scale invariant theories. In the last case of $\beta < 0$ the behaviour of the running is exactly opposite to that of $\beta > 0$. The coupling constant is very small in the ultraviolet and blows up in the infrared. This is the case for QCD. The beta function of QCD is, at one loop level,

$$\beta = \frac{g^3}{(4\pi)^2} \left(-\frac{11}{3} N + \frac{2}{3} N_f \right), \tag{1.5}$$

where N_f is the number of flavours and N is the number of colours. In QCD the number of colours is 3 and the number of flavours is 3-6 depending on the energy

scale. In this case (1.4) can be solved with (1.5) to give

$$g^2(\mu) = \frac{g^2(M)}{1 + \frac{7g^2(M)}{(4\pi)^2} \log \frac{\mu^2}{M^2}}. \tag{1.6}$$

Here M is a reference energy scale and μ the energy scale we are probing. The running of the coupling gives rise to confinement mentioned above, the quarks are coupled more strongly to each other the further they are apart. It also gives rise to a property of QCD called *asymptotic freedom* [3, 4]. A theory is called asymptotically free when two particles do not exert a force on each other when they are extremely close together. The large coupling constant at low energies means perturbation theory breaks down in physics at energies below those typical of nuclear physics, which is why we cannot use perturbation theory for calculations in this so called strong-coupling regime. This happens at $g \approx 1$ which occurs at an energy scale of approximately $\Lambda_{QCD} \approx 200\text{MeV}$ [6], the QCD scale. The large spectrum of confined QCD states (hadrons) has masses of order Λ_{QCD}. The best efforts of calculating QCD in the strong coupling regime have so far been made by introducing lattice gauge theory [7]. In this work we focus on holographic methods to calculate properties of strongly coupled field theories.

1.2.2 Chiral Symmetry Breaking

Another low energy property of QCD is chiral symmetry breaking. The discussion below is loosely based on [8]. The six quark flavours have very different masses and they can be divided into the light flavours, the up, down and strange, and the heavy flavours, the charm, top and bottom. Suppose we have QCD with only the two lightest flavours, up and down. Then we can neglect their mass in (1.1), as the masses are well below the QCD scale. Let us set $m = 0$ and look at the global symmetries of the new Lagrangian

$$\mathcal{L} = i\overline{\psi}\not{D}\psi - \frac{1}{4}F^a_{\mu\nu}F^{\mu\nu a} \tag{1.7}$$

$$\mathcal{L} = i\overline{\psi}_L\not{D}\psi_R + i\overline{\psi}_R\not{D}\psi_L - \frac{1}{4}F^a_{\mu\nu}F^{\mu\nu a}, \tag{1.8}$$

where in the second line ψ_R and ψ_L are the chiral projections of ψ. This new Lagrangian is invariant under $\mathrm{U}(2)_L\times\ \mathrm{U}(2)_R$ symmetry transformations. This means that we can rotate the ψ_R independently from the ψ_L under a U(2) and vice versa. This can also be expressed as $\mathrm{SU}(2)_L\times\ \mathrm{SU}(2)_R\times\ \mathrm{U}(1)_L\times\ \mathrm{U}(1)_R$. The $\mathrm{SU}(2)_L\times\ \mathrm{SU}(2)_R$ transformation can be expressed as

$$\psi_L(x) \to e^{-i\tau\cdot\theta_L}\ \psi_L(x) \quad \text{and} \quad \psi_R(x) \to e^{-i\tau\cdot\theta_R}\ \psi_R(x), \tag{1.9}$$

with $\tau = \frac{\sigma}{2}$ and σ being the Pauli matrices. This symmetry of the massless quark formulation is called *chiral symmetry*. The symmetry group can also be reformulated in terms of vector and axial-vector transformations, so the Lagrangian is invariant under $\mathrm{SU}(2)_V\times\ \mathrm{SU}(2)_A\times\ \mathrm{U}(1)_V\times\ \mathrm{U}(1)_A$. We can express the $\mathrm{SU}(2)_V\times\ \mathrm{SU}(2)_A$ transformation as

$$\psi(x) \to e^{-i\tau\cdot\theta_V}\ \psi(x) \quad \text{and} \quad \psi(x) \to e^{-i\gamma_5\tau\cdot\theta_A}\ \psi(x). \tag{1.10}$$

It turns out that $\mathrm{U}(1)_A$ is a global symmetry of the Lagrangian, but is broken by quantum corrections due to quark loop graphs. For a detailed description of this chiral anomaly see [5]. The $\mathrm{U}(1)_V$ is a global symmetry which is responsible for conservation of baryon number. The chiral symmetry can be explicitly broken by introducing a mass term for the quarks of the form

$$\mathcal{L}_m = -m\left(\overline{\psi}_L\psi_R + \overline{\psi}_R\psi_L\right) \tag{1.11}$$

This breaks the SU(2)×SU(2) down to the vector $\mathrm{SU}(2)_V$. In this case of two massless flavours this is isospin, which in the standard model is broken by the different electromagnetic charges of the up and the down quarks. The $\mathrm{SU}(2)_A$ symmetry can also be broken spontaneously by the formation of a quark condensate

$$\left\langle\overline{\psi}\psi\right\rangle = \left\langle\overline{\psi}_L\psi_R\right\rangle + \left\langle\overline{\psi}_R\psi_L\right\rangle \neq 0. \tag{1.12}$$

This breaks the chiral symmetry to the same $\mathrm{SU}(2)_V$. Indeed one can think of this condensation as a dynamical mass generation method for the quarks. The

formation of this vacuum expectation value (vev) is generated by strong dynamics. As for every spontaneously broken symmetry, we expect three massless Goldstone bosons, one for each broken generator. These are the three pions. The creation of the pion π^a with momentum p from the vacuum by the isospin axial vector current $j^{\mu 5a}(x) = \overline{\psi}\gamma^\mu\gamma^5\frac{\sigma^a}{2}\psi$ can be expressed with the following matrix element [5]

$$\langle 0 \left| j^{\mu 5a}(x) \right| \pi^b(p) \rangle = -ip^\mu f_\pi \delta^{ab} e^{-ip\cdot x}, \tag{1.13}$$

where a and b are isospin indices and f_π is the dimensionful pion decay constant. Its value $f_\pi = 93\text{MeV}$ is of order Λ_{QCD}, which sets the scale for chiral symmetry breaking. As the masses of the up and down quarks are not exactly zero, the chiral symmetry is just an approximate symmetry. The pions therefore gain mass due to the small mass of the quarks but are considerably lighter than the other mesons. We can also include the strange quark in the above argument and find eight Goldstone bosons, which consists of the pions, the kaons and the eta.

The pion decay constant f_π can also be used to write down a low energy effective Lagrangian describing QCD. At sufficient low energy only massless degrees of freedom can be produced in the theory, while massive particles can be integrated out. In this way we can write down a Lagrangian only including Goldstone modes in a non-linear representation [9] with the unitary matrix

$$U = \exp\left(2i\frac{\pi^a\tau^a}{f_\pi}\right). \tag{1.14}$$

Here $\pi^a (a = 1 \ldots 3)$ are the Goldstone bosons (pions) and τ^a the generators of SU(2). U transforms linearly under $\text{SU}(2)_L$ (L) and $\text{SU}(2)_R$ (R) as

$$U \to U' = LUR^\dagger. \tag{1.15}$$

When taking $U' = \exp(2i\frac{\pi'^a\tau^a}{f_\pi})$, we can see from (1.15) that the Goldstone fields do not transform linearly. The effective Lagrangian should include all chirally invariant terms [9]. At low energies we can perform an expansion in powers of momentum to

get the low energy effective chiral Lagrangian in normal parametrisation

$$\mathcal{L} \approx V_0 + \frac{1}{4} f_\pi^2 \mathrm{Tr} \left(D_\mu U D^\mu U^\dagger \right). \tag{1.16}$$

We will use this Lagrangian in chapter 2.

1.2.3 The QCD Phase Diagram

Now we will introduce the phase diagram of QCD, which tells us about the possible phases QCD displays depending on the thermodynamic variables temperature T and chemical potential μ. [10] gives a good overview of the QCD phase diagram. It is important to investigate QCD's thermodynamics, as we need this information to describe the interior of neutron stars or physics of heavy ion collisions at CERN and Brookhaven. The chemical potential shifts the energy of quarks by $\Delta\mathcal{L} = \overline{\psi}\mu\gamma^0\psi$ and induces quarks to fill the vacuum. We are interested in the chiral symmetry breaking transition and neglect any superconducting phases in the following.

For two massless quarks the phase diagram is shown in figure 1.1. At low chemical potential and low temperature chiral symmetry is broken and there exists a pion gas, as QCD is confining at low energies. At large energies we expect quarks and gluons to be the fundamental degrees of freedom, as QCD is asymptotically free. Indeed, a quark-gluon plasma forms, in which quarks and gluons are not confined and can move within the plasma freely. The vacuum expectation value $\langle\overline{\psi}\psi\rangle$ which breaks chiral symmetry also vanishes at high energies. This diagram arises from theoretical models and lattice calculations. Lattice calculations work quite well at high temperature. The transition between the two phases at zero μ is widely believed to be of second order. Lattice calculations are difficult at non-zero chemical potential, but possible for very small chemical potential. The high temperature and low chemical potential regime is where heavy ion collisions take place. Even though the lattice calculations are hard at large chemical potential, other models suggest that the order of the phase transition is first order at zero temperature. Between these two regimes lies a tri-critical point. It is not exactly known where this is.

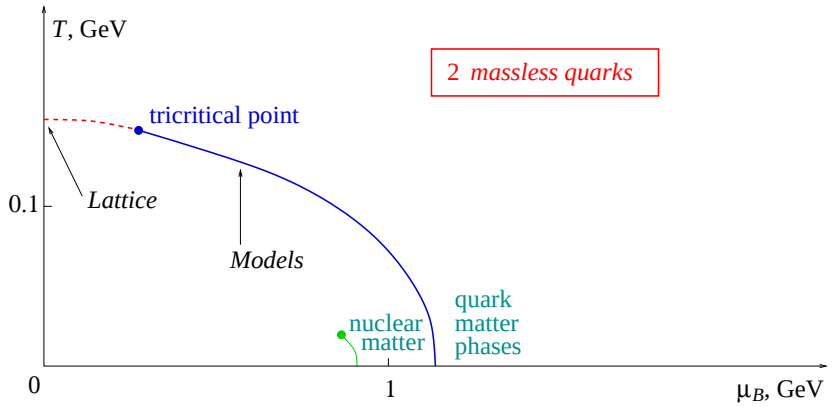

Figure 1.1: *The phase diagram of QCD with two massless and one massive quarks. This figure is taken from [10]. The red dashed line is the second order transition, the solid blue line is the first order transition. They meet at a tri-critical point. At low temperature and low chemical potential chiral symmetry is broken. Superconducting phases are neglected.*

When giving the two quarks a small mass, the phase diagram changes just a little. The second order transition at high temperature becomes a smooth crossover transition, as chiral symmetry is explicitly broken. The tri-critical point becomes the endpoint of the sharp first order transition line, the critical point. To the left of the critical point the two phases (hadrons and quark-gluon plasma) become indistinguishable. It is very important to note that the orders of the transitions in the phase diagram are still being questioned [11]. After all, the diagram is based on lattice calculations and models only and has not been backed up experimentally. The nature of the transitions seem to depend on the exact set of parameters, such as quark mass, that are hard to achieve in lattice calculations.

1.2.4 Electro-Weak Symmetry Breaking and Current Quark Mass Generation

While we have mentioned dynamical mass generation when we talked about chiral symmetry breaking in (1.2.2), we still need to explain where the current quark masses in the QCD Lagrangian come from. In fact, the answer lies in the investigation of electro-weak (EW) symmetry breaking. The weak force is generated by a gauged SU(2) symmetry of the chiral left handed fermion fields. QED is incorporated by an additional $U(1)_Y$ hypercharge gauge symmetry. Mass terms

(quadratic terms) for gauge bosons and Dirac fermions are thus forbidden in the SM Lagrangian, as they are not gauge-invariant. EW symmetry breaking accounts for the masses of the $W^{\pm}$ and the Z boson. It also explains the origin of mass for the fermions in the SM Lagrangian.

The Higgs Model

The easiest and most popular way of breaking EW symmetry is by introducing a complex scalar field ϕ, the *Higgs field* [12, 13]. It is a doublet of SU(2) with a hypercharge of $Y_\phi = \frac{1}{2}$ and takes part in EW interactions. The part of the SM Lagrangian containing this complex scalar field is

$$\mathcal{L}_\phi = (D^\mu\phi)^\dagger (D_\mu\phi) - V(\phi) \tag{1.17}$$

$$= (D^\mu\phi)^\dagger (D_\mu\phi) - \mu^2\phi^\dagger\phi - \lambda\left(\phi^\dagger\phi\right)^2, \tag{1.18}$$

where D_μ is the covariant derivative $D_\mu = \left(\partial_\mu - \frac{i}{2}g_2 A^a_\mu \sigma^a - g_1 Y_\phi B_\mu\right)$. A^a_μ and B_μ are the $SU(2)_L$ and U(1) gauge bosons respectively, while the g_2 and g_1 are coupling constants and the λ and μ are constants. For positive λ and negative μ^2, the Higgs field acquires a non-zero vev, which we can express as $v = \sqrt{-\frac{\mu^2}{\lambda}}$. v sets the EW scale, which is around 250 GeV. This vev breaks the symmetry in the SM from $SU(2)_L \times U(1)_Y$ to $U(1)_{em}$. The three Goldstone bosons associated with the broken generators are 'eaten' by the $W^{\pm}$ and Z bosons. These get a longitudinal component and thus become massive, which can explicitly be seen when introducing the vev into the Lagrangian in (1.17) and multiplying out the interaction terms of the scalar field and the gauge bosons. This is called the *Higgs mechanism*. The masses of the $W^{\pm}$ and Z are $M_W = \frac{v}{2}g_2$ and $M_Z = \frac{v}{2}\sqrt{g_2^2 + g_1^2}$. From EW physics we can relate the coupling constants g and g' to the Weinberg angle θ_W in the following way $\frac{g_1}{g_2} = \tan(\theta_W)$. The photon stays massless as expected for the gauge boson associated with the $U(1)_{em}$. The remaining degree of freedom from the complex scalar doublet is the real scalar Higgs boson, which has a mass of $M_h = \sqrt{2\lambda v^2}$.

Fermion masses can now be introduced via gauge invariant interaction terms

between the fermions and the scalar ϕ with Yukawa coupling λ_Y like

$$\mathcal{L}_{\psi\phi} = -\lambda_Y \left(\bar{\psi}_L \phi \psi_R + \bar{\psi}_R \phi \psi_L\right). \tag{1.19}$$

These terms are not only interaction terms but also give mass to the fermions when a non-vanishing vev for the scalar field is introduced. The Yukawa couplings in this fermion sector are free parameters, thus they do not give a satisfactory reason for why there is such a great mass difference between the different quark flavours. The SM Higgs does not give any explanation of flavour physics at all. Furthermore, this model exhibits the hierarchy problem, which is concerned with the large difference in mass scales in the SM. Namely, the GUT scale of order 10^{16} GeV and the EW scale of about 250 GeV need to be put into the model by hand. The Higgs mass has loop corrections of quadratic order and needs to be fine-tuned in order not to be driven to high energies [14], i.e. it is not *natural*. This points towards the idea that this theory might be an effective theory at low energies, which has to be replaced by some other theory in the UV.

Large particle colliders like the Large Hadron Collider in CERN are searching for the Higgs boson, but as of now the existence of this particle remains of a theoretical nature only. For all these reasons, the search for alternative models to the scalar Higgs boson goes on. One of these models, Technicolour, is important to some of the research in this thesis. We will discuss it in the following.

Technicolour

Technicolour (TC) [15, 16] is a higgsless model of EW symmetry breaking. The EW symmetry is broken dynamically by the vev of a composite fermion condensate. This seems much more natural, as a scalar particle has not yet been observed in nature. In fact, two of the most successful theories of spontaneous symmetry breaking exhibit a composite condensate, namely superconductors and chiral symmetry breaking in QCD. The model of technicolour introduces a new gauge interaction, the technicolour force. The simplest form is modelled on QCD and has a gauge group of SU(N_{TC}). Only new particles, the technifermions, are charged

under this new force. We look at a model with fundamental technifermions U_{TC} (up) and D_{TC} (down). In the following we will call the technifermions ψ_{TC}, when we mean either up or down. The theory possesses a chiral symmetry $SU(2)_L \times SU(2)_R$ for the right-handed and left-handed technifermions. Like in QCD, the TC coupling is asymptotically free and breaks chiral symmetry dynamically by forming a condensate at some scale Λ_{TC}, when the coupling constant becomes larger than 1. This condensate is of the form

$$\langle \overline{U}_L U_R \rangle + \langle \overline{D}_R D_L \rangle \neq 0. \tag{1.20}$$

The condensate breaks $SU(2)_L \times SU(2)_R$ down to $SU(2)_V$ generating three Goldstone bosons, the technipions $\pi^{\pm}_{TC}$ and π^0_{TC}, just like in QCD. Now we can assign weak charge to the technifermions. The $SU(2)_L$ is now gauged and the gauged $U(1)_Y$ is included in the $SU(2)_R \times U(1)_V$. The left-handed technifermions build a weak doublet under the $SU(2)_L$, while the right-handed up and down are singlets. The condensate is now also charged under $SU(2)_L \times U(1)_Y$. The formation of the condensate breaks $SU(2)_L \times U(1)_Y$ to $U(1)_{em}$ and the three Goldstone bosons are 'eaten' by $W^{\pm}$ and Z. They become massive. As in the case of the Higgs boson, the W mass is $M_W = \frac{1}{2} g_2 v$. The vacuum expectation value v is equal to the technipion decay constant $f_{\pi TC}$ [6], such that the mass of the W can be written in terms of $f_{\pi TC}$ as $M_W = \frac{1}{2} g_2 f_{\pi TC}$. To give the W its SM mass of $M_W \approx 80$ GeV, the technipion decay constant has to have a value of $f_{\pi TC} \approx 250$ GeV. This sets the scale at which the chiral symmetry is broken, Λ_{TC}, to order 1 TeV. We expect a large number of TC bound states to exist above this scale.

Technicolour gives a good explanation for the mass of the W and Z, but since there is no scalar field available in this theory, we cannot write down Yukawa mass terms for the SM fermions in the Lagrangian. In order to obtain masses for the SM fermions, we can introduce a class of models called *extended technicolour* (ETC) [17]. In ETC models there is a new symmetry group G_{ETC} at high energies. SM fermions and technifermions are both in the same irreducible representation of G_{ETC}. Therefore, there exists a gauge boson ε, which is in G_{ETC} but not in

$SU(N)_c$ or $SU(N_{TC})$. It mixes SM fermions and technifermions. The ETC gauge group is broken at a scale Λ_{ETC} to $SU(N)_c$ and $SU(N_{TC})$, which are exact symmetries. ε becomes massive and at lower energy scales, one can write down an effective Lagrangian for the interaction between SM fermions and technifermions containing a 4-fermion coupling of the form

$$\mathcal{L}_{eff} \propto \frac{g_{ETC}^2}{M_\varepsilon^2} \overline{\psi}\psi\overline{\psi}_{TC}\psi_{TC}. \tag{1.21}$$

As chiral symmetry is broken by the techniquark condensate, (1.21) becomes an effective Yukawa coupling term for the SM fermions. The mass of the SM fermions will be

$$m_f = \frac{1}{\Lambda_{ETC}^2} \left\langle \overline{\psi}_{TC}\psi_{TC} \right\rangle, \tag{1.22}$$

This mechanism can happen for different SM fermion flavours at different scales Λ_{ETC}, such that different flavour masses are dynamically generated. This model provides some hints about dynamical flavour symmetry breaking. However, many ETC models have the problem of generating many particles, which is phenomenologically not favourable. Another problem is that it is hard in TC not to violate EW precision restrictions. Furthermore, there needs to be a mechanism for setting different mass scales for the flavour physics, i.e. for breaking the ETC gauge group. It is also hard to produce a high enough top mass in ETC models, as the energy scale of ETC breaking would need to be too low (of order Λ_{TC}). This all makes building a working ETC model rather complicated. In addition to these problems ETC models can usually not avoid flavour changing neutral currents. These are strongly suppressed in the SM and are experimentally shown to be very small.

Walking Technicolour can solve some of these problems. In walking technicolour theories [18, 19], the behaviour of the β-function is not assumed to be that of QCD. The beta function can be modelled in such a way that the techniquark condensate in (1.22) gets enhanced and a larger mass for the SM fermions is possible. The techniquark condensate in (1.22) is evaluated at Λ_{ETC}. The relation between the value of the condensate at Λ_{TC}, where the chiral symmetry is broken, and at Λ_{ETC},

where ETC is broken, can be determined through the renormalisation group equations to be

$$\left\langle \overline{\psi}_{TC}\psi_{TC}\right\rangle_{ETC} = \left\langle \overline{\psi}_{TC}\psi_{TC}\right\rangle_{TC} \exp\left(\int_{\Lambda_{TC}}^{\Lambda_{ETC}} \frac{d\mu}{\mu}\gamma\left(g\left(\mu\right)\right)\right), \tag{1.23}$$

where γ is the anomalous dimension of the quark mass operator. In a theory similar to QCD the running of the coupling and the anomalous dimension γ fall off like $\frac{1}{\ln(\mu)}$ [20]. Inserting this behaviour into (1.23), we get a behaviour like

$$\left\langle \overline{\psi}_{TC}\psi_{TC}\right\rangle_{ETC} \propto \left\langle \overline{\psi}_{TC}\psi_{TC}\right\rangle_{TC} \left(\frac{\ln\Lambda_{ETC}}{\ln\Lambda_{TC}}\right)^{\gamma}. \tag{1.24}$$

The condensate is more or less of the same order at the ETC scale as at the TC scale due to the logarithmic suppression. In a *walking technicolour* theory the coupling g is approximately constant at some value $g*$ between the ETC and the TC scales. This theory can still be asymptotically free and confining. In this walking regime both the coupling constant and the anomalous dimension are approximately constant. We can use this behaviour to evaluate (1.23) once again and get

$$\left\langle \overline{\psi}_{TC}\psi_{TC}\right\rangle_{ETC} \propto \left\langle \overline{\psi}_{TC}\psi_{TC}\right\rangle_{TC} \left(\frac{\Lambda_{ETC}}{\Lambda_{TC}}\right)^{\gamma(g*)}. \tag{1.25}$$

The condensate is enhanced in walking technicolour models and so is e.g. the top quark mass.

1.2.5 Large N Field Theories

Another method of tackling the calculations in QCD was introduced by 't Hooft in the 1970s [21]. As the perturbative expansion in the gauge coupling g turns out not to be useful in all energy regimes, 't Hooft introduced an expansion around a different dimensionless parameter of an SU(N) gauge theory, $1/N$. The idea is that gauge theories may simplify in the limit of $N \to \infty$ and that they have a perturbative expansion in $1/N$, which in QCD equals 1/3. Indeed, gauge theories do simplify in the large N limit, as we will discuss here. The following discussion is along the lines of [22] .

The beta-function for pure SU(N) gauge theory, i.e. without fundamental matter, is given by

$$\beta(g) = -\frac{11}{3}\frac{g^3}{(4\pi)^2}N + \mathcal{O}(g^5). \tag{1.26}$$

$\beta(g)$ has no sensible large N limit. However if we replace $g \to \frac{g}{\sqrt{N}}$, then $\beta(g)$ does not blow up. In the following we will be considering the limit of $N \to \infty$ with a new coupling constant $\lambda \equiv g^2 N$ which we keep fixed. This limit is called 't Hooft limit and the constant λ the 't Hooft coupling constant.

We will now consider Feynman diagrams of large U(N) gauge theory in double-line notation. U(N) turns out to be equivalent to SU(N) at large N, as the correction is proportional to $1/N$. In the double-line notation a propagator of an adjoint field Φ is represented by a propagator of fundamental representation and one of anti-fundamental representation. In this notation a progagator of a gluon consists of two parallel lines. Let us assume that, like in QCD, the 3-point vertex of these fields is proportional to g and the 4-point vertex is proportional to g^2. Then the Lagrangian can schematically be written as

$$\mathcal{L} \sim \mathrm{Tr}\,(d\Phi_i d\Phi_j) + g\ c^{ijk}\mathrm{Tr}\,(\Phi_i\Phi_j\Phi_k) + g^2\ d^{ijkl}\mathrm{Tr}\,(\Phi_i\Phi_j\Phi_k\Phi_l), \tag{1.27}$$

where the Φ_i are adjoint fields with flavour index i, the d is a spacetime derivative and c^{ijk} and d^{ijkl} are constants. Rescaling the fields by $\tilde{\Phi}_i \equiv g\Phi_i$ gives

$$\mathcal{L} \sim \frac{1}{g^2}\left[\mathrm{Tr}\left(d\tilde{\Phi}_i d\tilde{\Phi}_j\right) + c^{ijk}\mathrm{Tr}\left(\tilde{\Phi}i_i\tilde{\Phi}_j\tilde{\Phi}_k\right) + d^{ijkl}\mathrm{Tr}\left(\tilde{\Phi}_i\tilde{\Phi}_j\tilde{\Phi}_k\tilde{\Phi}_l\right)\right]. \tag{1.28}$$

As mentioned above in the 't Hooft limit $1/g^2 = N/\lambda$. We can now read the Feynman rules directly from the Lagrangian. There is a factor of N/λ associated with every vertex, while every propagator contributes with a factor of λ/N. For every loop we have to sum over the different colours, so a factor of N arises. We find that every diagram with E propagators, V vertices and F loops has a coefficient proportional to

$$N^{V-E+F}\lambda^{E-V} = N^{\chi}\lambda^{E-V}, \tag{1.29}$$

where $\chi \equiv V - E + F$ is the Euler character of the diagram. It is a topological

invariant and depends only on the number of handles (genus) g in the diagram $\chi = 2 - 2g$. Planar diagrams with $g = 0$ dominate all diagrammatic expansions in the 't Hooft limit. Furthermore, when this large number of planar diagrams are added up, they become very dense. It looks like there is a sheet of gluons forming between two fundamental degrees of freedom. This sheet can be thought of as a worldsheet for perturbative string theory with strings being the fundamental degrees of freedom. This suggests that string theories and gauge theories are related, with large N playing a big role. Indeed, we will find that large N supersymmetric Yang-Mills (SYM) theory is connected to string theory. It is very important for gauge/gravity dualities, as we will also see below. But for now let us introduce string theory first.

1.3 String Theory

String theory was born in the 1970s. In the early days of string theory it was seen as a candidate to model strong interactions. Meson states were observed to lie on a straight line in the angular momentum vs. mass squared plane, so called Regge trajectories. A good model for this behaviour is a rotating open string. The mass of the open string which is proportional to the tension of the string has the same dependence on the angular momentum of the rotation as meson masses in Regge trajectories. But with the establishment of the standard model and QCD as the theory describing strong interactions, theorists lost interest in string theory. It became more interesting for the physics community when a graviton was discovered in the spectrum of string theory and as problems of early string theories where solved. This section contains a brief introduction to string theory and D-branes. For a more detailed introduction to string theory we recommend [23, 24].

1.3.1 String Action

In string theory elementary objects are taken to be one dimensional strings with string length $l_s = \sqrt{\alpha'}$ rather than zero dimensional particles. The action of a

relativistic string is given by the area of the worldsheet the string sweeps out as it moves in time. This is the analogue to the worldline of the relativistic particle. We are considering only bosonic strings in this part, as we add fermions at a later point. The string action, also known as the Nambu-Goto action, is [23]

$$S = -T \int d^2\sigma \sqrt{-\text{det} G_{\mu\nu} \frac{dX^\mu}{d\sigma^a} \frac{dX^\nu}{d\sigma^b}}, \tag{1.30}$$

where $T = \frac{1}{2\pi\alpha'}$ is the string tension, $G_{\mu\nu}$ the background metric, $\sigma^a = (\tau, \sigma)$ the coordinates on the worldsheet, the X^μ bosonic fields living on the worldsheet and the determinant is for the indices a and b. The square root structure of this action makes it hard to work with. We can instead introduce a new auxiliary field, the worldsheet metric h_{ab}, and construct an equivalent action [23]

$$S = -T \int d^2\sigma \sqrt{-h} h^{ab} G_{\mu\nu} \frac{dX^\mu}{d\sigma^a} \frac{dX^\nu}{d\sigma^b}, \tag{1.31}$$

which is called the Polyakov action. When we introduce this new field we also need to introduce a constraint obtained from h^{ab}'s equation of motion to be able to recover the Nambu-Goto action

$$\partial_a X^\mu \partial_b X_\mu - \frac{1}{2} h_{ab} h^{cd} \partial_c X^\mu \partial_d X_\mu = 0. \tag{1.32}$$

When quantising this bosonic string theory, one finds that there are tachyons contained in the theory. In order to remove these tachyon states and to include fermionic fields ψ, supersymmetry is introduced into string theory. It turns out that the fermions, ψ, and the bosons, X^μ have to live in 10 dimensions to make the theory free of tachyons and anomalies.

1.3.2 5 Theories and States of Type II

There exist five different consistent superstring theories, depending on which boundary conditions for the strings are chosen. When solving the equations of motion for the strings one needs for example to specify a boundary condition at the ends of the string. We can use periodic boundary conditions which effectively

corresponds to tying the ends of an open string together and make a closed string. We could instead choose Neumann boundary conditions where the ends of the string are free to move. Or we could fix the ends of the string, such that the ends do not move. This condition is called Dirichlet boundary condition and we will see later that there are objects in the space of string theory where the strings are attached. These objects are called D-branes. We will come to open string theories later but will for now focus on string theories containing closed strings only.

We are especially interested in type IIA and type IIB string theory. Both of these theories possess closed strings only and have $\mathcal{N} = 2$ supersymmetry. Both type II theories are oriented theories which means that we can distinguish between left-moving and right-moving modes on the strings. In the supersymmetric theory we need to specify if we have *Neveu-Schwartz* (NS) or *Ramond* (R) boundary conditions for each end which we tie together. Which gives us four different possible closed string sets of states: NS-NS, R-R, NS-R and R-NS. The first two sets are bosonic string states and the latter two are fermions. The low energy spectrum of these theories includes in the NS-NS sector the metric tensor $G_{\mu\nu}$, the scalar dilaton Φ and a two index anti-symmetric tensor $B_{\mu\nu}$. The metric $G_{\mu\nu}$ plays the usual role of measuring distances and lowering indices to form a scalar product. It also naturally incorporates gravitons. This is why string theory is such a good candidate for the theory of everything. The dilaton plays the role of the theory's coupling. It sets the string coupling to $g_s = e^{\Phi}$. The anti-symmetric tensor $B_{\mu\nu}$ is the string theory generalisation of the one-form potential A_μ of electrodynamics. The part of the action of a particle coupling to electromagnetism is $\int dx^\mu A_\mu$. The string moving in the influence of such a anti-symmetric tensor $B_{\mu\nu}$, also called the Kalb-Ramond field, has the action $\int dx^\mu dx^\nu B_{\mu\nu}$. Remember, we have integrated here over the worldsheet and not the worldline.

Type II string theory also possesses a set of R-R states. In IIA the chirality of the right movers and the left movers are opposite while in IIB they have the same chirality. This results in different sets of R-R states for those theories. We will focus on IIB in this work, which is important to the AdS/CFT correspondence applied to 3+1 dimensional field theories. Type IIB possesses a number of $C^{(p)}$ R-R potentials.

These are p-forms with p =0, 2, 4, 6 and 8. $C^{(0)}$ and $C^{(2)}$ are electromagnetic duals to $C^{(8)}$ and $C^{(6)}$ respectively. $C^{(4)}$ is self-dual. The low-energy limit of type IIB is especially important to the AdS/CFT correspondence. The massless states treated as point-like particles with only tree-level diagrams give classical supergravity.

Just for completeness we shall mention the other three string theories which are also consistent.

- *Type I Superstrings* have $\mathcal{N} = 1$ supersymmetry. This theory includes open and closed strings and also contains a spacetime metric, a dilaton and a two-index antisymmetric tensor. It has unoriented strings which are charged under a SO(32) gauge group.

- *Heterotic Superstrings* are closed strings with $\mathcal{N} = 1$ supersymmetry. Left-movers in this theory are bosonic while right-movers are fermionic. The strings are charged either under a SO(32) (*H0*) gauge symmetry or a $E_8 \times E_8$ gauge symmetry (*HE*). This theory also possesses a spacetime metric, a dilaton and a two-index antisymmetric tensor.

When all these different consistent superstring theories were discovered, it was a setback for scientists who wanted to find the theory of everything. How could it be possible that there are five seemingly different consistent copies of the theory of everything? The answer is that there are dualities which link all these theories. After all there is just one theory called M-theory. One of these dualities is T-duality, which we would like to introduce in the following. It not only links different string theories but also supplies a natural way of introducing D-branes into string theory.

1.3.3 T-Duality

T-duality is a unique property of string theory and it cannot be found in field theories where the fundamental matter consists of point-like particles. The important difference is that strings are extended objects and thus have different properties on different topologies. Let us suppose that we have a closed bosonic string theory on a background with D dimensions with one of them compactified,

e.g. on a circle with radius R. The momentum of the closed string in the compactified direction is quantised as the momentum of a particle would be. This leads to an additional mass term

$$M_{KK}^2 = \frac{n^2}{R^2}, \tag{1.33}$$

with n being an integer number. At a large compact dimension $R \to \infty$ the quantised tower of states becomes a continuous spectrum. But if we take the limit of a very small compact dimension $R \to 0$ then we see that these Kaluza-Klein modes get very heavy, such that the strings effectively do not propagate in this direction. The degrees of freedom associated with it are no longer accessible.

This is not the whole story as we need to consider that the closed string can be wrapped around the extra dimension. The string gains an additional term to its momentum and mass such that the total mass squared is

$$M^2 \propto \frac{n^2}{R^2} + (\omega 2\pi R)^2 T^2 = \frac{n^2}{R^2} + \frac{\omega^2 R^2}{\alpha'^2}, \tag{1.34}$$

where the integer ω denotes the winding number. There is a symmetry in the mass formula as we can easily see when exchanging

$$\omega \leftrightarrow n \quad \text{and} \quad R \leftrightarrow \frac{\alpha'}{R}. \tag{1.35}$$

This symmetry is called T-symmetry. We can also match state operators to get a T-dual theory. This implies that our theory is physically identical to a theory with inverse radius $R' = \frac{\alpha'}{R}$, if we change the two quantum numbers ω and n. Looking at the limit of $R \to 0$ again, we see that the Kaluza-Klein tower of states become very massive. But the winding modes are becoming a continuous spectrum of states and replace the momentum modes. The smallness of the compact direction does not matter any longer, a new direction opens up. The theory still lives in the original number of D dimensions. It is equivalent to a theory with one direction having a very large radius $R' = \frac{\alpha'}{R} \to \infty$.

Now we consider open strings rather than closed strings. Putting them in a

spacetime with one compact direction yields the normal Kaluza-Klein tower of states. On the contrary to closed strings, there is no winding number associated with open strings, as they can unwind after being wrapped around the compact direction. Taking the radius $R \to 0$ gives a theory with only D-1 dimensions for the open strings and D dimensions for the closed strings in the spectrum. Actually, only the endpoints of the open strings live on D-1 dimensional surfaces, but the string itself can oscillate in all D dimensions. Such D-1 dimensional surfaces are called D-branes, where the 'D' stands for Dirichlet boundary conditions. Due to T-duality all open strings have to end on a D-brane.

When supersymmetry is added type IIA theory transforms to type IIB and vice versa when T-duality is applied. This is due to the switching of chirality during the T-dualisation.

1.3.4 D-Branes

D-branes are sometimes called Dp-branes, where 'p' stands for the D-brane's number of spatial dimensions. In type IIB there are only Dp-branes with odd p allowed, while in type IIA there are branes with even p. As mentioned above, D-branes are higher dimensional surfaces where open strings end. We can attach additional degrees of freedom to the ends of the open strings, the so called *Chan-Paton* factors. Stacking a number of N Dp-branes on top of each other, we can label the branes in this way. Each string has two labels, one from each brane it is attached to. These labels run from 1 to N and we find that this labelling process gives rise to a U(N) gauge theory with gauge (open string) coupling $g_{YM} = \sqrt{g_s}$. The massless low energy excitations of the strings are then the N^2 adjoint degrees of freedom of the gauge group. It is even possible to break the gauge symmetry by moving one of the branes away from the stack. If e.g. we have N =2 branes then the U(2) gauge group is broken to U(1)×U(1). The two strings which have both ends on one brane remain massless, but the two strings stretching between the two branes acquire tension and therefore mass. This is a nice string theory model of the Higgs mechanism.

It has been shown by Polchinski [25] that the Dp-branes are not only specific points where open strings end, but that they also carry R-R charge and therefore source the C-form potentials. The action of a D-brane is called the Dirac-Born-Infeld (DBI) action. It is an analogue to the Nambu-Goto string action, as it minimises the worldvolume of the brane. It includes the pullback of the metric $G_{\mu\nu}$ and the background Kalb-Ramond field $B_{\mu\nu}$ as well as the dilaton Φ and the field strength F_{ab} of the U(1) gauge field living on the Dp-brane. The pullback e.g. of $G_{\mu\nu}$ is defined as

$$P\left[G\right]_{ab} = G_{\mu\nu}\frac{dX^{\mu}}{d\xi^{a}}\frac{dX^{\nu}}{d\xi^{b}}. \tag{1.36}$$

The bosonic Dirac-Born-Infeld action in string frame can be written as [8]

$$\begin{aligned} S_{Dp} &= -\mu_p \int d^{(p+1)}\xi e^{-\Phi}\sqrt{-\det\left(P\left[G+2\pi\alpha' B\right]_{ab}+2\pi\alpha' F_{ab}\right)} \\ &+ \frac{\left(2\pi\alpha'\right)^2}{2}\mu_p \int P[C^{(p+1)}]\wedge F\wedge F, \end{aligned} \tag{1.37}$$

where $\mu_p = (2\pi)^{-p}\,\alpha'^{\frac{-(p+1)}{2}}$ is the string tension. We included a Chern-Simons term for F_{ab}, which is a topological term. It will not be of relevance for the rest of this work, so we will neglect it from now on. There can also be Chern-Simons terms for the Kalb-Ramond field, but we will not need to consider these terms in this work.

1.4 The Gauge/Gravity Duality

In this section we will introduce the AdS/CFT correspondence, first suggested by Maldacena in 1997 [26]. It arises when looking at the physics of D3 branes, as we will see. On one side of the correspondence stands a conformal field theory while on the other side is a gravity theory. We will also look at some ways of modifying the gravity side such that the field theory side mimics some properties of QCD, rather than being a pure gauge conformal field theory.

Firstly, let us motivate the correspondence. The correspondence has so far not been proven, but there are some heuristic arguments why we expect it to hold. It has also been tested and the tests have not proven it wrong. To motivate the correspondence

we will consider a system of D3 branes from two different points of view, the string theory view and the supergravity view following the discussion in [22].

1.4.1 The String Theory View of N D3 Branes

We start by introducing a stack of a large number N of D3 branes into a ten dimensional space. The string excitations and interactions we expect are of three different types. There will be interaction between open strings on the brane described at low energy by a gauge theory as mentioned in section 1.3.4. There will be supergravity type IIB interactions between closed strings in the background, the so called bulk. And finally we expect interactions between open and closed strings, e.g. when two open strings join to form a closed string that dissipate into the bulk. Let us look at the low energy limit of this theory. The effective Lagrangian will be of the form

$$\mathcal{L} = \mathcal{L}_{\text{open}} + \mathcal{L}_{\text{closed}} + \mathcal{L}_{\text{int}}. \tag{1.38}$$

By low energy we mean, that the energies of the states are smaller than the string scale $E \ll \frac{1}{l_s} = \frac{1}{\sqrt{\alpha'}}$. However, it is more convenient to send the string (energy) scale to infinity, or equivalently the string length to zero, $\alpha' \to 0$, while keeping the energies and all dimensionless parameters fixed. In the low energy limit only massless string states can be excited, such that a gauge theory with massless degrees of freedom forms. The supergravity theory describing the closed strings will become free in the low energy limit, as the coupling between the closed strings is proportional to the ten dimensional Newton constant $G^{(10)}$, which in turn is proportional to $g_s^2(\alpha')^4$. Finally, the interaction term in (1.38) is proportional to $g_s\alpha'^2$, which goes to zero in the low energy limit. The interaction term vanishes. Thus we are left with two decoupled theories: the open string sector and free supergravity. Before we discuss the supergravity view of this system, let us introduce the fields of the open string sector in detail.

The open string theory is a U(N) gauge theory, as seen in section 1.3.4. The U(N) factorises into SU(N)×U(1), where the U(1) is related to a centre of mass motion of the stack of N D3 branes. Thus, the gauge group can be treated as a SU(N). The

field content of the gauge theory on the D3 brane can be obtained by a dimensional reduction of an $\mathcal{N} = 1$ gauge multiplet in ten dimensions to four dimensions. The arising gauge theory is $\mathcal{N} = 4$ super Yang-Mills (SYM) theory in 3+1 dimensions. The low energy field content on the brane is a massless gauge field A_μ ($\mu = 0 \ldots 3$), six real massless scalars and four massless Weyl fermions, the gauginos. The six scalars arise from six degrees of freedom from the ten dimensional gauge field. The scalars and gauginos transform via a global SU(4) R-symmetry. The scalars are in a **6** of SU(4) and the gauginos in a **4** of SU(4), while the gauge field is a singlet. All fields are in the adjoint representation of the gauge group. The one-loop beta function of $\mathcal{N} = 4$ SYM is

$$\beta(g) = \frac{g^3}{16\pi^2}\left(\frac{11}{3} \times 1 \times N - \frac{2}{3} \times 4 \times N - \frac{1}{6} \times 6 \times N\right) = 0, \tag{1.39}$$

where the first term comes from the gauge field, the second from the gauginos and the last from the scalar fields. This calculation yields zero, as all the fields are in the adjoint representation. In fact, it can be shown that the beta-function vanishes to all orders of perturbation theory. This feature leads to more global symmetry in the theory. $\mathcal{N} = 4$ SU(N) SYM is not only invariant under the usual Poincaré transformation, but is also scale invariant and invariant under special conformal transformations. Therefore, the theory is a *conformal field theory* (CFT) with the global conformal symmetry group SO(4,2).

1.4.2 The Supergravity View of N D3 Branes

Embedding the stack of D3 branes into a ten dimensional background has the consequence of warping the spacetime. Branes have tension and thus act as a $T^{\mu\nu}$ term in a gravitational theory. They are also the source of some of the supergravity fields. D3 branes are solutions [27] of supergravity with the metric

$$ds^2 = \left(1 + \tfrac{R^4}{r^4}\right)^{-\frac{1}{2}} \eta_{ij} dx^i dx^j + \left(1 + \tfrac{R^4}{r^4}\right)^{\frac{1}{2}} \left(dr^2 + r^2 d\Omega_5^2\right) \tag{1.40}$$

$$\text{with } \int_{S_5} dC^{(4)} = N \text{ and } R^4 = 4\pi g_s N \alpha'^2, \tag{1.41}$$

where η_{ij} is the Minkowski metric and $d\Omega_5^2$ is the line element of a 5-sphere. We take now the point of view of an observer at infinity. As g_{00} is not constant, the energy E_r of an object observed at some point r is red-shifted for an observer at infinity. The relation between the energies is $E_\infty = \left(1 + \frac{R^4}{r^4}\right)^{-\frac{1}{4}} E_r$. This means that an object with the same energy would have lower and lower E_∞ as we bring it closer and closer to $r = 0$. Now we take the same low energy limit as before ($\alpha' \to 0$). The low energy spectrum of the theory will have two sets of different excitations. Firstly there are the low energy (long wavelength) excitations in the bulk. Then there are excitations of any kind of energy near $r = 0$, as the energies are all very small for the observer at infinity. At the low energy limit these two kinds of excitations become decoupled. It becomes harder for the excitations near $r = 0$ to climb the potential well genarated by the D3 branes. And the bulk excitations decouple, because their wavelengths become larger than the gravitational extent of the D3 brane. Thus, the low energy supergravity picture of the D3 branes contains two decoupled systems. The first system is free low energy type IIB supergravity in the bulk and the second one is type IIB supersymmetric string theory near $r = 0$ or in other words near the horizon. The near horizon limit $r \ll R$ of the metric in (1.40) is

$$ds^2 = \frac{r^2}{R^2}\eta_{ij}dx^i dx^j + \frac{R^2}{r^2}dr^2 + R^2 d\Omega_5^2. \tag{1.42}$$

This is the metric of $AdS_5 \times S^5$. The AdS_5 stands for a five dimensional Anti-de Sitter space with radius R. AdS_5 space has a boundary at $r \to \infty$. This boundary has the metric of four dimensional Minkowski space. The S^5 is a five-sphere with radius R.

We found two different descriptions of the same system, the string and the supergravity description. In both descriptions we find two decoupled theories, one of which is low energy type IIB supergravity. The AdS/CFT correspondence is built on the conjecture that when one part of the two descriptions is the same, the other part should also match. It conjectures that the CFT $\mathcal{N} = 4$ SU(N) SYM in 3+1 dimensions is dual to type IIB superstring theory on an $AdS_5 \times S^5$ spacetime.

This duality means that the two different theories describe the same physics. The AdS/CFT correspondence is a *open-closed string duality*, as one of the dual theories consists of an open and the other one of a closed string theory.

1.4.3 Symmetry Matching

Another way of arguing that the $\mathcal{N} = 4$ SU(N) SYM in 3+1 dimensions and type IIB superstring theory on an $AdS_5 \times S^5$ could describe the same physics is to look at the global symmetries in both theories. We have already discussed the symmetries of $\mathcal{N} = 4$ SU(N) SYM in section 1.4.1. There is a SU(4) R-symmetry present and the conformal symmetry of SO(4,2). Now looking at the geometry of $AdS_5 \times S^5$, we find that the AdS_5 has a spacetime symmetry of SO(4,2), as it can be constructed as a surface embedded into a 2+4 dimensional spacetime. The five-sphere has an isometry of SO(6) $\simeq$ SU(4). Thus we can match the global symmetries on either side of the correspondence to each other. We can consider the theories as dual.

1.4.4 The Holographic Duality

Let us have a closer look at the nature of the correspondence now. We have a CFT in 3+1 dimensions, which is dual to a closed string theory (a theory of gravity) in 9+1 dimensions. Five of these 9+1 dimensions on the gravity side are compact, so they do not add much to the theory other than a Kaluza-Klein tower of states. So effectively, the correspondence is between a 3+1 dimensional gauge theory and a 4+1 dimensional string theory. These kind of dualities are called *holographic* dualities. Information in a d-dimensional theory is encoded in a lower dimensional theory, like in a hologram. The CFT can be thought of as living on the boundary of AdS_5.

The additional dimension is the radial direction r of the AdS space. But what does this extra direction correspond to in the gauge theory? To answer this question, we need to look at the SO(4,2) global symmetry on both sides of the correspondence. In detail, let us look at dilatations ($x^i \to e^\alpha x^i$) in the gauge theory. The action of the CFT is invariant under these rescaling transformations, as it is a symmetry of

the field theory. If we e.g. introduce a massless scalar field ϕ into the field theory and look at its kinetic term

$$S = \int d^4x(\partial\phi)^2, \tag{1.43}$$

we see that under dilatations the ϕ needs to be scaled as $\phi \to e^{-\alpha}\phi$ to keep the action invariant. This means ϕ has energy dimension. On the gravity side of the correspondence, the SO(4,2) is a global symmetry of the metric. Thus rescaling ($x^i \to e^{\alpha}x^i$) should keep the metric in (1.42) invariant. For the metric to be invariant the radial direction r needs to have scaling properties of $r \to e^{-\alpha}r$. Therefore, r has energy dimension and not dimension of a distance like the x^i. One can think of r as the renormalisation scale of the CFT. This is a quite intuitive result in a sense, as we have seen before that the energy of an object seen by an observer at the boundary will be red-shifted. If we place the observer on a point with smaller r the energy will be less red-shifted.

1.4.5 The Parameters of the AdS/CFT Correspondence

Let us now investigate which parameter space will be of use. The strongest form of the correspondence is that $\mathcal{N} = 4$ SU(N) SYM in 3+1 dimensions and type IIB superstring theory on $AdS_5 \times S^5$ are dual to each other throughout parameter space. Now this is not testable, as we cannot do perturbation theory in the gauge theory for arbitrary coupling. There is also no method of quantising string theory on a curved background with RR-flux. We need to make some approximations to be able to do calculations. In order to reach the perturbative regime on the gauge theory side, the 't Hooft coupling needs to be small

$$\lambda = g_{YM}^2 N = g_s N = \frac{R^4}{4\pi l_s^4} \ll 1, \tag{1.44}$$

where we have used (1.41). We also take a large N limit to be able to only have planar diagrams in the gauge theory. It is only possible to do calculations on the gravity side when we can approximate string theory with supergravity. This classical theory of gravity becomes reliable when the the radius of AdS is much

larger than the string length

$$\frac{R^4}{l_s^4} = 4\pi g_s N = 4\pi g_{YM}^2 N = 4\pi\lambda \gg 1. \tag{1.45}$$

In this approximation N needs to be large as well, because g_s needs to be small in order to preserve the classical supergravity limit. In this regime the 't Hooft coupling constant is very large, so we can see that these two regimes are not compatible. If the gauge theory side is weakly coupled, the gravity side is strongly coupled and vice versa. This leads to the conclusion that the duality is a *weak-strong duality*. This property makes it hard to prove the duality in any kind of regime, because it is always hard to calculate on at least one of the sides. However, this also means that we found a tool which we can use to extract information about a strongly coupled field theory by using simple classical supergravity. This is exactly the tool we will be using during the remainder of this work. We will assume that $g_s \ll 1$ and that we have a large number of colours N in our gauge theory.

1.4.6 Field-Operator Matching

Having established the nature of the duality we would like to be able to do some calculations with it. A *field-operator map* has been developed in [28] and [29] to allow one to extract some physical values from the duality. The authors of [28] suggest a mathematical formulation for the duality. It states that the generating functional of the correlation functions of operators $\mathcal{O}$ with sources $\phi_0(\vec{x})$ in the CFT is the same as the supergravity partition function, where the values for the fields $\phi(r, \vec{x})$ are $\phi_0(\vec{x})$ at the boundary of $\mathrm{AdS}_5 \times \mathrm{S}^5$

$$\left\langle e^{\int d^d x \phi_0(\vec{x})\mathcal{O}(\vec{x})} \right\rangle_{CFT} = Z_{Sugra}|_{\phi(\infty,\vec{x})=\phi_0(\vec{x})}. \tag{1.46}$$

In other words (1.46) suggests that the boundary values ϕ_0 of supergravity fields $\phi(r, \vec{x})$ which live in the bulk are the sources of operators $\mathcal{O}$ in the CFT.

We will now look at an explicit example of this procedure, a supergravity scalar field ϕ with mass m in AdS_5. The ten dimensional supergravity is Kaluza-Klein

reduced to five dimensions to obtain the five dimensional field. The action is

$$S = \int d^4x dr \sqrt{-g} \left(g^{ab} \partial_a \phi \partial_b \phi - m^2 \phi^2 \right) \tag{1.47}$$

where g_{ab} is the metric of the AdS_5. Solving the equations of motions for the radial dependence of the scalar $\phi(r)$ gives a solution of the form

$$\phi(r) = A \frac{1}{r^{2+\sqrt{4+m^2R^2}}} + B \frac{1}{r^{2-\sqrt{4+m^2R^2}}}, \tag{1.48}$$

with factors A and B. This can be reformulated as

$$\phi(r) = A \frac{1}{r^{\Delta}} + B \frac{1}{r^{4-\Delta}} \tag{1.49}$$

with $\Delta = 2 + \sqrt{4 + R^2 m^2}$. The supergravity field does not carry a mass dimension, whereas r has mass dimension 1. This implies that A and B carry mass dimensions of Δ and $4 - \Delta$ respectively. Now let us look at the near horizon value of $\phi(\epsilon)$ where $\epsilon \to \infty$. The second part of (1.48) will dominate the expression. Formally we should replace the boundary condition on the right-hand side (RHS) of (1.46) with the limit $\epsilon \to \infty$ of

$$\phi(\epsilon, \vec{x}) = \epsilon^{\Delta - 4} \phi_0(\vec{x}), \tag{1.50}$$

where we have identified B with the source $\phi_0(\vec{x})$ of an operator $\mathcal{O}$. Naturally the operator $\mathcal{O}$ has dimension Δ. It turns out that we can identify A in (1.49) with the vev of the operator $A = \langle \mathcal{O} \rangle$. We have found a relation between the mass m of the scalar field and the mass dimensions Δ of the corresponding operator. Note, that when the gravity scalar field has a small mass-squared $(-4\lambda R^2 m^2 \lambda - 3)$, it can be associated with field theory operators of two possible dimensions [30]. Here, this means that either A or B can be interpreted as $\langle \mathcal{O} \rangle$. There is a further constraint on mapping the scalar field to an operator and vice versa, as both need to be in the same irreducible representation of $SO(6) \simeq SU(4)_R$.

1.4.7 Adding Flavour

Now we have got an exciting method which allows us to explore properties of $\mathcal{N} = 4$ SU(N) SYM with $N \to \infty$ in the strong coupling regime. Physicists hope to be able to describe strongly coupled QCD with this method one day. This is a hard task, as these two field theories differ in many aspects. QCD only has 3 flavours rather than infinitely many, it has no supersymmetry, it has a running coupling rather than being conformal and it possesses quarks. We hope that we can modify the gravity side of the correspondence to be able to make the gauge theory side more QCD like. Even though we have not succeeded in doing this completely, there is hope that we can describe e.g. phenomena which do not depend on the differences of the theories or phenomena which display common features of strongly coupled theories. It is indeed possible to introduce quarks and a running coupling into the correspondence. Let us first introduce quarks and briefly mention the running of the coupling later.

As mentioned above $\mathcal{N} = 4$ SU(N) SYM only has adjoint degrees of freedom. Quarks are in the fundamental representation of the gauge group, so they can be represented by adding strings with only one end on a colour D3 brane as done in [31] and [32]. This can be achieved by introducing a different kinds of D-brane. The fundamental degrees of freedom have their other end attached to new flavour branes. These new kind of D-branes break some of the supersymmetry. If we introduce D7 branes the quarks are found in $\mathcal{N} = 2$ hypermultiplets.

The strings stretching between flavour branes holographically describe mesonic operators and their sources. In the future we will mainly consider the case of introducing a number N_f of D7 branes [33, 34, 31], where N_f stands for the number of flavours. The number N_f of D7 branes needs to be small compared to the number of D3 branes to avoid backreaction on the geometry resulting from the D3 branes. As usual we work in the 't Hooft limit and at low energies (i.e. $\alpha' \to 0$) to avoid interactions between the D7-D7 strings and the other strings. In this set-up the D3 branes can be replaced by $AdS_5 \times S^5$ space on the gravity side and the D7 branes are referred to as probe branes. This approximation is called the quenched approximation on the field theory side. It is used in the context of lattice field

theory when considering a theory with the dynamics of gluonic degrees of freedom, their effect on the quarks, but not the effect of quarks on the gluons. The D7 branes can minimise their worldvolume in the geometry, such that a stable configuration is reached. The low energy fluctuations of the D7 branes are dual to meson-fluctuation, while the gauge fields on the D7 brane are dual to global flavour currents on the field theory side.

Let us insert the D7 brane into the 01234567 directions of the ten dimensional space, while the D3 branes lie in the 0123 directions as seen in table 1.1. Here the 0 direction is time. It is apparent that the original spacetime symmetry of SO(6) is

	0	1	2	3	4	5	6	7	8	9
D3	X	X	X	X						
D7	X	X	X	X	X	X	X	X		

Table 1.1: *The extension of the D3 and D7 branes in flat spacetime coordinates.*

broken to SO(4)×SO(2). The SO(4) rotates the 4567 directions and the SO(2) rotates the 89 directions. These spacetime symmetries are also present on the field theory side of the duality.

Now we can find the equation of motion for the D7 brane, which is called the embedding equation, as it determines where there are stable configurations of the D7 lying in the spacetime. We will follow [8] for this analysis. We will work in the string frame and assume that the dilaton is constant, i.e. the string coupling is constant. The metric in (1.42) can be rewritten as

$$ds^2 = \frac{r^2}{R^2}\eta_{ij}dx^i dx^j + \frac{R^2}{r^2}\left(d\rho^2 + \rho^2 d\Omega_3^2 + dw_5^2 + dw_6^2\right), \tag{1.51}$$

with $r^2 = \rho^2 + w_5^2 + w_6^2$ and $\rho^2 = w_1^2 + w_2^2 + w_3^2 + w_4^2$. The D7 is now embedded along the gauge theory x^i, the 3-sphere Ω_3 and the new radial direction of the 3-sphere ρ. The EOM is obtained from the DBI action

$$S_{D7} = -\mu_7 \int d^8\xi \sqrt{-\det\left(P\left[G\right]_{ab} + 2\pi\alpha' F_{ab}\right)} + \frac{\left(2\pi\alpha'\right)^2}{2}\mu_7 \int P[C^{(4)}] \wedge F \wedge F, \tag{1.52}$$

with $\mu_7 = \left((2\pi)^2 g_s \alpha'^4\right)^{-1}$. If we consider a static D7 brane with no gauge field F_{ab}

on its worldvolume the action is proportional to

$$S_{D7} \propto -\mu_7 \int d^8\xi \sqrt{1 + (\partial_\rho w_5)^2 + (\partial_\rho w_6)^2}, \tag{1.53}$$

We find that there are solutions with w constant which minimise this action, where w denotes either w_5 or w_6. The D7 branes are indeed localised in what we called the 89 directions above as proposed in table 1.1. The geometrical set-up can be seen in figure 1.2.

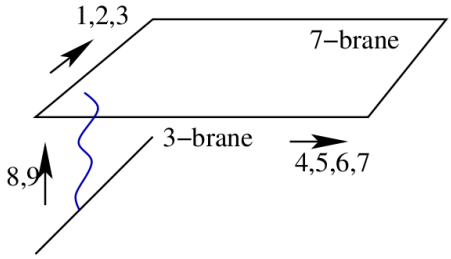

Figure 1.2: *A schematic of the D3/D7 showing our conventions. The D3-D3 strings generate the $\mathcal{N} = 4$ theory, the D3-D7 string represent the quarks and D7-D7 strings describe mesonic operators.*

When the D7 branes are separated by a distance L in the w_5 or w_6 direction, the SO(2)$\sim$U(1)$_R$ is broken. This is an axial symmetry on the field theory side. Simultaneously we find that the D3-D7 strings get a finite mass due to their tension. In the field theory this corresponds to a quark mass of $m_q = L/2\pi\alpha'$. We can interpret this finite quark mass as breaking the chiral U(1)$_R$ symmetry, such that we interpret this axial U(1) as our chiral symmetry in this system. In general the solutions minimising the action (1.53) have asymptotically with $\rho \to \infty$ the form

$$w = L + \frac{c}{\rho^2} + \ldots, \tag{1.54}$$

where up to some factors of of $2\pi\alpha'$, c can be interpreted as the chiral condensate on the field theory side, as it must be a vev of an operator with the same symmetries as the mass and mass dimension 3. This fermionic bilinear operator also breaks chiral symmetry. Note that the generation of a condensate is forbidden by supersymmetry.

It is interesting to look at the induced metric on the D7 brane when it is separated

by a length L from the stack of D3 branes. The induced metric is

$$ds^2 = \frac{\rho^2 + L^2}{R^2}\eta_{ij}dx^i dx^j + \frac{R^2}{\rho^2 + L^2}d\rho^2 + \frac{R^2\rho^2}{\rho^2 + L^2}d\Omega_3^2. \tag{1.55}$$

This is the metric of $AdS_5 \times S^3$ in the limit of $\rho \to \infty$, which is the UV regime on the field theory side. For $\rho \to 0$ (i.e. $r^2 = L^2$) the radius of the 3-sphere shrinks to zero size. This is the IR limit in the field theory. From the field theory point of view we would expect that heavy quarks are absent in the IR of the theory and present in the UV. This is precisely what is happening here, as the D7 branes seem to vanish due to this shrinking of the 3-sphere radius in the IR.

Chiral symmetry in this model can be broken by generating a chiral condensate. One method of doing so is by introducing a non-trivial dilaton profile depending on the radial coordinate of AdS in the background [35, 36, 37]. This introduces a running of the coupling on the field theory side. We will not go into detail here, but postpone the discussion to chapter 2. A condensate can also be generated by introducing a magnetic field on the flavour brane's surface [38]. Due to the magnetic field the action of the flavour brane blows up when approaching $r = 0$, such that the brane bends around the origin creating a slope at infinity and therefore a condensate. We discus this topic further in chapter 3. These two methods will be very useful to us for the remainder of this work.

1.4.8 Mesons Fluctuations

Now we will briefly describe how to calculate mesonic fluctuations and their mass spectrum. The aim of this section is to sketch the calculation rather than going into much detail. We will focus on scalar fluctuations (fluctuations with spin equal to zero) on the system introduced above. We will follow the calculations in [32] and [8] closely.

Scalar fluctuations correspond to fluctuations of the D7 in the transverse directions, i.e. w_5 or w_6. The embedding including the fluctuations is

$$w_6 = 0 + \delta w_6 \ , \quad w_5 = L + \delta w_5 \ . \tag{1.56}$$

It is sufficient to work in quadratic order of the fluctuations here, as the fluctuations are taken to be very small. The relevant part of the Lagrangian density for the scalars is then

$$\mathcal{L} = -\mu_7 \sqrt{-\det g_{ab}} \left(1 + \frac{1}{2}\frac{R^2}{r^2} g^{cd} \left(\partial_c \delta w_5 \partial_d \delta w_5 + \partial_c \delta w_6 \partial_d \delta w_6\right)\right) \tag{1.57}$$

Note that we used the induced metric g_{ab} from (1.55) here. We work in the same coordinates as above such that $r^2 = \rho^2 + L^2$. The equation of motion for δw_5 is independent of δw_6 and vice versa. These equations of motion are

$$\partial_a \left(\frac{\rho^3 \sqrt{\epsilon_3}}{\rho^2 + L^2} g^{ab} \partial_b \Phi\right) = 0 \tag{1.58}$$

where ϵ_3 is the metric of the unit 3-sphere and Φ stands for either fluctuation. The equation of motion can be expanded as

$$\frac{R^4}{(\rho^2 + L^2)^2} \partial^\mu \partial_\mu \Phi + \frac{1}{\rho^3} \partial_\rho \left(\rho^3 \partial_\rho \Phi\right) + \frac{1}{\rho^2} \nabla^i \nabla_i \Phi = 0 \tag{1.59}$$

where ∇_i is the covariant derivative on the 3-sphere. We can now use separation of variables to solve this differential equation. We can write the fluctuations as

$$\Phi = \phi(\rho) e^{ik\cdot x}\ \mathcal{Y}^l(S^3) \tag{1.60}$$

where the $\mathcal{Y}^l(S^3)$ are the scalar spherical harmonics on the 3-sphere. They satisfy

$$\nabla^i \nabla_i \mathcal{Y}^\ell = -\ell(\ell+2)\mathcal{Y}^\ell \tag{1.61}$$

In the x^i directions these fluctuations are plane wave excitations. The meson mass is defined as $M^2 = -k^2$, where k is the wavevector from (1.60). This is the usual ansatz for finding this type of meson fluctuation. After redefinition of variables

$$\varrho = \frac{\rho}{L}\ , \quad \bar{M}^2 = \frac{-k^2 R^4}{L^2}\ , \tag{1.62}$$

the equation for $\phi(\rho)$ becomes

$$\partial_\varrho^2\phi + \frac{3}{\varrho}\partial_\varrho\phi + \left(\frac{\bar{M}^2}{(1+\varrho^2)^2} - \frac{\ell(\ell+2)}{\varrho^2}\right)\phi = 0. \tag{1.63}$$

This equation can be solved using hypergeometric functions. We impose normalisability such that the solution is

$$\phi(\rho) = \frac{\rho^\ell}{(\rho^2+L^2)^{n+\ell+1}} F\left(-(n+\ell+1), -n; \ell+2; -\rho^2/L^2\right) \tag{1.64}$$

with

$$\bar{M}^2 = 4(n+\ell+1)(n+\ell+2). \tag{1.65}$$

The four dimensional mass spectrum of the scalar fluctuations can now be calculated using (1.62)

$$M_s(n,\ell) = \frac{2L}{R^2}\sqrt{(n+\ell+1)(n+\ell+2)} \tag{1.66}$$

The normalisable modes have a mass spectrum which is discrete. It is interesting to note that the mass is proportional to the separation L of the D3 and D7. It sets the mass scale for the mesonic fluctuations.

1.4.9 Holographic Confinement and Finite Temperature

We now have a way of describing holographic quarks and holographic mesons, but are the quarks confined like they are in QCD? One way of investigating if the quarks are confined is to put two heavy quarks into the geometry and look at their interaction energy as done in [39, 40]. In the analysis of [39] a single probe-D3 brane is introduced at large radial distance from the stack of N D3 branes. Adding two strings stretching between the probe-D3 and the stack gives a heavy quark and anti-quark. There is no interaction between the quarks in this configuration. The authors of [39] found that it is energetically more favourable for the two strings to join up creating a single string with both ends on the probe-brane. They used the Nambu-Goto action to find the favourable configuration. The energy of this

configuration depends on the separation L of the endpoints (i.e. the separation of the quarks). The energy is then

$$E = -\frac{4\pi^2 \left(2g_{YM}N\right)^{\frac{1}{2}}}{\Gamma\left(\frac{1}{4}\right)^4 L}. \tag{1.67}$$

The energy goes as $1/L$, which means there are strongly coupled Coulomb interactions between the quarks. They form bound states similar in nature with atomic bound states. This $1/L$ factor comes from the conformal invariance of the gauge theory. It was also found that the larger the distance L the further the string dips into the geometry towards the origin where the stack of N D3 branes is located.

Now we can ask ourselves what happens to the confinement when a temperature is added to the system. A temperature is added by replacing the AdS_5 part of the geometry with the AdS_5 Schwarzschild black hole geometry

$$ds^2 = \frac{r^2}{R^2}\left(-\left(1-\frac{r_H^4}{r^4}\right)dt^2 + dx_3^2\right) + \frac{R^2}{r^2}\left(1-\frac{r_H^4}{r^4}\right)^{-1} dr^2 \ , \tag{1.68}$$

where r_H is the position of the black hole horizon. The Hawking temperature of the black hole is proportional to its horizon

$$T = \frac{r_H}{\pi R^2}. \tag{1.69}$$

Witten identified this as the thermal description of the gauge theory in [28]. If we think about the radial direction as energy scale, we will see that the black hole cuts off all energies below r_H, so it is natural to identify it with the temperature. The black hole is the natural candidate since it has intrinsic thermodynamic properties such as entropy and temperature.

Now looking at gluonic physics we will find that at zero temperature the theory is conformal. At finite temperature there is a scale to break this conformality, such that the gluonic degrees of freedom are deconfined even for infinitesimal T. The equations describing this theory now display N degrees of freedom, while this factor was not found in the case of zero temperature. We can also investigate mesons in a finite temperature background. In this theory mesons are not confined in the

traditional meaning of the word. As the mesonic string dips further into the geometry when separating the ends, it reaches the horizon eventually. As soon as the string touches the black hole the two strings separate and cannot interact any longer. This means that a finite amount of energy can separate the quarks. In this sense the meson bound states are closer in spirit to atomic bound states than QCD-like mesons. Nevertheless, we can ask if the theory exhibits stable bound states in the finite temperature regime. To answer this question we need to investigate the embedding of the flavour branes. The embeddings of the D7 branes calculated in section 1.4.7 change. In the UV they are still flat with separation L from the ρ axis. Remember that this separation is dual to the quark mass. Near the origin the embeddings either fall into the black hole for small L (i.e. m_q) or they avoid it for large L (i.e. m_q). The embeddings not touching the black hole are called Minkowski embeddings while the others are called black hole embeddings. Meson fluctuations can be calculated for both cases. The energy of the mesonic fluctuations on the black hole embeddings dissipate into the black hole, the mesons melt. There is a critical value of the quark mass for the transition between stable mesons (Minkowski embedding) and melted mesons (black hole embedding) [41].

We would like to add that holographic dualities have been used to study transport properties at finite temperature [42, 43]. Holographic mesons have also been widely studied and for a detailed review we recommend [8]

We will use these methods we have introduced in the following chapters to investigate properties of QCD. We will manipulate the gravity side of the duality to introduce QCD-like physics on the gauge theory side. Although it is somewhat hard to dial a particular gauge theory, we instead work in tractable models that lie close to $\mathcal{N} = 4$ super Yang-Mills theory and hope that these gauge theories show similar behaviours to realistic cases. In the cases we will be looking at the UV behaviour of our gravity side is $AdS_5 \times S^5$, such that in the UV the gravity side is dual to $\mathcal{N} = 4$ super Yang-Mills theory.

Chapter 2

Holographic Integral Equations and Walking Technicolour

The D3/D7 system in AdS-like spaces has allowed the study, through gauge/gravity duality or holography, of many aspects of strongly interacting gauge theories with quarks [8]. The system has been used to study chiral symmetry breaking in the presence of a running coupling [35, 36, 37] or a magnetic field [38]. In this chapter we wish to present a very simple model of chiral symmetry breaking and the associated Goldstone boson (essentially pion) in this system. The simple model consists of embedding the D7s in pure $AdS_5 \times S^5$ but with an arbitrary dilaton profile to represent the running coupling of the dual gauge theory. This basic model, although the metric is not affected by the dilaton's presence, provides a simple encapsulation of the chiral symmetry breaking mechanism in the D3/D7 system. In particular it will allow us to elucidate in the holographic equations of motion why there is a Goldstone boson present for the symmetry breaking. Further, it will allow us to write integral equations for the parameters of the low energy chiral Lagrangian involving just the form of the running coupling and the quark self-energy function (the D7 brane embedding function). These equations are very similar in spirit to the Pagels-Stokar formula [44] for the pion decay constant, f_π, and constituent quark model [45] estimates of the chiral condensate and so forth.

The formulae we will present for these low energy parameters allow one to develop

intuition about how the low energy theory depends on the underlying gauge dynamics. We explore this and as a particular example look at walking technicolour theories to see if the holographic model matches the folklore from constituent quark models. Our results support the expectation that a walking regime will enhance the quark condensate relative to the pion decay constant.

In the final section of this chapter we will perform a similar study for the non-supersymmetric D3/D5 system with a four dimensional overlap. We interpret this system as a walking gauge theory where the quark condensate has a dimension of $2+\sqrt{3}$ in the far UV. This theory is not of any obvious phenomenological use but the walking paradigm does seem to explain the physics of the system.

2.1 A Simple D3/D7 Chiral Symmetry Breaking Model

We will consider a gauge theory with a holographic dual described by the Einstein frame geometry $AdS_5 \times S^5$

$$ds^2 = \frac{1}{g_{uv}}\left[\frac{r^2}{R^2}dx_4^2 + \frac{R^2}{r^2}\left(d\rho^2 + \rho^2 d\Omega_3^2 + dw_5^2 + dw_6^2\right)\right], \tag{2.1}$$

where we have split the coordinates into the x_{3+1} of the gauge theory, the ρ and Ω_3 which will be on the D7 brane worldvolume and two directions transverse to the D7, w_5, w_6. The radial coordinate, $r^2 = \rho^2 + w_5^2 + w_6^2$, corresponds to the energy scale of the gauge theory. The radius of curvature is given by $R^4 = 4\pi g_{uv}^2 N \alpha'^2$ with N the number of colours. g_{uv}^2 is the $r \to \infty$ value of the dilaton. In addition we will allow an arbitrary running as $r \to 0$ to represent the gauge theory coupling

$$e^{\phi} \;=\; g_{YM}^2(r^2) \;=\; g_{uv}^2\ \beta(\rho^2 + w_5^2 + w_6^2) \tag{2.2}$$

where the function $\beta \to 1$ as $r \to \infty$. The $r \to \infty$ limit of this theory is dual to the $\mathcal{N} = 4$ super Yang-Mills theory and g_{uv}^2 is the constant large r asymptotic value of the gauge coupling.

We will introduce a single D7 brane probe [31] into the geometry to include quarks

— by treating the D7 as a probe we are working in a quenched approximation although we can reintroduce some aspects of quark loops through the running coupling's form if we wish (and know how). Although this system only has a U(1) axial symmetry on the quarks corresponding to rotations in the $w_5 - w_6$ plane we believe it is a good setting for studying the dynamics of the quark condensation. That process is driven by the strong dynamics rather than the global symmetries, i.e. the dynamics of the formation of the quark condensate is flavour independent, so the absence of a non-Abelian axial symmetry should not be important[1].

We must find the D7 embedding function e.g. $w_5(\rho), w_6 = 0$. The Dirac-Born-Infeld action in the Einstein frame is given by

$$\begin{aligned} S_{D7} &= -T_7 \int d^8\xi e^{\phi} \sqrt{-\mathrm{det} P[G]_{ab}} \\ &= -\overline{T_7} \int d^4x \; d\rho \; \rho^3 \beta \sqrt{1 + (\partial_\rho w_5)^2} \end{aligned} \tag{2.3}$$

where $T_7 = 1/(2\pi)^7 \alpha'^4$ and $\overline{T_7} = 2\pi^2 T_7 / g_{uv}^2$ when we have integrated over the 3-sphere on the D7. The equation of motion for the embedding function is therefore

$$\partial_\rho \left[\frac{\beta \rho^3 \partial_\rho w_5}{\sqrt{1 + (\partial_\rho w_5)^2}} \right] - 2 w_5 \rho^3 \sqrt{1 + (\partial_\rho w_5)^2} \frac{\partial \beta}{\partial r^2} = 0. \tag{2.4}$$

The UV asymptotic limit of this equation, provided the dilaton returns to a constant so the UV dual is the $\mathcal{N} = 4$ super Yang-Mills theory, has solutions of the form

$$w_5 = m + \frac{c}{\rho^2} + ... \tag{2.5}$$

where we can interpret m as the quark mass ($m_q = m/2\pi\alpha'$) and c is proportional to the quark condensate as we will see below.

The embedding equation (2.4) clearly has regular solutions $w_5 = m$ when g_{YM}^2 is independent of r — the flat embeddings of the $\mathcal{N} = 2$ Karch-Katz theory [31]. Equally clearly if $\partial\beta/\partial r^2$ is non-trivial in w_5 then the second term in (2.4) will not vanish for a flat embedding. We conclude that for any non-trivial gauge coupling

[1] The Sakai Sugimoto model [46] is an example of a gravity dual with a non-Abelian chiral symmetry but it is fundamentally five dimensional and a clear prescription for including a quark mass is lacking - the result is that we would not know how to do this analysis in that model since we can not identify the quark self-energy nor the quark condensate.

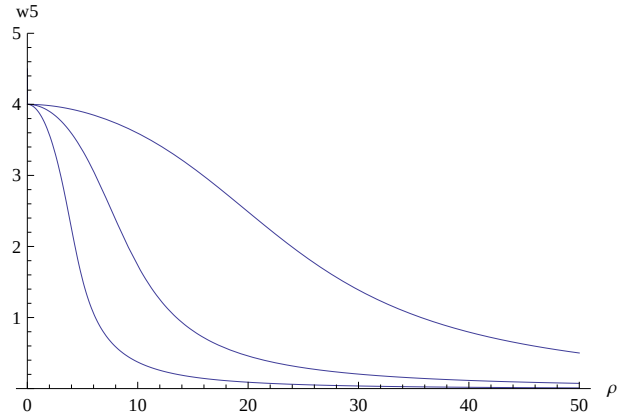

Figure 2.1: *The D7 brane embeddings/quark self-energy plots for the coupling ansatz in (2.6) - in each case the parameter* $a = 3$ *and from left to right:* $\lambda = 3.19, \Gamma = 1$*;* $\lambda = 4.55, \Gamma = 0.3$*;* $\lambda = 10.4, \Gamma = 0.1$.

the asymptotic solutions must contain the parameter c, a quark condensate. Whether $c \to 0$ or not as $m \to 0$ depends on the precise form of the running coupling chosen (note that $w_5 = 0$ is always a solution of (2.4)). However, if the coupling grows towards $r = 0$ as one would expect in a confining theory then there is clearly a growing penalty in the action for the D7 to approach the origin and we expect c to be non-zero. So there is chiral symmetry breaking present for $m = 0$.

As an example one can consider a gauge coupling running with a step function of the form

$$\beta = a + 1 - a \tanh\left[\Gamma(r - \lambda)\right]. \tag{2.6}$$

This form introduces conformal symmetry breaking at the scale $\Lambda = \lambda/2\pi\alpha'$ which triggers chiral symmetry breaking. The parameter a determines the increase in the coupling across the step but the solutions have only a small dependence on the value chosen because the area of increasing coupling is avoided by the D7 brane. An extreme choice of the profile is to let the coupling actually diverge at the barrier to represent the one loop blow up in the running of the QCD coupling - the solutions show the same behaviour as for a finite step provided the transition is not infinitely sharp. The parameter Γ spreads the increase in the coupling over a region in r of order Γ^{-1} in size - the effect of widening the step is to enhance the tail of the self-energy function for the quark. We show the symmetry breaking embeddings in figure 2.1. We will interpret the D7 embedding function as the dynamical

self-energy of the quark, similar to that emerging from a gap equation. The separation of the D7 from the ρ axis is the mass at some particular energy scale given by ρ — in the $\mathcal{N}=2$ theory where the embedding is flat the mass is not renormalised, whilst with the running coupling an IR mass forms — we have picked parameters in figure 2.1 that generate the same dynamical quark mass at $\rho=0$. We call the embedding function Σ_0 below.

2.1.1 Goldstone Mode

The embedding above lies at $w_6=0$ but there is clearly a set of equivalent solutions given by rotating that solution in the w_5-w_6 plane. That degeneracy of the solutions is the vacuum manifold. We therefore expect a Goldstone mode associated with a fluctuation of the vacuum in the angular direction. For small fluctuations about the embedding above we may look at fluctuations in w_6. The action expanded to quadratic order for such a fluctuation is

$$\begin{aligned} S_7 &= -\overline{T_7}\int \mathrm{d}\rho dx^4\rho^3\beta\sqrt{1+(\partial_\rho\Sigma_0)^2}\left(1+\frac{\partial_{r^2}\beta}{\beta}w_6^2\right. \\ &\qquad \left.+\frac{1}{2}\frac{(\partial_\rho w_6)^2}{1+(\partial_\rho\Sigma_0)^2}+\frac{1}{2}\frac{R^4}{r^4}(\partial_\mu w_6)^2+...\right) \end{aligned} \tag{2.7}$$

note r, β and $\partial_{r^2}\beta$ are evaluated on the solution Σ_0 here and henceforth.

As usual we will seek solutions of the form $w_6(\rho,x)=f_n(\rho)e^{ik.x},\ k^2=-M_n^2$. Here n takes integer values - the solutions are associated with the Goldstone boson and its tower of radially excited states. The f_n satisfy the equation

$$\partial_\rho\left(\frac{\beta\rho^3\partial_\rho f_n}{\sqrt{1+(\partial_\rho\Sigma_0)^2}}\right)-2\rho^3\sqrt{1+(\partial_\rho\Sigma_0)^2}(\partial_{r^2}\beta)f_n+\frac{1}{r^4}\rho^3\beta\sqrt{1+(\partial_\rho\Sigma_0)^2}R^4M_n^2f_n=0 \tag{2.8}$$

The presence of a Goldstone boson is now immediately apparent - there is a solution with $M_n^2=0$ and $f_0=\Sigma_0$. With these substitutions the equation is exactly the embedding equation (2.4), a result of the symmetry between w_5 and w_6. This is the pion like bound state of this theory — although there is only a broken U(1) axial symmetry, the absence of anomaly effects at large N make it closer in nature

to the pions than the η' of QCD.

Naively the argument just given makes it appear there is a massless Goldstone for any w_5 solution including those where there is an explicit quark mass in the asymptotic fall-off in (2.5). This is not the case though because to interpret the solution as a Goldstone requires f_0 to fall off at large ρ as $1/\rho^2$ (i.e. we only allow fluctuations of the normalisable mode). The naive massless solution is related to the fact that the theory has a spurious symmetry where $\bar{\psi}_L\psi_R \to e^{i\alpha}\bar{\psi}_L\psi_R$ and simultaneously $m \to e^{-i\alpha}m$. This spurious symmetry must be present in the string construction. The naive massless solution would also not be normalisable.

2.1.2 The Low Energy Chiral Lagrangian

The Goldstone field's low energy Lagrangian must take the form of a chiral Lagrangian, non-linear realisation of the broken symmetry [47]. We can substitute the form $w_6^a = f_0(\rho)\pi^a(x) = \Sigma_0\pi^a(x)$ into (2.7) and integrate over ρ to obtain this Lagrangian, where the x-directions are the directions of the gauge theory

$$\begin{aligned}\mathcal{L} &= -\overline{T_7}\int \mathrm{d}\rho\rho^3\beta\sqrt{1+(\partial_\rho\Sigma_0)^2}\left(1+\frac{1}{2}\frac{R^4}{r^4}\Sigma_0^2\left(\partial_\mu\pi^a(x)\right)^2\right.\\ &\left.+\frac{1}{4}\frac{R^4}{r^4}\left(\frac{2}{\beta}\frac{d\beta}{dr^2}\Sigma_0^4+\frac{\Sigma_0^2(\partial_\rho\Sigma_0)^2}{1+(\partial_\rho\Sigma_0)^2}\right)\ \mathrm{Tr}\left([\partial_\mu\Pi,\Pi]^2\right)+...\right) \quad (2.9)\end{aligned}$$

We have used the equation of motion (2.8) to eliminate the second and third terms in (2.7) in the massless limit. We have also included the $[\partial_\mu\Pi,\Pi]^2$ term from the fourth order expansion from which we will determine f_π, where $\Pi = \pi^a(x)\tau^a$ and τ^a are the generators of $\mathrm{U}(N_f)$.

This should be compared to the standard chiral Lagrangian form where $U = \exp(2i\Pi/f_\pi)$

$$\begin{aligned}\mathcal{L} &= V_0+\frac{f_\pi^2}{4}\mathrm{Tr}\left(\partial_\mu U^\dagger\partial^\mu U\right)+\mathcal{O}(p^4)\\ &= V_0+\frac{1}{2}\left(\partial_\mu\pi^a(x)\right)^2+\frac{1}{48f_\pi^2}\ \mathrm{Tr}\left([\partial_\mu\Pi,\Pi]^2\right)+\mathcal{O}(\pi(x)^6)+\mathcal{O}(p^4) \quad (2.10)\end{aligned}$$

where V_0 is the vacuum energy and f_π is the pion decay constant.

We must rescale $\pi(x)$ in (2.9) to the canonical normalisation in (2.10) and then we can read off an integral expression for the pion decay constant. To ensure all factors of α' are absent from physical answers, as they must be, we must express our answer as the ratio of two physical scales. Here we will use the scale Λ in the gauge coupling running (2.6) that encodes the scale of the chiral symmetry breaking as our reference - we have

$$\frac{f_\pi^2}{\Lambda^2} = \frac{-N}{48\pi^2\lambda^2} \left. \frac{\left[\int d\rho\rho^3\beta\sqrt{1+(\partial_\rho\Sigma_0)^2}\frac{\Sigma_0^2}{(\rho^2+\Sigma_0^2)^2}\right]^2}{\left[\int d\rho\rho^3\beta\sqrt{1+(\partial_\rho\Sigma_0)^2}\frac{1}{4(\rho^2+\Sigma_0^2)^2}\left(\frac{2}{\beta}\frac{d\beta}{dr^2}\Sigma_0^4+\frac{\Sigma_0^2(\partial_\rho\Sigma_0)^2}{1+(\partial_\rho\Sigma_0)^2}\right)\right]}\right|_{r^2=\rho^2+\Sigma_0^2} \tag{2.11}$$

Note that $\partial_{r^2}\beta$ is typically negative for the embeddings we have explored above so that f_π^2 is positive. Employing the embedding equation (2.4) the denominator may be simplified leaving

$$\frac{f_\pi^2}{\Lambda^2} = \frac{-N}{12\pi^2\lambda^2} \frac{\left[\int d\rho\rho^3\beta\sqrt{1+(\partial_\rho\Sigma_0)^2}\frac{\Sigma_0^2}{(\rho^2+\Sigma_0^2)^2}\right]^2}{\left[\int d\rho\frac{\Sigma_0^2}{(\rho^2+\Sigma_0^2)^2}\partial_\rho\left(\frac{\beta\rho^3\Sigma_0(\partial_\rho\Sigma_0)}{\sqrt{1+(\partial_\rho\Sigma_0)^2}}\right)\right]}. \tag{2.12}$$

We can also extract an integral equation for the quark condensate (evaluated in the UV where there is no running) from our analysis. We use the fact that the expectation value of $\bar{q}_L q_R$ is given by $\frac{1}{Z}\frac{\partial Z}{\partial m_q}|_{m_q\to 0}$. For an infinitesimal value of m in the boundary embedding (2.5) we expect the full embedding, to leading order, to simply take the form $w_5 = 2\pi\alpha' m_q + \Sigma_0$. We insert this form into the vacuum energy and expand to leading order in m_q - the coefficient is just the quark condensate

$$\frac{\langle\bar{q}_L q_R\rangle}{\Lambda^3} = \frac{-N}{4\pi\lambda^3 g_{uv}^2 N} \int d\rho\ \rho^3\Sigma_0\sqrt{1+(\partial_\rho\Sigma_0)^2}\partial_{r^2}\beta\Big|_{r^2=\rho^2+\Sigma_0^2} \tag{2.13}$$

One may use the embedding equation (2.4) to turn this into a surface term that is then, given that β becomes unity asymptotically, proportional to $\rho^3\partial_\rho\Sigma_0|_{\rho\to\infty}$ which is just proportional to the constant c in (2.5) confirming the interpretation of c as the condensate. The integral form of the equation provides intuition for the value of the condensate from the shape of the embedding as we will see. Note that

if the 't Hooft coupling $g_{uv}^2 N$ is kept fixed both f_π and the condensate grow as N as expected.

The integral equations (2.12) and (2.13) that link low energy parameters to the underlying UV physics are the main results of this chapter. They are very reminiscent of constituent quark model [45] results which input the quark self-energy, $\Sigma(q)$, (for example determined from a gap equation [19]) to determine the same quantities. In particular those models give for the condensate

$$\langle \bar{q}q \rangle = \frac{N}{2} \int q^3 dq \frac{\Sigma}{q^2 + \Sigma^2} \tag{2.14}$$

and the Pagels Stokar formula [44] for the pion decay constant

$$f_\pi^2 = \frac{N}{8\pi^2} \int q^3 dq \frac{\Sigma^2 - \frac{1}{2} q^2 \Sigma \Sigma'}{(q^2 + \Sigma^2)^2} \tag{2.15}$$

where a prime indicates a derivative with respect to q^2. Although our formulae are more complex and include the underlying gauge coupling's running there are nevertheless a number of common features. We will compare them for the case of walking technicolour below.

It must be stressed that we have derived our expressions (2.12) and (2.13) in a toy holographic model of chiral symmetry breaking. Of course one can not just impose any random running of the gauge coupling and assume one is in a real gauge theory. We have also not included any response of the metric to the presence of a non-trivial dilaton. The analysis is very similar in spirit to the chiral quark model assumption of an arbitrary choice of $\Sigma(q^2)$. Despite these flaws, we hope the simplicity of the expressions allows one to analytically understand the typical response of the holographic descriptions to different types of running coupling.

2.2 Walking Technicolour

The constituent quark model expressions (2.14) and (2.15) have underpinned much of the folklore for walking technicolour theories [18, 19]. As elaborated in section

1.2.4, the gauge coupling in walking technicolour is assumed to transition from perturbative to non-perturbative behaviour at one scale, Λ_1 but then the running slows, only crossing some critical value for inducing chiral symmetry breaking at a scale, Λ_2, several orders of magnitude below Λ_1. In the region between Λ_1 and Λ_2 we imagine that the anomalous dimension ϵ of the quark condensate is larger than zero (so $\bar{q}q$ has scaling dimension less than three) - the condensate evaluated in the UV is then enhanced taking the rough value $\Lambda_2^{3-\epsilon}\Lambda_1^{\epsilon}$.

Gap equation analysis [19] provides an alternative but equivalent explanation for the enhancement of the quark condensate. There walking, which has a larger coupling value further into the UV, enhances the large q tail of the quark self-energy $\Sigma(q)$. Looking at the constituent quark model expressions for low energy parameters one can see that f_π is largely determined by the small q region (there is a q^4 in the denominator) and so f_π is broadly unchanged by walking. In a technicolour model f_π sets the W and Z masses and hence the weak scale. On the other hand the condensate in (2.14) is given by a simple integral over $\Sigma(q)$ and hence grows if the tail of $\Sigma(q)$ is raised. The condensate is enlarged in walking theories relative to the weak scale. In extended technicolour models [17] the condensate determines the standard model fermion masses — increasing it drives up the extended technicolour scale, potentially suppressing flavour physics below current experimental bounds.

Do our holographic expressions agree with this story? The challenge is to simulate walking in a holographic setting. The problem is that we are always at strong coupling (large N) if we have a weakly coupled gravity dual. We cannot therefore reproduce directly the physics at the scale Λ_1 discussed above where the theory moved from weak to strong coupling.

As a first attempt to address this point we can be led by the solutions in figure 2.1 as a result of the coupling ansatz in (2.6). If we decrease the parameter Γ we effectively smear the scale at which the chiral symmetry breaking is induced over a range of $r \sim \Gamma^{-1}$. Could we use this smeared range to represent the separation between Λ_1 and Λ_2 above? The effect of the smearing is to enhance the tail of the self-energy just as expected in walking theories.

If we now turn to the holographic expressions (2.12) & (2.13) we see that they naively share the same response to enhancing the tail of Σ_0 as the constituent quark model expressions (2.14) & (2.15) did to raising the tail of $\Sigma(q)$. In particular again f_π has a $1/\rho^4$ factor in the denominator of each integral involved, making it, one would expect, insensitive to changes in the tail of Σ_0. The expression for the condensate though is sensitive to the tail and should grow as walking is introduced. In fact though this analysis neglects the dependence of these functions on the derivatives of the gauge coupling and the self-energy function Σ_0 — this additional understanding of dynamics coming from the gauge coupling running lies beyond the constituent quark model pictures. Both (2.12) and (2.13) are dominated around the points of maximum change in the coupling and Σ_0. Note though that the derivative of the coupling, $\partial_{r^2}\beta$, is evaluated on the brane, which in the cases above has precisely embedded itself so as to avoid large derivatives in β. By smoothing these functions through decreasing Γ we include extra functional behaviour. In fact these changes in the derivatives are more numerically important than the rise in the tail of Σ_0 for the plots in figure 2.1. This means that the more 'walking' looking self-energies in fact give a slightly lower condensate for a fixed value of f_π. The simple coupling ansatz in (2.6) does not therefore accommodate a behaviour we can interpret in the usual walking picture. The model does suggest that there could be considerable variation in the ratio of the condensate to f_π in gauge theories with rather different speeds of IR running though. A recent lattice analysis suggest this ratio could vary as the number of quark flavours is changed in QCD [48].

To take advantage of the similarities between (2.12) & (2.13) and (2.14) & (2.15) one would need to keep the derivatives of the coupling and Σ_0 roughly fixed as the scale at which that change occurred was moved out to larger ρ. Our equations would in such a scenario provide the enhancement of the condensate that one looks for in a walking theory. Essentially one would want a self-energy that rose sharply at large ρ but then flattened to meet the w_5 axis at the same value as the curves in figure 2.1. This in fact matches the crucial signal of walking that one would expect $\Sigma_0(\rho = 0) \ll \Lambda$ with Λ the scale at which the high scale running occurs. Within holographic models this should be the crucial signal of walking.

This scenario suggests we are mimicking a slightly different walking dynamics in the gauge theory than that discussed above — imagine a theory in which the coupling ran to strong coupling (call this scale Λ_1 again) and then entered a conformal regime with coupling value slightly above the critical value needed to form a condensate. If the coupling was tuned from above sufficiently close to the critical value in its conformal window then a self-energy, $\Sigma(\rho = 0)$ would form but with a size considerably below Λ_1.

Realising this sort of walking behaviour can be done in a straightforward, if ad hoc, fashion. We need to break the symmetry between ρ and w_5, w_6 in the coupling ansatz β. A simple ansatz is just to shift our previous ansatz out to larger ρ:

$$\begin{aligned} \beta &= a + 1 - a \tanh\left[\Gamma(\sqrt{(\rho - \lambda_1)^2 + w_5^2 + w_6^2} - \lambda)\right] \quad \rho \geq \lambda_1 \\ \beta &= 1 \qquad\qquad\qquad\qquad\qquad\qquad\qquad\qquad\qquad\qquad \rho < \lambda_1 \end{aligned} \tag{2.16}$$

This ansatz, which we sketch in figure 2.2, leaves the derivative of β unchanged but shifted by λ_1 in ρ — this will ensure the condensate, which is given by (2.13) and dominated around λ_1 where the derivative of β is non-zero, will grow as λ_1^3. The embedding will still plateau around the same value of w_5 since above the step (which is quite sharp) the space is AdS and the embeddings must be flat. Below λ_1 the embedding becomes flat since the geometry is AdS (the first derivative of Σ_0 at $\rho = \lambda_1$ is smooth). Obviously this choice of β below λ_1 looks peculiar - one could though imagine that in that region there is a sharp step function to large coupling at small w_5, w_6 - the embeddings would remain the same.

With the embeddings from this walking β ansatz we can analytically see how the expressions for f_π and $\langle \bar{q}q \rangle$ change with λ_1. In (2.12) the numerator will become independent of λ_1 as it grows whilst the denominator, which is proportional to the derivatives of Σ_0 and β will fall as $1/\lambda_1$. f_π will therefore scale as $\lambda_1^{1/2}$. The condensate expression (2.13) is dominated around λ_1 where the derivative of β is non-zero — it will grow as λ_1^3. Therefore if we raise λ_1 at fixed f_π the condensate will grow as $\lambda_1^{3/2}$. The rise is consistent with the usual claims that a walking theory

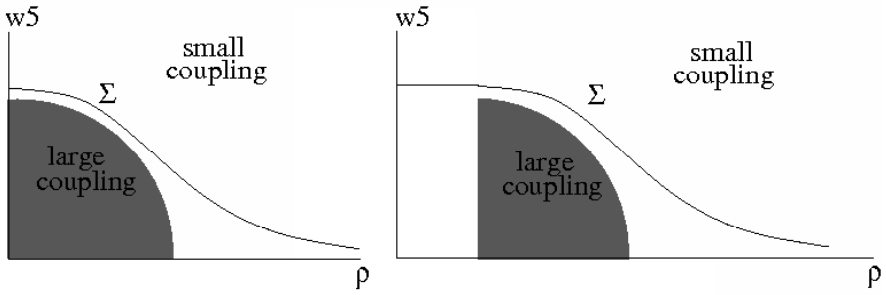

Figure 2.2: *A sketch of the area in which the coupling is large in our ansatz in (2.16) and the resulting form of the embeddings* Σ_0 *— on the left for* $\lambda_1 = 0$ *and on the right for a non-zero* λ_1

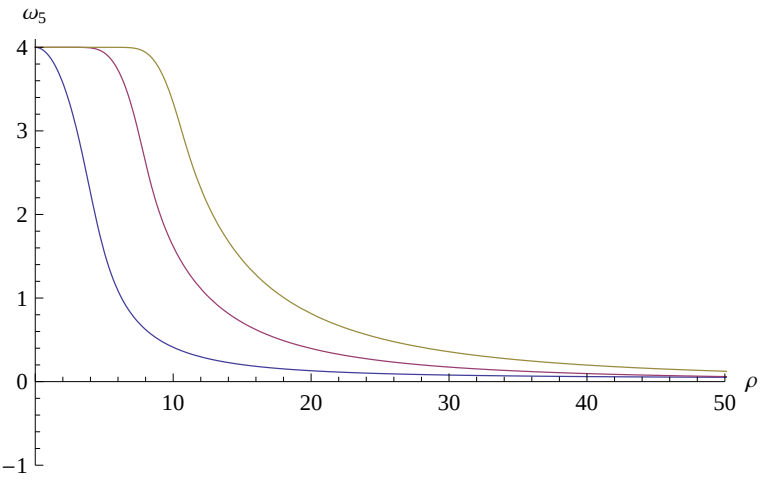

Figure 2.3: *Numerically determined embeddings for the coupling ansatz in (2.16). These curves all have* $a = 3$ *and* $\lambda = 3.19$ *in addition the curves from from left to right correspond to the parameter choices* $\lambda_1 = 0, \Gamma = 1$, $\lambda_1 = 5, \Gamma = 3.51$,$\lambda_1 = 8, \Gamma = 3.63$.

will enhance the condensate.

It is also possible to numerically confirm this behaviour at least for small λ_1. In figure 2.3 we show numerical embeddings, displaying the behaviour shown in figure 2.2, as λ_1 is increased from 0 to 8. To keep the plateau value exactly equal we have tuned Γ in the coupling ansatz (it changes from 1 to 3.6 across these plots). The condensate grows by an order of magnitude across these plots and in the large λ_1 limit will presumably match the analytic behaviour discussed although more and more tuning of Γ would be needed. Note that breaking the symmetry between ρ and w_5, w_6 in the β ansatz is still consistent with the symmetries of the D3/D7 system. In fact interestingly a distinction between the ρ and w_5, w_6 directions is precisely what one would expect in a geometry backreacted to the D7 branes

[33, 49]. It is therefore plausible that one could fine tune the number of quark flavours in some D3/D7 system to obtain these forms of ansatz for the dilaton.

2.3 The D3/D5 System

We now turn to an alternative attempt to describe aspects of walking dynamics with holography. On first meeting the specific D3/(probe)D7 configuration discussed above it seems as if that system should fundamentally be a walking gauge theory — the $\mathcal{N} = 4$ gauge dynamics is conformal and strongly coupled in the UV. When we introduce running in the IR that triggers chiral symmetry breaking, should the physics not be closer in spirit to that of a walking theory rather than QCD? Why did we have to work so hard in section 2.2 to make that system walk? The reason it is not a walking theory is that the UV of the D3/D7 system possesses $\mathcal{N} = 2$ supersymmetry which both forbids a quark condensate and protects the dimension of the $\bar{q}q$ condensate at three. That the self-energy profiles Σ_0 fall off as $1/\rho^2$ in the analysis above is driven by that UV supersymmetry and mimics the behaviour of asymptotically free QCD.

It is natural then to look for a way to introduce quarks into $\mathcal{N} = 4$ super Yang-Mills which breaks supersymmetry even in the far UV. Using a D5 probe to introduce quarks seems the simplest example to explore. Here we consider the system with a four dimensional overlap of the D3 and the D5 not a three dimensional overlap as studied in [50]. This D3/D5 system is a specific example with broken supersymmetry, while i.e. the D3/D5 configuration studied in [50] is supersymmetric. Note that the strings between the D3 and D5 remain bi-fundamental fields of the gauge symmetry and global symmetry. The lowest energy modes of those strings are still at heart the gauge field that would be present if the strings were free to move in the whole space, which become scalar fields, and the gaugino partners that become the fermionic quarks. In a non-supersymmetric theory the scalars will most likely become massive leaving fermionic quark multiplets in the $\mathcal{N} = 4$ theory.

The metric of $AdS_5 \times S^5$ can be written in coordinates appropriate to the D5 embedding as:

$$ds^2 = \frac{1}{g_{uv}}\left[\frac{r^2}{R^2}\eta_{ij}dx^i dx^j + \frac{R^2}{r^2}\left(d\rho^2 + \rho^2 d\Omega_1^2 + d\omega_3^2 + d\omega_4^2 + d\omega_5^2 + d\omega_6^2\right)\right], \quad (2.17)$$

with $r^2 = \rho^2 + \omega_3^2 + \omega_4^2 + \omega_5^2 + \omega_6^2$ and $\rho^2 = \omega_1^2 + \omega_2^2$. R is the radius of AdS $R^4 = 4\pi g_{uv}^2 N\alpha'^2$ The D3 brane is extended in the x_i dimensions. The D5-brane will also be extended in the ρ and Ω_1 directions. The $\omega_3, \omega_4, \omega_5$ and ω_6 are perpendicular to the D5-brane. g_{uv}^2 is the value of the dilaton for $r \to \infty$.

Let us first analyse the system with a constant dilaton

$$e^{\phi} = g_{uv}^2. \quad (2.18)$$

The action for a probe D5 brane assuming the embedding $\omega_5(\rho), \omega_3 = \omega_4 = \omega_6 = 0$ is:

$$\begin{aligned} S_{D5} &= -T_5 \int d^8\xi \; e^{\phi}\sqrt{-\mathrm{det}P\left[G\right]_{ab}} \\ &= -\overline{T_5}\int d^4x d\rho \; r^2\rho\sqrt{1+\left(\partial_\rho w_5\right)^2}, \end{aligned} \quad (2.19)$$

where $T_5 = 1/(2\pi)^5\alpha'^3$ and $\overline{T_5} = T_5 2\pi/R^2 g_{uv}$. The embedding equation is

$$\partial_\rho\left[r^2\rho\frac{\left(\partial_\rho\omega_5\right)}{\sqrt{1+\left(\partial_\rho\omega_5\right)^2}}\right] - 2\omega_5\rho\sqrt{1+\left(\partial_\rho\omega_5\right)^2} = 0. \quad (2.20)$$

The large ρ behaviour of these solutions is

$$\omega_5 \sim m\rho^{\sqrt{3}-1} + c/\rho^{1+\sqrt{3}}. \quad (2.21)$$

The full embeddings are shown on the left hand of figure 2.4. Note that as $m \to 0$ in the UV asymptotics the full solutions lie along the ρ axis indicating that the condensate $c = 0$ and there is no spontaneous chiral symmetry breaking — this is a simple result of the absence of a scale in the conformal field theory.

We continue to interpret the parameter m in the D5 brane embedding as the quark

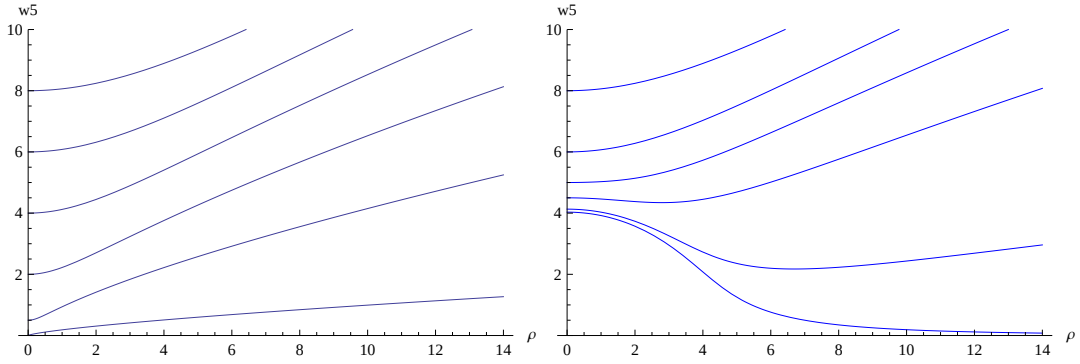

(a) (b)

Figure 2.4: *The regular embeddings of a D5 brane in pure AdS with $\beta = 1$ on the left. On the right the chiral symmetry breaking embeddings for the ansatz for β in (2.6) with $\Gamma = 1, \lambda = 3, a = 5$.*

mass. Then from (2.21) we can see that there is an effective anomalous dimension present for that mass — its dimension is $2 - \sqrt{3}$. The parameter c is then the quark condensate and has dimension $2 + \sqrt{3}$. The change in the dimension of these operators in the UV conformal regime is exactly the physics that underlies the walking idea. Amusingly though here the anomalous dimension of the quark condensate is smaller than zero rather than larger as usually envisaged in walking theories. The D3/D5 system will not apparently be much use for constructing a phenomenological technicolour model. On the other hand here we are simply interested in testing the intuition for walking theories so we will continue to investigate for more formal reasons.

2.3.1 D3/D5 Embedding with a Non-Trivial Dilaton

Let us now include a non-trivial dilaton (gauge coupling) profile as we did above in the D3/D7 system

$$e^{\phi} = g_{YM}^2(r^2) = g_{uv}^2 \beta(r^2). \tag{2.22}$$

For $r \to \infty$ $\beta \to 1$. The action is now

$$S_{D5} = -\overline{T_5} \int d^4x d\rho \; r^2 \beta \rho \sqrt{1 + (\partial_\rho w_5)^2}. \tag{2.23}$$

The embedding equation is

$$\partial_\rho \left[r^2 \beta \rho \frac{(\partial_\rho \omega_5)}{\sqrt{1+(\partial_\rho \omega_5)^2}} \right] - 2\omega_5 \rho \sqrt{1+(\partial_\rho \omega_5)^2} \left[\beta + r^2 (\partial_{r^2} \beta) \right] = 0 \tag{2.24}$$

The embeddings can be seen on the right in figure 2.4 for the ansatz for β in (2.6). There is again chiral symmetry breaking with a non-zero $w_5(\rho = 0)$ as $m \to 0$ in the UV. The self-energy curves fall off faster at large ρ which matches expectations from gap equations in a theory where the quark condensates dimension grows in the walking regime.

The embedding breaks the SO(4) symmetry in the $\omega_3 - \omega_6$ directions so we expect there to be Goldstone modes present. For example, there should be an equivalent solution when rotating the embedding in e.g. the $\omega_5 - \omega_6$ plane. Let's look at small fluctuations around the embedding Σ_0 in the ω_6 direction to find a Goldstone boson. The action for such fluctuations in quadratic order is

$$\begin{aligned} S_5 &= -\overline{T_5} \int d^4x d\rho \; r^2 \beta \rho \sqrt{1+(\partial_\rho \Sigma_0)^2} \left[1 + (\partial_{r^2}\beta) w_6^2 \right. \\ &\qquad \left. + \frac{1}{2} \frac{(\partial_\rho \omega_6)^2}{1+(\partial_\rho \Sigma_0)^2} + \frac{1}{2} \frac{R^4}{r^4} (\partial_\mu \omega_6)^2 + \ldots \right], \end{aligned} \tag{2.25}$$

where again r^2, β and $\partial_{r^2}\beta$ are all evaluated on the the D7 brane worldvolume Σ_0. We seek fluctuations of the form $\omega_6(x,\rho) = f_n(\rho) e^{ik\cdot x}$ with $k^2 = -M_n^2$. The equation of motion for the fluctuations give the following equations for f_n

$$\begin{aligned} \partial_\rho \left[r^2 \beta \rho \frac{(\partial_\rho f_n)}{\sqrt{1+(\partial_\rho \Sigma_0)^2}} \right] + \frac{R^4}{r^2} \beta \rho \sqrt{1+(\partial_\rho \Sigma_0)^2} M_n^2 f_n \\ - 2\rho \sqrt{1+(\partial_\rho \Sigma_0)^2} \left[\beta + r^2 \partial_{r^2} \beta \right] f_n = 0. \end{aligned} \tag{2.26}$$

The equation with $M^2 = 0$ and $f_0 = \Sigma_0$ is the embedding equation (2.4) revealing the presence of the Goldstone mode.

The Lagrangian for the Goldstone field is found by writing
$\omega_6^a = f_0(\rho)\pi^a(x) = \Sigma_0 \pi^a(x)$ in (2.25) and integrating the Lagrangian density over ρ. We can expand $r^2\beta$ with $r^2 = \rho^2 + \Sigma_0^2 + \Sigma_0^2 (\pi^a(x))^2$ as

$r^2\beta(r^2) = r^2\beta(r^2)|_{r^2=\rho^2+\Sigma_0^2} + \Sigma_0^2\left(\pi^a(x)\right)^2 \partial_{r^2}(r^2\beta)|_{r^2=\rho^2+\Sigma_0^2}$ and then use the equation of motion (2.26) to eliminate the second and third terms in (2.25) for $M_n = 0$. This procedure gives the Lagrangian to quadratic order

$$\mathcal{L} = -\overline{T_5}\int d\rho\; r^2\beta\rho\sqrt{1+(\partial_\rho\Sigma_0)^2}\left[1+\frac{1}{2}\frac{R^4}{r^4}\Sigma_0^2\left(\partial_\mu\pi^a(x)\right)^2 \right.$$
$$\left. +\frac{1}{4}\frac{R^4}{r^4}\left(\frac{(\partial_\rho\Sigma_0)^2\Sigma_0^2}{1+(\partial_\rho\Sigma_0)^2}+2\Sigma_0^4\frac{\partial_{r^2}\left(\beta r^2\right)}{\beta r^2}\right)\mathrm{Tr}\left([\partial_\mu\Pi,\Pi]^2\right)+\ldots\right], \tag{2.27}$$

where again $\Pi = \pi^a(x)\tau^a$. We can now rescale $\pi(x)$ in (2.27) and get an expression for f_π. We find

$$\frac{f_\pi^2}{\Lambda^2} = \frac{-N^{1/2}}{24\pi^{3/2}\lambda^2}\frac{\left[\int d\rho\beta\rho\sqrt{1+(\partial_\rho\Sigma_0)^2}\frac{\Sigma_0^2}{\rho^2+\Sigma_0^2}\right]^2}{\left[\int d\rho\frac{\Sigma_0^2}{(\rho^2+\Sigma_0^2)^2}\partial_\rho\left(\frac{(\rho^2+\Sigma_0^2)\beta\rho\Sigma_0(\partial_\rho\Sigma_0)}{\sqrt{1+(\partial_\rho\Sigma_0)^2}}\right)\right]} \tag{2.28}$$

We also want to find out the value of the quark condensate. We expand $r^2\beta$ in (2.27) with $r^2 = \rho^2 + (\Sigma_0 + m\rho^{\sqrt{3}-1})^2$ as
$r^2\beta = r^2\beta|_{r^2=\rho^2+\Sigma_0^2} + \partial_{r^2}(r^2\beta)|_{r^2=\rho^2+\Sigma_0^2}(2m\rho^{\sqrt{3}-1}\Sigma_0 + \mathcal{O}(m^2))$. Then we can compare the vacuum energy, V_0, in (2.27) with the vacuum energy of the chiral Lagrangian to find the quark condensate

$$\frac{\langle\bar{q}q\rangle}{\Lambda^{2+\sqrt{3}}} = \frac{-N^{1/2}}{2g_{uv}^2N\pi^{1/2}\lambda^{2+\sqrt{3}}}\int d\rho\;\rho^{\sqrt{3}}\sqrt{1+(\partial_\rho\Sigma_0)^2}\Sigma_0\partial_{r^2}(r^2\beta)\Big|_{r^2=\rho^2+\Sigma_0^2}. \tag{2.29}$$

These expressions for f_π and $\langle\bar{q}q\rangle$ are in some ways similar to those in the D3/D7 system. f_π is again dominated at low ρ whilst the condensate is more sensitive to the tail of Σ_0. In the D5 setting Σ_0 falls off more quickly in the UV and will suppress the condensate. This matches the chiral quark model results. On the other hand the factor of $N^{1/2}$ before each expression suggests some radical redistribution of the degrees of freedom in the UV conformal regime which we can offer no explanation for.

It is important also to note that one can not directly compare the condensates in

the D5 and D7 cases since they have different intrinsic dimension even in the far UV. In fact to convert the D3/D5 theory to the usual walking set-up would require the inclusion of extra UV physics (equivalent to that at the scale Λ_1 in the walking discussion above) where the condensate's dimension changes to three. The condensate above that scale would be suppressed by a further factor of roughly $\Lambda_1^{\sqrt{3}-1}$.

Whilst the D3/D5 system may not form the basis of any helpful phenomenological model we do believe that the walking paradigm is the correct way to interpret the system and the anomalous dimensions present in the UV.

2.4 Conclusions

We have presented a general description of chiral symmetry breaking in the D3/D7 system that describes a strongly coupled gauge theory with quarks. The model allows one to compute the dependence of the parameters of the low energy chiral Lagrangian on the running coupling or dilaton form. Our integral formulae for f_π and the quark condensate allow analytic understanding of how these quantities depend on the coupling and the dynamical mass of the quark in a similar way to the results of chiral quark models and the Pagels-Stokar formula. Our model is not complete since we do not backreact the geometry to the dilaton. However, we view this as a necessary evil to construct intuition in this type of set-up to the response to different dilaton profiles. This toy environment should provide good guidance for those wishing to construct fully backreacted solutions that show specific phenomena.

We have used our results to understand how walking-like gauge dynamics could be included in a holographic framework. The crucial signal of walking should be that the quark self-energy at zero momentum should be much less than the scale at which conformal symmetry breaking is introduced. We displayed in figure 2.2 the form a dilaton profile must take to achieve walking. Our integral equations support the usual hypothesis that walking in a gauge theory would tend to boost the value

of the quark condensate relative to the value of f_π.

Finally we studied the non-supersymmetric D3/D5 system with a four dimensional overlap and proposed that the conformal UV of the theory should be considered as a walking phase of a gauge theory. The anomalous dimensions of the quark mass and condensate were computed - in this theory the dimension of the quark condensate is $2 + \sqrt{3}$ which is greater than the canonical dimension 3. Normally walking is constructed to lower this dimension but this theory hopefully nevertheless adds to our knowledge of walking behaviour.

Chapter 3

Holographic Description of the Phase Diagram of a Chiral Symmetry Breaking Gauge Theory

The phase diagram in the temperature and chemical potential (or density) plane is a matter of great interest in both QCD and more widely in gauge theory [51, 10, 11]. As discussed in section 1.2.3 there is in QCD believed to be a transition from a confining phase with chiral symmetry breaking at low temperature and density to a phase with deconfinement and no chiral symmetry breaking at high temperature. In the standard theoretical picture for QCD with massless quarks, the transition is first order for low temperature but growing density, whilst second order at low density and growing temperature. The second order transition becomes a cross over at finite quark mass. There is a (tri-)critical point where the first order transition mutates into the (second order) cross over transition. In fact as mentioned in section 1.2.3 though there could still be room in QCD for a more exotic phase diagram [11] as we will discuss in the context of our results in our final section.

In this chapter we will present a precise holographic determination of the phase

diagram in the temperature chemical potential plane for a gauge theory that displays many of the features of the QCD diagram, although the precise details differ. A pictorial comparison of our theory to QCD can be made by comparing figure 3.5 to figure 3.10.

The theory we will consider is the large N $\mathcal{N}$=4 gauge theory with quenched $\mathcal{N}$=2 quark matter. An immediate difference between the $\mathcal{N}$=4 glue theory and QCD is that the thermal phase transition to a deconfined phase occurs for infinitesimal temperature since the massless theory is conformal [28]. Essentially the entire temperature chemical potential phase diagram of our theory is therefore characterised by strongly coupled deconfined glue.

The quark physics is more subtle though — the phase diagram in the temperature chemical potential (density) plane for the $\mathcal{N} = 2$ quark matter has been studied in [52, 53, 54, 55, 56, 57]. When the quark mass is zero the theory is conformal. Immediately away from zero quark mass, in either temperature or chemical potential, a first order transition moves the theory to a non-conformal theory with melted mesons [58, 59, 60, 61].

When a quark mass is present in the $\mathcal{N}$=2 theory the meson melting transition occurs away from the origin. This transition has been reported as first order with a second order transition point where the first order transition line touches the $T = 0$ chemical potential axis [53, 54] (in the grand canonical ensemble). Interestingly there is a phase transition line in the temperature versus density plane (in the canonical ensemble) in which the quark condensate jumps [55, 52]. This area of the phase diagram is intrinsically unstable though and not realisable by imposing any chemical potential [53].

The crucial ingredient we will add to the theory is chiral symmetry breaking which will also bring the theory closer in spirit to QCD. As shown in [38, 62, 63, 64, 65, 66, 67] the $\mathcal{N} = 2$ theory in the presence of a magnetic field displays chiral symmetry breaking through the generation of a quark anti-quark condensate. At zero density the finite temperature behaviour has been studied [38, 62, 63, 64] and there is a first order transition from a chiral symmetry broken

phase at low temperature to a chiral symmetry restored phase at high temperature. In this chapter we will include chemical potential as well to map out the full phase diagram in the temperature chemical potential plane. We will find a chiral symmetry restoration phase transition, which is first order for low density and second order for low temperature — there is a critical point where these transitions meet. This physics is in addition to a meson melting transition which is first order at large temperature but apparently second order at low temperature. This latter region of transition is interesting because it is associated with a discontinuous jump from an embedding off the black hole to one that ends on it and it looks naively first order. However, we see a second order transition in the free energy.

We will also track the movement of these transition lines and critical points as the quark mass rises relative to the magnetic field. The infinite mass limit corresponds to the pure $\mathcal{N}$=2 theory without magnetic field [53, 56]. The second order chiral symmetry restoration transition becomes a cross over the moment a mass is introduced. The first order transition structure remain however, even in the infinite mass limit, with two critical points: one is the end point of the first order transition and the other is the the end point of the second order meson melting transition. This structure was not reported in the results in [53, 56][2] but this is not surprising since the structure, in that limit, is on a very fine scale. We have only found it by following the evolution of the larger structure present at low quark mass with a magnetic field. In addition we present evidence to suggest the parameter space with a second order meson melting transition extends away from just the $T = 0$ axis, again, even in the infinite mass limit. We have confirmed these results in the strict $B = 0$ limit also.

The theory we study may appear to be a rather vague relative of QCD with magnetic field induced chiral symmetry breaking. On the other hand it is a theory of strongly coupled glue with the magnetic field inducing conformal symmetry breaking in the same fashion as $\Lambda_{\rm QCD}$ in QCD. In fact the magnetic field case in

[2]The existence of two critical points is related with the existence of the black hole to black hole transition. It is actually just visible in Fig 2c of [56] but the authors had not probed it in detail previously. After discussion of our results with the authors of [56], they have refined their computations and confirmed our results.

the basic $\mathcal{N}$=4 dual is the cleanest known example of chiral symmetry breaking in a holographic environment. The magnetic field case provides a smooth IR wall where we have more control but the results are likely to be the same in those more complex cases. We can hope to learn some lessons for a wider class of gauge theories. Such studies are potentially of interest for QCD, more exotic gauge theories and even for condensed matter systems.

3.1 The Holographic Description

The $\mathcal{N}$=4 gauge theory at finite temperature has a holographic description in terms of an AdS_5 black hole geometry (with N D3 branes at its core). The geometry is

$$ds^2 = \frac{r^2}{R^2}(-f dt^2 + d\vec{x}^2) + \frac{R^2}{r^2 f} dr^2 + R^2 d\Omega_5^2 \ , \tag{3.1}$$

where $R^4 = 4\pi g_s N \alpha'^2$ and

$$f := 1 - \frac{r_H^4}{r^4} \ , \qquad r_H := \pi R^2 T \ . \tag{3.2}$$

The black hole with its horizon at $r = r_H$ introduces a temperature T into the theory as seen in section 1.4.9.

We will find it useful to make the coordinate transformation

$$\frac{dr^2}{r^2 f} \equiv \frac{dw^2}{w^2} \implies w := \sqrt{r^2 + \sqrt{r^4 - r_H^4}} \ , \tag{3.3}$$

with $w_H = r_H$. This change makes the presence of a flat 6-plane perpendicular to the horizon manifest. We will then write the coordinates in that plane as ρ and L according to

$$w = \sqrt{\rho^2 + L^2} \ , \quad \rho := w \sin\theta \ . \quad L := w \cos\theta \ , \tag{3.4}$$

The metric is then

$$ds^2 = \frac{w^2}{R^2}(-g_t dt^2 + g_x d\vec{x}^2) + \frac{R^2}{w^2}(d\rho^2 + \rho^2 d\Omega_3^2 + dL^2 + L^2 d\Omega_1^2) \ ,$$

where

$$g_t := \frac{(w^4 - w_H^4)^2}{2w^4(w^4 + w_H^4)} \ , \qquad g_x := \frac{w^4 + w_H^4}{2w^4} \ . \tag{3.5}$$

3.1.1 Quarks/D7 Brane Probes

Quenched ($N_f \ll N$) $\mathcal{N}$=2 quark superfields are included in the $\mathcal{N}$=4 gauge theory through probe D7 branes in the geometry. The D7 probe can be described by its DBI action

$$S_{DBI} = -T_{D7} \int d^8\xi \sqrt{-\det(P[G]_{ab} + 2\pi\alpha' F_{ab})} \ , \tag{3.6}$$

where $P[G]_{ab}$ is the pullback of the metric and F_{ab} is the gauge field living on the D7 worldvolume. We will use F_{ab} to introduce a constant magnetic field (e.g. $F_{12} = -F_{21} = B$) [38, 62, 63] and a chemical potential associated with baryon number $A_t(\rho) \neq 0$ [52, 68, 69].

We embed the D7 brane in the ρ and Ω_3 directions of the metric but to allow all possible embeddings we must include a profile $L(\rho)$ at constant Ω_1. The full DBI action we will consider is then

$$S = \int d\xi^8 \mathcal{L}(\rho) = \left(\int_{S^3} \epsilon_3 \int dt d\vec{x}\right) \int d\rho \ \mathcal{L}(\rho) \ , \tag{3.7}$$

where ϵ_3 is a volume element on the 3-sphere and

$$\begin{aligned} \mathcal{L} \ := \ & -N_f T_{D7} \frac{\rho^3}{4}\left(1 - \frac{w_H^4}{w^4}\right) \times \sqrt{\left(1 + (\partial_\rho L)^2 - \frac{2w^4(w^4 + w_H^4)}{(w^4 - w_H^4)^2}(2\pi\alpha'\partial_\rho A_t)^2\right)} \\ & \times \sqrt{\left(\left(1 + \frac{w_H^4}{w^4}\right)^2 + \frac{4R^4}{w^4}B^2\right)} \ . \end{aligned} \tag{3.8}$$

Since the action depends on $\partial_\rho A_t$ and not on A_t, there is a conserved quantity d

$\left(:= \frac{\delta S}{\delta F_{\rho t}}\right)$ and we can use the Legendre transformed action

$$\widetilde{S} = S - \int d\xi^8 F_{\rho t} \frac{\delta S}{\delta F_{\rho t}} = \left(\int_{S^3} \epsilon_3 \int dt d\vec{x}\right) \int d\rho \; \widetilde{\mathcal{L}}(\rho) \; , \tag{3.9}$$

where

$$\widetilde{\mathcal{L}} := -N_f T_{D7} \frac{(w^4 - w_H^4)}{4w^4} \sqrt{K(1 + (\partial_\rho L)^2)} \; , \tag{3.10}$$

$$K := \left(\frac{w^4 + w_H^4}{w^4}\right)^2 \rho^6 + \frac{4R^4 B^2}{w^4}\rho^6 + \frac{8w^4}{(w^4 + w_H^4)} \frac{d^2}{(N_f T_{D7} 2\pi\alpha')^2} \; . \tag{3.11}$$

To simplify the analysis we note that we can use the magnetic field value as the intrinsic scale of conformal symmetry breaking in the theory — that is we can rescale all quantities in (3.10) by B to give

$$\widetilde{\mathcal{L}} = -N_f T_{D7} (R\sqrt{B})^4 \; \frac{\widetilde{w}^4 - \widetilde{w}_H^4}{\widetilde{w}^4} \sqrt{\widetilde{K}(1 + \widetilde{L}'^2)} \; , \tag{3.12}$$

$$\widetilde{K} = \left(\frac{\widetilde{w}^4 + \widetilde{w}_H^4}{\widetilde{w}^4}\right)^2 \widetilde{\rho}^6 + \frac{1}{\widetilde{w}^4}\widetilde{\rho}^6 + \frac{\widetilde{w}^4}{(\widetilde{w}^4 + \widetilde{w}_H^4)} \widetilde{d}^2 \; , \tag{3.13}$$

where the dimensionless variables are defined as

$$(\widetilde{w}, \widetilde{L}, \widetilde{\rho}, \widetilde{d}) := \left(\frac{w}{R\sqrt{2B}}, \frac{L}{R\sqrt{2B}}, \frac{\rho}{R\sqrt{2B}}, \frac{d}{(R\sqrt{B})^3 N_f T_{D7} 2\pi\alpha'}\right) \; . \tag{3.14}$$

In all cases the embeddings become flat at large ρ taking the form

$$\widetilde{L}(\widetilde{\rho}) \sim \widetilde{m} + \frac{\widetilde{c}}{\widetilde{\rho}^2} \; , \widetilde{m} = \frac{2\pi\alpha' m_q}{R\sqrt{2B}} \; , \widetilde{c} = \langle \bar{q} q \rangle \frac{(2\pi\alpha')^3}{(R\sqrt{2B})^3} \; . \tag{3.15}$$

In the absence of temperature, magnetic field and density the regular embeddings are simply $L(\widetilde{\rho}) = \widetilde{m}$, which is the minimum length of a D3-D7 string, allowing us to identify it with the quark mass as shown in section 1.4.7. $\tilde{c}$ should then be identified with the quark condensate with the relation shown.

We will classify the D7 brane embeddings by their small $\widetilde{\rho}$ behaviour. If the D7 brane touches the black hole horizon, we call it a black hole embedding, otherwise, we call it a Minkowski embedding. We have used Mathematica to solve the equations of motion for the D7 embeddings resulting from (3.12). Typically in what

follows, we numerically shoot out from the black hole horizon (for black hole embeddings) or the $\widetilde{\rho} = 0$ axis (for Minkowski embeddings) with Neumann boundary condition for a given $\widetilde{d}$. Then by fitting the embedding function with (3.15) at large $\widetilde{\rho}$ we can read off $\widetilde{m}$ and $\widetilde{c}$.

3.1.2 Thermodynamic Potentials

The Hamilton equations from (3.9) are $\partial_\rho d = \frac{\delta \widetilde{S}}{\delta A_t}$ and $\partial_\rho A_t = -\frac{\delta \widetilde{S}}{\delta d}$. The first simply means that d is the conserved quantity. The second reads as

$$\partial_{\widetilde{\rho}} \widetilde{A}_t = \widetilde{d}\, \frac{\widetilde{w}^4 - \widetilde{w}_H^4}{\widetilde{w}^4 + \widetilde{w}_H^4} \sqrt{\frac{1 + (\widetilde{L}')^2}{\widetilde{K}}}\ , \tag{3.16}$$

where $\widetilde{A}_t := \frac{\sqrt{2} 2\pi\alpha' A_t}{R\sqrt{2B}}$.

There is a trivial solution of (3.16) with $\widetilde{d} = 0$ and constant $\widetilde{A}_t$ [53]. The embeddings are then the same as those at zero chemical potential. For a finite $\widetilde{d}$, $\widetilde{A}_t'$ is singular at $\widetilde{\rho} = 0$ and requires a source. In other words the electric displacement must end on a charge source. The source is the end point of strings stretching between the D7 brane and the black hole horizon. The string tension pulls the D7 branes to the horizon resulting in black hole embeddings [52]. For such an embedding the chemical potential $\widetilde{\mu}$ is defined as [52, 68, 69]

$$\begin{aligned} \widetilde{\mu} &:= \lim_{\widetilde{\rho}\to\infty} \widetilde{A}_t(\widetilde{\rho}) \\ &= \int_{\widetilde{\rho}_H}^{\infty} d\widetilde{\rho}\ \widetilde{d}\, \frac{\widetilde{w}^4 - \widetilde{w}_H^4}{\widetilde{w}^4 + \widetilde{w}_H^4} \sqrt{\frac{1 + (\widetilde{L}')^2}{\widetilde{K}}}\ , \end{aligned} \tag{3.17}$$

where we fixed $\widetilde{A}_t(\widetilde{\rho}_H) = 0$ for a well defined A_t at the black hole horizon.

The Euclideanised on-shell bulk action can be interpreted as the thermodynamic potential of the boundary field theory. The grand potential ($\widetilde{\Omega}$) is associated with the action (3.8) while the Helmholtz free energy ($\widetilde{F}$) is associated with the Legendre

transformed action (3.9):

$$\begin{aligned}\widetilde{F}(\widetilde{w}_H,\widetilde{d}) &:= \frac{-\widetilde{S}}{N_f T_{D7}(R\sqrt{B})^4\mathrm{Vol}} \\ &= \int_{\widetilde{\rho}_H}^{\infty} d\widetilde{\rho}\ \frac{\widetilde{w}^4-\widetilde{w}_H^4}{\widetilde{w}^4}\sqrt{\widetilde{K}(1+(\widetilde{L}')^2)} \end{aligned} \tag{3.18}$$

$$\begin{aligned}\widetilde{\Omega}(\widetilde{w}_H,\widetilde{\mu}) &:= \frac{-S}{N_f T_{D7}(R\sqrt{B})^4\mathrm{Vol}} \\ &= \int_{\widetilde{\rho}_H}^{\infty} d\widetilde{\rho}\ \frac{\widetilde{w}^4-\widetilde{w}_H^4}{\widetilde{w}^4}\sqrt{\frac{(1+(\widetilde{L}')^2)}{\widetilde{K}}}\times\left(\left(\frac{\widetilde{w}^4+\widetilde{w}_H^4}{\widetilde{w}^4}\right)^2\widetilde{\rho}^6+\frac{1}{\widetilde{w}^4}\widetilde{\rho}^6\right)\end{aligned} \tag{3.19}$$

where Vol denote the trivial seven dimensional volume integral except $\widetilde{\rho}$ space, so the thermodynamic potentials defined above are densities, strictly speaking. Since $\widetilde{K}\sim\widetilde{\rho}^6$, both integrals diverge as $\widetilde{\rho}^3$ at infinity and need to be renormalised. Thermodynamic potentials, (3.17),(3.18) and (3.19) are reduced to $B=0$ case if we simply omit all $\frac{\widetilde{\rho}^6}{\widetilde{w}^4}$ and then tildes. See for example (3.20).

3.2 Chiral Symmetry Breaking and the Thermal Phase Transition

We begin by reviewing the results of [38, 62, 63, 64] on magnetic field induced chiral symmetry breaking and the thermal phase transition to a phase in which the condensate vanishes. While those works show the embeddings for fixed T and different values of B, we will show the embeddings for fixed B and different values of T. By fixing B we are using it as the intrinsic scale of symmetry breaking in the same fashion as Λ_{QCD} plays that role in QCD.

Let us digress here to explain how to understand the figures we will present in this chapter. For example, in figure 3.1 we have three columns. The left is the D7 brane embedding configuration. The middle shows a plot of the allowed values of the condensate $\widetilde{c}$ as a function of the quark mass $\widetilde{m}$ — these are thermodynamical conjugate variables. The right is the corresponding thermodynamic potential. Each

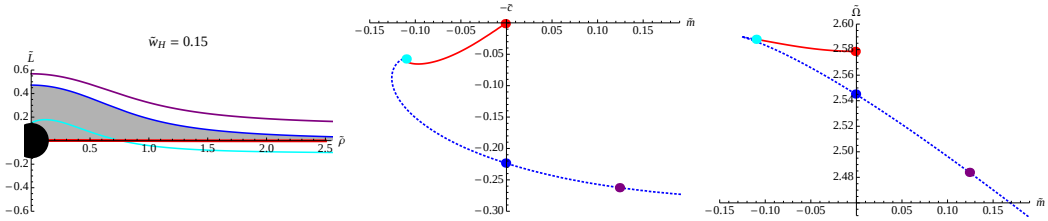

(a) Low temperature - $\widetilde{w}_H = 0.15$. Here we see chiral symmetry breaking with the blue embedding thermodynamically preferred over the red at $\widetilde{m} = 0$.

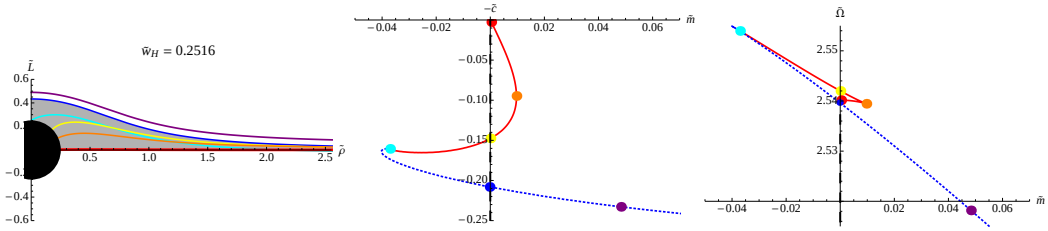

(b) Transition temperature - $\widetilde{w}_H = 0.2516$. This shows the point where the first order chiral symmetry phase transition occurs from the blue to the red embedding. The transition can be identified by considering Maxwell's construction (middle) or the lowest free energy (right).

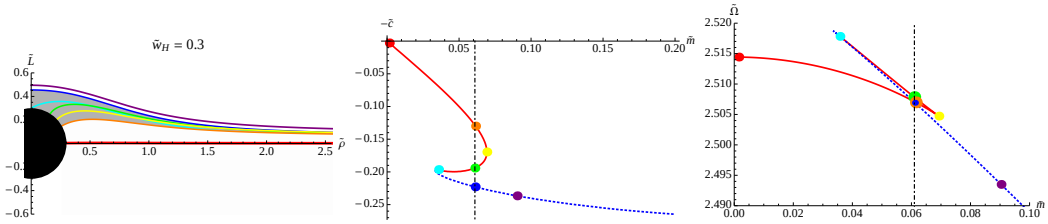

(c) Above the transition - $\widetilde{w}_H = 0.3$. This is the chiral restored phase with the $\widetilde{m} = 0$ curve lying along the $\widetilde{\rho}$ axis (red).

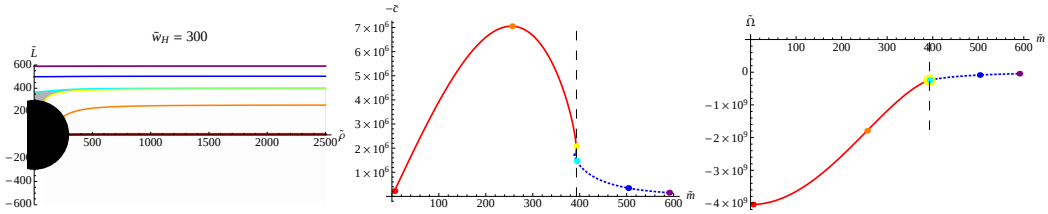

(d) High temperature - $\widetilde{w}_H = 300$. Here the magnetic field is negligible and the embeddings show the usual finite temperature meson melting transition.

Figure 3.1: *The D7 brane embeddings (left), their corresponding $\widetilde{m} - \widetilde{c}$ diagrams (middle), and the free energies (right) in the presence of a magnetic field at finite temperature. (Parameters are scaled or $B = 1/2R^2$ in terms of parameters without tilde.)*

row is for a fixed parameter we are varying — here it is temperature. The left and middle plots are plotted by solving the equation of motion (3.12) with the black hole boundary condition that the embedding is orthogonal to the horizon.

The right hand plot is calculated using (3.18) or (3.19). Both are the same at zero density. We subtract $\lim_{\widetilde{\rho}\to\infty} \frac{1}{4}\widetilde{\rho}^4$ to remove the common infinite component.

Every point in the middle and right plots corresponds to one embedding curve in

the left plot. These points are colour coded with the colours common across each of the three plots. The order of colours follows the rainbow from the bottom embedding as a mnemonic.

In the middle plot we can find any transition point by a Maxwell construction (an equal area law), which is also confirmed by the minimum of the grand potential on the right. The vertical dashed line in the middle and right hand plots corresponds to the transition point.

In the left plots the grey region contains embeddings that are excluded since they are unstable, as shown in the middle and on the right.

The results for the case of a constant magnetic field and varying temperature are displayed in figures 3.1(a)-(d). The figure 3.1(a) (left) shows the D7 embeddings when $T \ll B$ and the black hole is small. The embeddings are driven away from the origin of the $\widetilde{L} - \widetilde{\rho}$ plane - this behaviour is a result of the inverse powers of $\widetilde{w}$, when $\widetilde{w}_H \ll 1$, in the Lagrangian (3.12) which lead the action to grow if the D7 approaches the origin (note that the factor of $\widetilde{\rho}^3$ multiplying the action means the action will never actually diverge). There are also embeddings that end on the black hole (shown in red) but they are thermodynamically disfavoured as shown in figure 3.1(a) (right).

At large $\widetilde{\rho}$ the stable embedding with $\widetilde{m} = 0$ has a non-zero derivative so $\widetilde{c}$ is non-zero and there is a chiral condensate, i.e. chiral symmetry breaking. The U(1) symmetry in the Ω_1 direction is clearly broken by any of these embedding too. We can numerically read off the values of $\widetilde{m}$ and $\widetilde{c}$ from the embeddings and their values are shown in figure 3.1(a) (middle), where the dotted blue curves are for Minkowski embeddings, whilst the red curves are for black hole embeddings.

If the temperature is allowed to rise sufficiently then the black hole horizon grows to mask the area of the plane in which the inverse $\widetilde{w}$ terms in the Lagrangian are large. At a critical value of T the benefit to the $\widetilde{m} = 0$ embedding of curving off the axis becomes disfavoured and it instead lies along the $\tilde{\rho}$ axis — chiral symmetry breaking switches off. This first order transition occurs at $\tilde{w}_H = 0.2516$ as shown in figure 3.1(b) by Maxwell's construction (middle) and by lower grand potential

(right). Our value for the critical temperature agrees with the value $\widetilde{B} = 16$ in [64] since our $\widetilde{w}$ is the same as $\sqrt{\frac{1}{\widetilde{B}}}$ in [64].

We show an example of the embeddings above the critical temperature, their grand potential and the evolution of the curves in the $\widetilde{m} - \widetilde{c}$ plane in figure 3.1(c).

Figure 3.1(d) shows a case when $T \gg B$, here the area of the plane in which B is important is totally masked by the black hole and the results match those of the usual finite T version of the $\mathcal{N}$=2 theory. For $\widetilde{m} >> \tilde{w}_H$ the embeddings are Minkowski like whilst for small $\widetilde{m}$ they fall into the black hole. There is a first order phase transition between these two phases which is the meson melting phase transition discussed in detail in [35, 41, 70, 71, 72]. Minkowski embeddings have a stable and discrete linearised spectrum of fluctuations that correspond to the mesons of the theory [32] In the case of black hole embeddings the linearised fluctuations are now replaced by in-falling quasi-normal modes of the black hole which describe unstable mesonic fluctuations of a quark plasma, as they induce an imaginary component to the meson masses [58, 59]. We can see that the previously reported meson melting transition at large quark mass becomes also the chiral symmetry restoring transition at zero quark mass.

3.3 Finite Density or Chemical Potential at Zero Temperature

We can now turn to the inclusion of finite density or chemical potential in the theory with magnetic field. In this section we consider the zero temperature ($\tilde{w}_H = 0$) theory only, and will continue with finite temperature in the next section.

A finite density (chemical potential) at zero temperature has been studied in the $\mathcal{N}$=2 theory without a magnetic field in [54], where analytic solutions for both a black hole like embedding and a Minkowski embedding have been found. When a magnetic field is turned on, analytic solutions are not available any more, but we have found numerical solutions that continuously deform from the known analytic solutions at zero magnetic field.

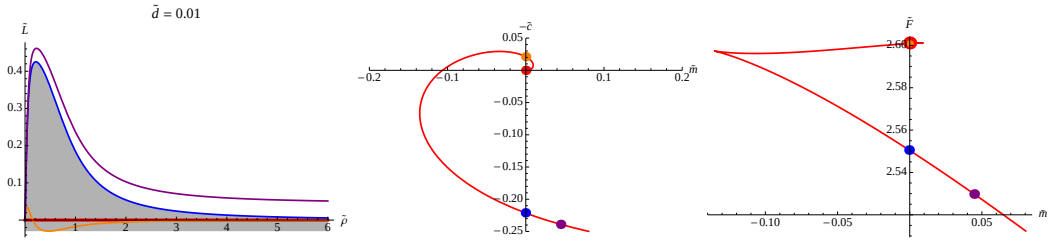

(a) Low density - $\widetilde{d} = 0.01$. Here we see chiral symmetry breaking (the blue embedding is preferred over the red embedding) and a spiral structure in the $\widetilde{m}$ vs. $\widetilde{c}$ plane.

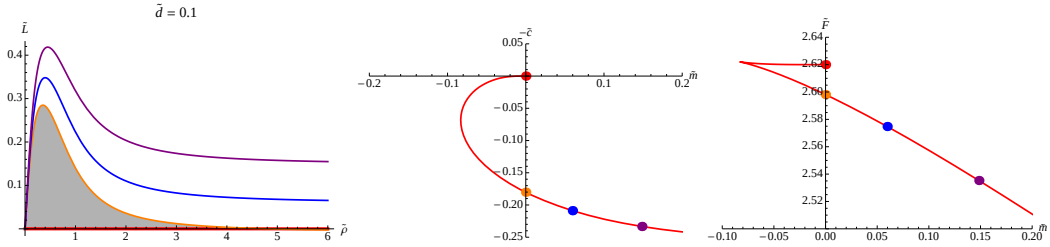

(b) Increasing density below the transition - $\widetilde{d} = 0.1$. There is still chiral symmetry breaking here with the orange embedding preferred to the red. Note the spiral structure in the $\widetilde{m} - \widetilde{c}$ plane has disappeared.

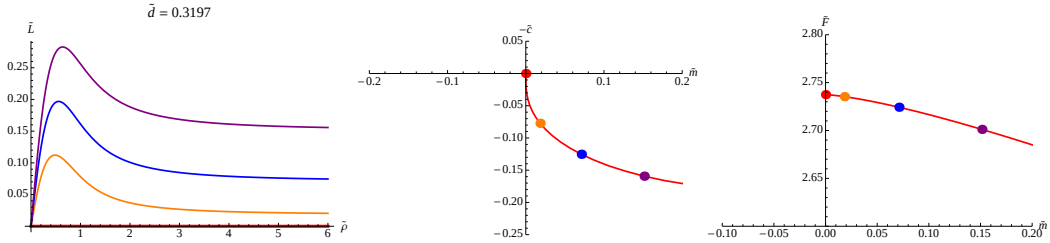

(c) Transition point - $\widetilde{d} = 0.3197$. This shows the point where the second order chiral symmetry phase transition occurs.

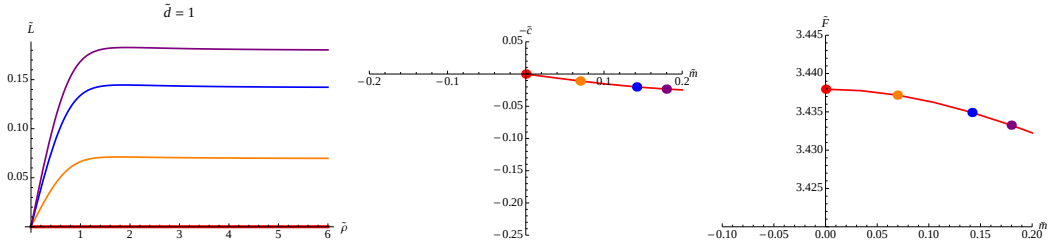

(d) High density $\widetilde{d} = 1$. This is the chiral restored phase with the $\widetilde{m} = 0$ curve lying along the $\widetilde{\rho}$ axis. For larger $\widetilde{m}$ the usual spike like embedding can be seen.

Figure 3.2: *The D7 brane embeddings (left), their corresponding $\widetilde{m} - \widetilde{c}$ diagrams (middle), and the free energies (right) in the presence of a magnetic field at finite density. (Parameters are scaled or $B = 1/2R^2$ in terms of parameters without tilde.)*

Minkowski embedding solutions correspond to zero density and finite chemical potential. The black hole like embedding is the embedding deformed by the density — a spike forms from the D7 down to the origin of the $\widetilde{L} - \widetilde{\rho}$ plane (figure 3.2(d) (left)) which has been interpreted as an even distribution of strings (i.e. quarks) forming in the vacuum of the gauge theory.

First of all it will be interesting to see how the repulsion from the origin induced by a magnetic field and the attraction to the origin by the density compete. Thus we start with the canonical ensemble (that is solutions with non-zero $\widetilde{d}$) and consider black hole like embeddings exclusively. The plot in figure 3.2a (left) shows the embeddings for a small value of density. The solutions show the chiral symmetry breaking behaviour induced by the magnetic field but then spike to the origin because of the density at small $\widetilde{\rho}$. For $\widetilde{m} = 0$ one should compare the blue and red embeddings — the blue one is thermodynamically preferred as shown in figure 3.2(a) (right). The theory shows similar behaviour to that seen at zero density: there is a spiral structure in the $\widetilde{m}$ vs. $\widetilde{c}$ plane (figure 3.2(a) (middle)) [38, 62, 63]. That will disappear as the density increases.

As the density increases the value of the condensate for the $\widetilde{m} = 0$ embeddings falls. We show a sequence of plots for growing $\tilde{d}$ in figures 3.2(b)-(d) (middle). There is a critical value of $\widetilde{d} = 0.3197$ where $\widetilde{c}$ becomes zero for the massless embeddings. Above this value of $\widetilde{d}$ the D7 embedding is flat and lies along the $\tilde{\rho}$ axis (figures 3.2(c)-(d) (left)) . One can see from the plots that there is a second order phase transition to a phase with no chiral condensate. In figures 3.2(c) (left) and 3.2(d) (left) we show embeddings at the critical value of $\widetilde{d}$ and above it respectively. At very large density the solutions become the usual spike embeddings of the $\mathcal{N} = 2$ theory at zero magnetic field.

We are not yet done though, since there are also Minkowski embedding with zero density but constant chemical potential. These can have lower energy and be the preferred vacuum at a given value of chemical potential — that is, they are important in the grand canonical ensemble. The relevant analysis is in figure 3.3(a) (figures 3.3(b)-(e) will be explained in the next section). On the left it shows the three possible types of embedding of the D7 for a given chemical potential at zero temperature. The black curve is the Minkowski embedding (with $\widetilde{d} = 0$), the blue the chiral symmetry breaking spike embedding (with $\widetilde{d} \neq 0$) and the red the chiral symmetry preserving black hole embedding (with $\widetilde{d} \neq 0$). Strictly speaking there is a fourth embedding which lies along the $\tilde{\rho}$ axis and has constant $A_t = \mu$. Its energy is equal for all $\tilde{\mu}$ to that of the red embedding at $\tilde{\mu} = 0$ and is never preferred over

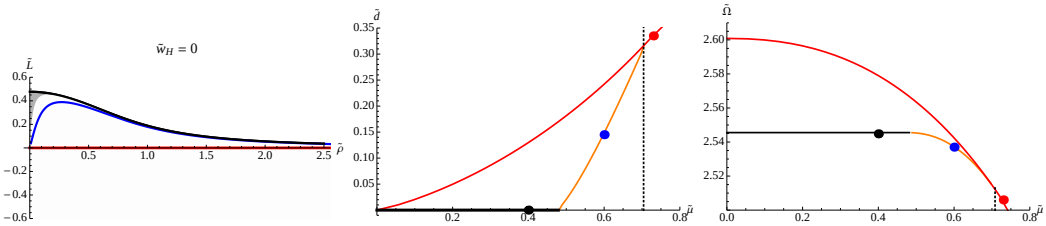

(a) Zero temperature - $\widetilde{w}_H = 0$. The second order meson melting transition and then the second order chiral restoration transition are apparent.

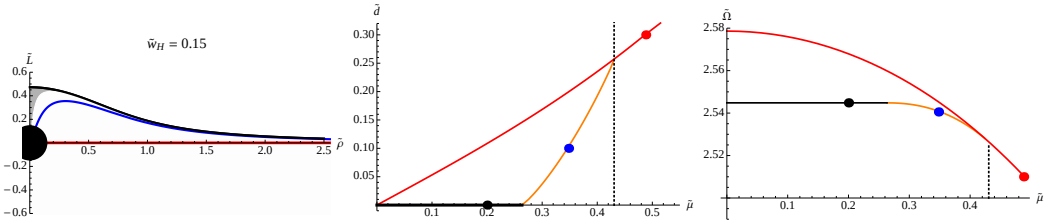

(b) Low temperature - $\widetilde{w}_H = 0.15$. The zero temperature structure remains.

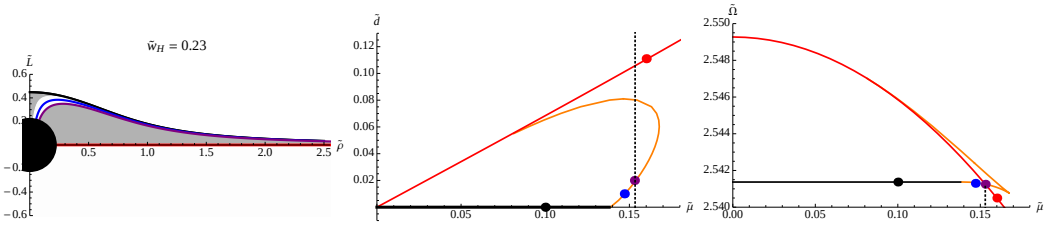

(c) Above the first tri-critical point - $\widetilde{w}_H = 0.23$. The meson melting transitions remains second order but the chiral symmetry restoration transition is first order.

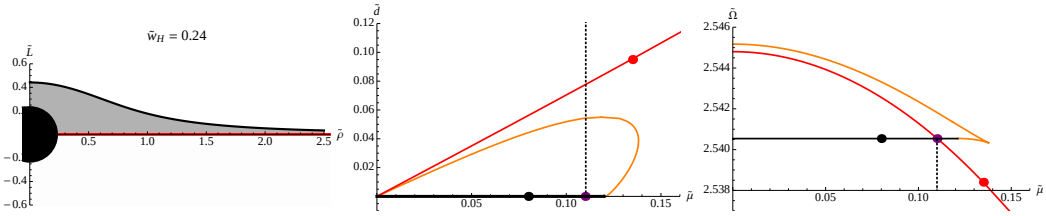

(d) Above the second tri-critical point - $\widetilde{w}_H = 0.24$. There is now only a single first order transition for meson melting and chiral symmetry restoration.

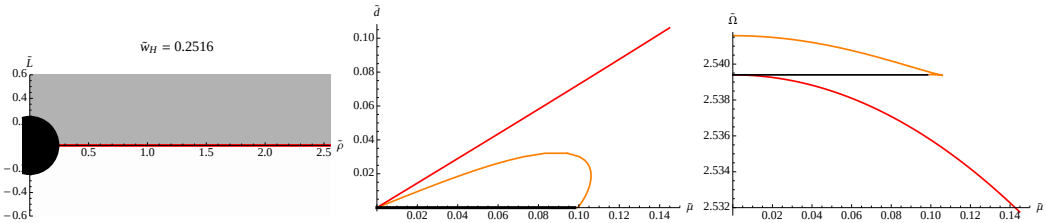

(e) High temperature - $\widetilde{w}_H = 0.2516$. The ground state preserves chiral symmetry for all values of $\tilde{\mu}$.

Figure 3.3: *The D7 brane embeddings (left), their corresponding $\widetilde{d} - \widetilde{\mu}$ diagrams (middle), and the grand potentials (right) for massless quarks in the presence of a magnetic field at a variety of temperatures that represent slices through the phase diagram figure 3.5. (Parameters are scaled or $B = 1/2R^2$ in terms of parameters without tilde.)*

the red embedding with density, so we will ignore it henceforth. The trajectory of the three key embeddings in the $\widetilde{d} - \tilde{\mu}$ space is shown in the middle plot (note that again these two variables are thermodynamical conjugate variables). Finally on the right the grand potential is computed. Clearly at low chemical potential the Minkowski embedding is preferred and $\widetilde{d} = 0$. There is a critical value of $\tilde{\mu} = 0.470$ at which a transition occurs to the spike embedding. This transition looks naively first order since it is a transition between a Minkowski embedding and a black hole embedding. However, we can see that the grand potential appears smooth and the quark density is continuous, which is shown again in figure 3.4(a). The solid lines in figure 3.4(a) are calculated from (3.17), which is based on the holographic dictionary. The dotted lines are obtained by numerically differentiating the grand potential ($\widetilde{d} = -\frac{\partial\widetilde{\Omega}}{\partial\widetilde{\mu}}$), which comes from a thermodynamic relation. This is a non-trivial consistency check of the holographic thermodynamics as well as our calculation [68, 69, 73].

Further in figure 3.4(b) we plot the behaviour of the quark condensate through this transition. The density and quark condensate are both smooth and the transition looks clearly second order. Here we have tested the smoothness numerically at better than the 1% level. Whether there is some other order parameter that displays a discontinuity is unclear. Nevertheless, it would be surprising to have a first order transition with any of the order parameters undergoing a smooth behaviour. We conclude the transition is second order (or so weakly first order that it can be treated as second order). This second order nature of the transition from a Minkowski to a spiky embedding has been shown also in the $B = 0, \widetilde{m} \neq 0$ case at zero temperature analytically [54] and numerically [53].

Finally, above the chemical potential corresponding to the meson melting transition ($\widetilde{\mu} = 0.470$), non-zero density is present and the physics already described in the canonical ensemble occurs, which turns out to be equivalent to the results from the current grand canonical ensemble. Both ensembles predict the second order transition to the flat embedding at the same point, $\widetilde{\mu} = 0.708$ or $\widetilde{d} = 0.3197$, which is the chiral symmetry restoration point. Notice that for the canonical ensemble we used ($\widetilde{m}$,$\widetilde{c}$) conjugate variables on constant $\widetilde{d}$ slices, while for the grand canonical

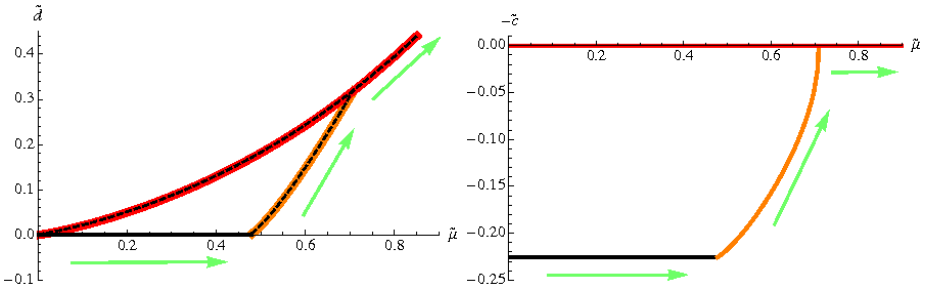

(a) Density: the solid lines are calculated from (3.17) and the dotted lines are obtained by numerically differentiating the grand potential ($\widetilde{d} = -\frac{\partial\widetilde{\Omega}}{\partial\widetilde{\mu}}$).

(b) The quark condensate.

Figure 3.4: *Plots of the order parameters vs. chemical potential at zero temperature and finite B. Both are continuous across the Minkowski to spiky embedding transition ($\widetilde{\mu} \sim 0.47$). The green arrows indicate the changes of phase.*

ensemble we used $(\widetilde{\mu},\widetilde{d})$ conjugate variables on constant $\widetilde{m} = 0$ slices. This agreement with different approaches is another consistency check of our calculation.

On the gauge theory side of the dual, the description is as follows. At zero density there is a theory with chiral symmetry breaking and bound mesons. As the chemical potential is increased $\widetilde{d}$ remains zero and the quark condensate remains unchanged. Then there is a second order transition to finite density (to a spike like embedding) which is presumably associated with meson melting induced by the medium. At a higher density there is then a further second order transition to a phase with zero quark condensate.

Finally we note a paper [74] that proposed an alternative ground state for a chiral symmetry breaking theory at finite density. They proposed that the string spike might end on a wrapped D5 brane baryon vertex in the centre of the geometry. We have not considered that possibility here but it might be interesting to investigate this in the future. The magnetic field induced chiral symmetry breaking provides a system in which this could be cleanly computed without the worries of the hard wall present in that geometry.

3.4 The Phase Diagram in the Grand Canonical Ensemble

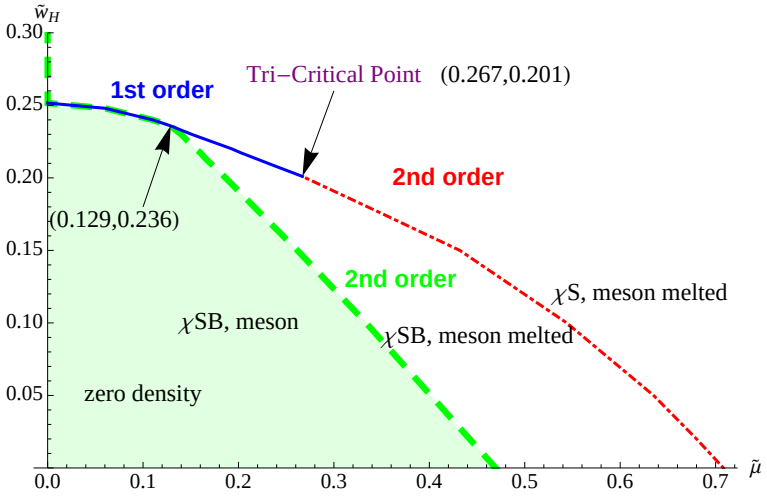

Figure 3.5: *The phase diagram of the $\mathcal{N} = 2$ gauge theory with a magnetic field. The temperature is controlled by the parameter $\tilde{w}_H$ and chemical potential by $\widetilde{\mu}$. (Parameters are scaled or $B = 1/2R^2$ in terms of parameters without tilde.)*

We have identified a first order phase transition from a chiral symmetry breaking phase with meson bound states to a chirally symmetric phase with melted mesons in our massless theory in the presence of a magnetic field with increasing pure temperature. On the finite density axis the meson melting transition is second order and separate from another second order chiral symmetry restoring phase transition. Clearly there must be at least one critical point in the temperature chemical potential phase diagram. We display the phase diagram of the massless theory, which we will discuss the computation of, in figure 3.5.

To construct the phase diagram we have plotted slices at fixed temperature and varying chemical potential. We display the results in figures 3.3(a)-(e) where we show the embeddings (left) relevant at different temperatures, their trajectories in the $\widetilde{d} - \widetilde{\mu}$ plane (middle) and the grand potential (right).

The phase diagram agrees with our previous results: At zero chemical potential we have the transition point $\widetilde{w}_H = 0.2516$. At zero temperature we have the transition point at $\widetilde{\mu} = 0.708$, which corresponds to $\widetilde{d} = 0.3197$. We also identify $\widetilde{\mu} = 0.470$ as the position of the second order transition to a meson melted phase with non-zero $\widetilde{d}$

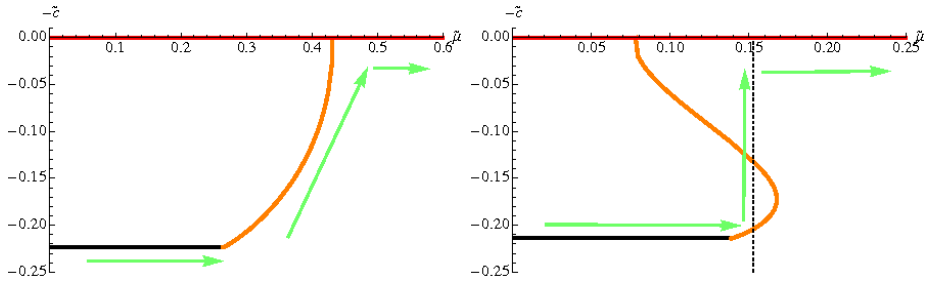

(a) $\widetilde{w}_H = 0.15$ (b) $\widetilde{w}_H = 0.23$

Figure 3.6: *Quark condensate vs. chemical potential at finite B. Both are continuous across the Minkowski (black) to black hole (orange) embedding transition. At $\widetilde{w}_H = 0.23$ the black hole (orange) to black hole (red) transition is discontinuous.*

and chiral condensate $\widetilde{c}$.

The dotted green line is the line along which $\widetilde{d} = 0$ and corresponds to the second order meson melting transition from a Minkowski embedding to a black hole embedding. The transition generates density continuously from zero. The quark condensate also smoothly decreases from its constant value on the Minkowski embedding. We display the continuous behaviour of the quark condensate across the transition in figure 3.6. Note this means that the slope of the embedding at the UV boundary is continuous through the transition even though the embedding in the IR is discontinuous and topology changing. Again we have checked the smoothness of these parameters numerically to better than the 1% level.

The blue line corresponds to a first order transition and the red dotted line is a second order transition in density, chiral condensate etc. The red dotted line is rather special in that this is a phase boundary only at $\widetilde{m} = 0$. This is because this phase boundary is related to the spontaneous breaking of chiral symmetry which only exists at $\widetilde{m} = 0$. At finite $\widetilde{m}$ it must be a cross over region as we will discuss further in section 3.6

The diagram then displays two tri-critical points. It is straightforward to identify where the points lie numerically. The chiral symmetry tri-critical point where the first and second order chiral symmetry restoration transitions join lies at the point $(\widetilde{\mu}, \widetilde{w}_H) = (0.267, 0.201)$. The second tri-critial point where the meson melting transitions join is at $(\widetilde{\mu}, \widetilde{w}_H) = (0.129, 0.236)$.

3.5 The Phase Diagram in the Canonical Ensemble

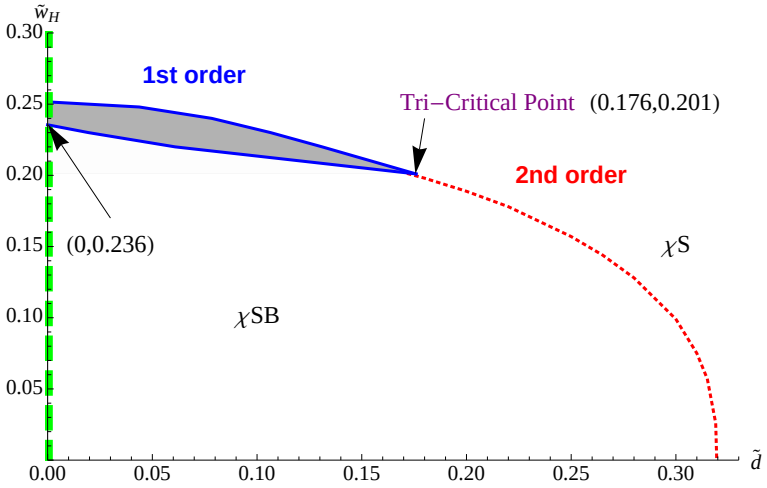

Figure 3.7: *The phase diagram of the $\mathcal{N} = 2$ gauge theory with a magnetic field. The temperature is controlled by the parameter $\tilde{w}_H$ and the density by $\tilde{d}$. (Parameters are scaled or $B = 1/2R^2$ in terms of parameters without tilde.)*

We can study the phase diagram also in the canonical ensemble. It is shown in figure 3.7 and has the same information as figure 3.5. The pale green region in figure 3.5 lies in the green dotted line along the $\tilde{w}_H$ axis of figure 3.7. The chiral symmetry breaking region enclosed by the red, green and blue lines in each figure map onto each other. Similarly the high temperature and density region to the upper right of all the lines in both plots map onto each other. The two double blue lines and the area between them in figure 3.7 correspond to the single blue line in figure 3.5, which is natural since the blue line in figure 3.5 is a first order transition line and the density change is discontinuous. Thus the grey region in figure 3.7 is an unstable density region which hides in the phase boundary in figure 3.5. That region may only be reached by super-cooling or super-heating since it is unstable. The true ground state at those densities and temperatures should be a mixture of the black hole and Minkowski embedding in analogy with the liquid-gas mixture between the phase transitions of water [53]. It's not clear how to realise that mixture in a holographic set-up.

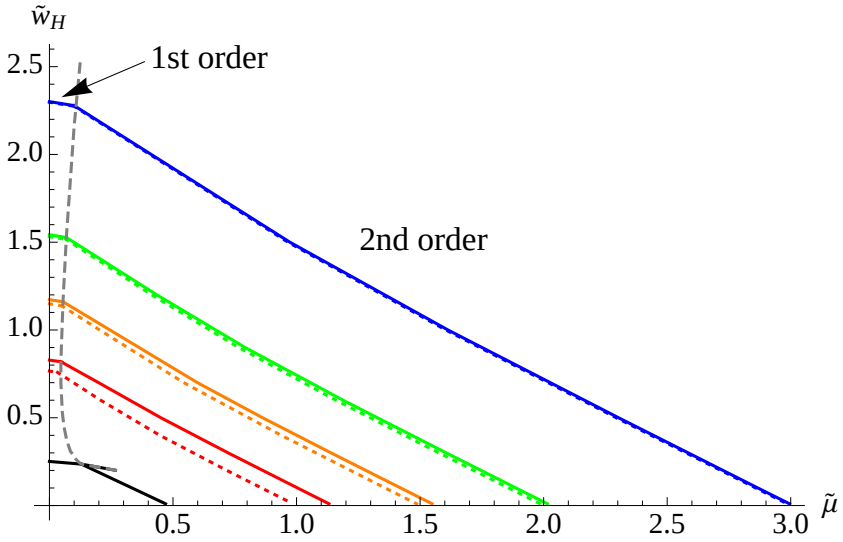

(a) The curves correspond to $\widetilde{m} = 0$(black), 1(red), 1.5(orange), 2(green), 3(blue) from bottom to top. The grey line is the path of the critical points.

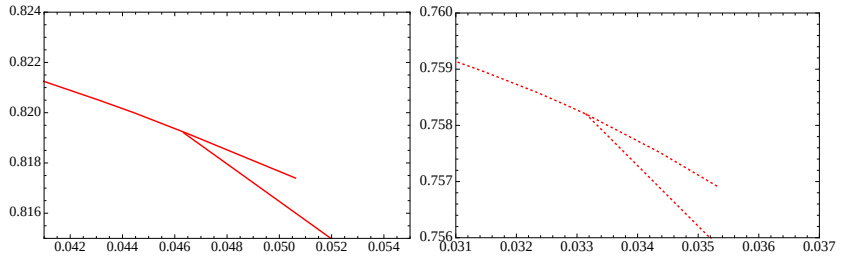

(b) A zoom into figure (a) to show the critical point structure at small chemical potential. Here we show the detail of $\widetilde{m} = 1$ case, but a similar structure exists for every case.

Figure 3.8: *The phase diagram at finite current quark mass with finite B (solid lines) and zero B (dotted lines).*

3.6 Finite Mass

We next describe the evolution of the phase diagram with quark mass. If we move away from zero quark mass then the second order chiral symmetry restoration phase transition at $T = 0$ but growing chemical potential becomes a cross over transition. This can be seen in figure 3.2 where for $\widetilde{m} \neq 0$ the non-zero value of the condensate can be seen to change smoothly with changing $\widetilde{\mu}$ and there is no jump in any order parameter. The (chiral) tri-critical point becomes a critical point. However, the other transition lines survive the introduction of a quark mass.

In figure 3.8. we plot the phase diagram for various quark mass, $\widetilde{m}$, at constant B. The colours represent different quark masses — $\widetilde{m} = 0, 1, 1.5, 2, 3$ from bottom to top are black, red, orange, green, and blue. The solid lines are for finite, fixed B.

To show the influence of the magnetic field we also display the $B = 0$ solution as the dotted lines. The grey line shows the motion of the critical points.

In general the magnetic field shifts the transition line up and right, meaning that the magnetic field makes the meson more stable against the temperature/density meson dissociation effect. This is important at small $\widetilde{m}$ but negligible at large $\widetilde{m}$ as expected.

Both critical points survive the introduction of a finite $\widetilde{m}$, even though it looks like there is no critical point in figure 3.8(a). Zooming in on the appropriate region at small chemical potential reveals the two critical point structure as shown in figure 3.8(b). Their positions, as $\widetilde{m}$ changes, are marked by the grey line in figure 3.8a. The one line represents the two critical points which are indistinguishable on the scale of figure 3.8(a). The chiral symmetry critical point moves very close to the other critical point even for a very small mass ($\widetilde{m} \sim 0.01$). The interpretation of the critical points and the phase boundaries are the same as in the $\widetilde{m} = 0$ case in the previous section.

Notice that the black hole to black hole transition exists even in the $B = 0$ case as shown in figure 3.8(b) (right), so it is not purely due to the magnetic field. Nevertheless this transition seems not to have been reported in the previous works [53, 56]. We believe that this is because the transition line between the two critical points is too small to be resolved on the scale of figure 3.8(a), which agrees qualitatively with the figures in [53]. In order to find those transitions we had to slice the temperature down to order 10^{-3} as shown on the vertical axis in figure 3.8(b) (right). Any coarser graining would miss it.

The final surprise relative to the previous work is that the meson melting transition below the critical point appears second order in our work even in the infinite mass limit. To emphasise this we show a number of plots in the $B = 0$ theory in figure 3.9.

Since the scaled variables (3.15) cannot be used at $B = 0$, (3.19) and (3.17) read in

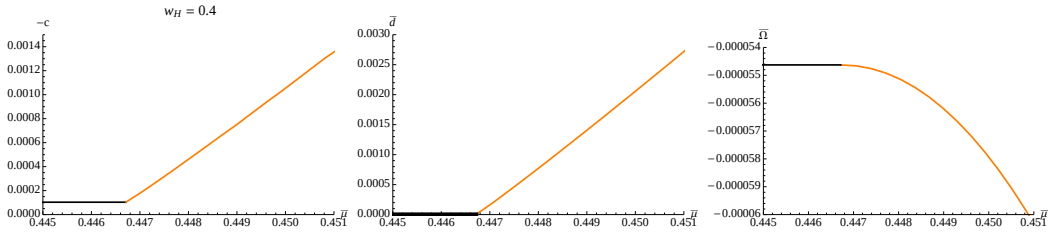

(a) $w_H = 0.4$. At $\bar{\mu} \sim 0.4467$ there is a Minkowski to black hole embedding transition, which is second order in both chiral condensation and density.

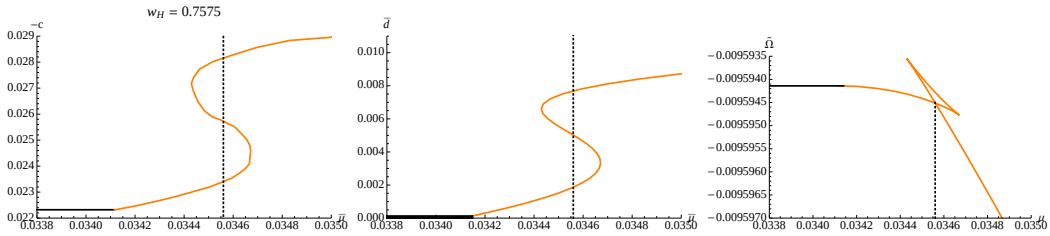

(b) $w_H = 0.7575$. There are two transitions. The first ($\bar{\mu} \sim 0.0341$) is a Minkowski to black hole transition and second order in condensation and density. The second ($\bar{\mu} \sim 0.03455$) is a black hole to black hole transition and first order.

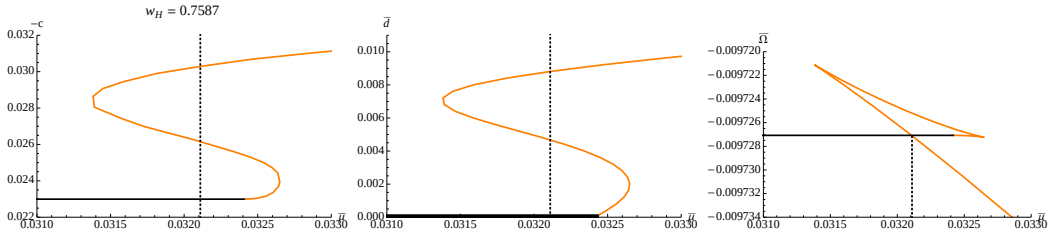

(c) $w_H = 0.7587$. At $\bar{\mu} \sim 0.0321$ there is a Minkowski to black hole embedding transition, which is first order in both chiral condensation and density.

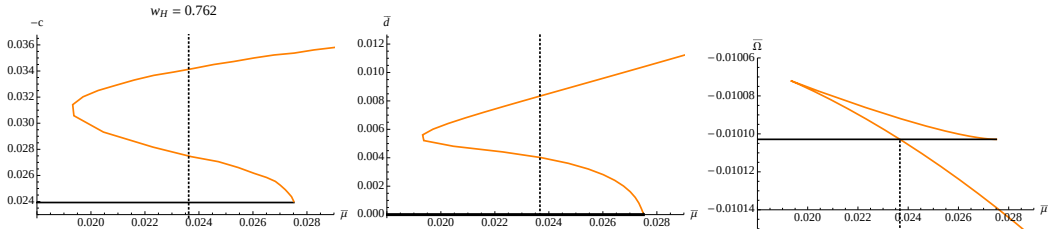

(d) $w_H = 0.762$. At $\bar{\mu} \sim 0.0235$ there is a Minkowski to black hole embedding transition, which is first order in both chiral condensation and density.

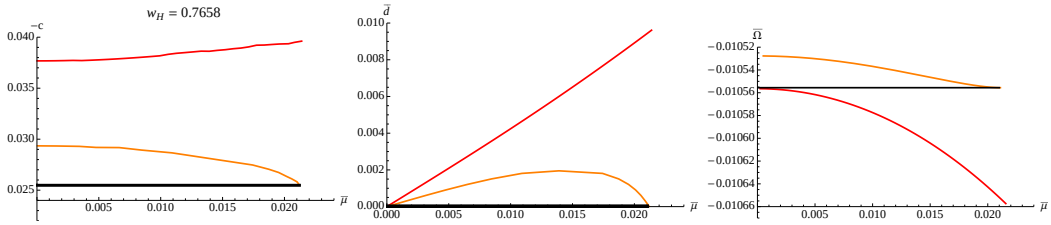

(e) Above $w_H = 0.7658$ only a black hole embedding (red) is stable configuration.

Figure 3.9: *Chiral condensation (left), density (middle), and the grand potentials (right) for massive quarks ($m = 1$) at $B = 0$ at a variety of temperatures that represent slices through the phase diagram figure 3.8(a).*

terms of the original coordinates:

$$\begin{aligned}\bar{\Omega}(w_H,\bar{\mu}) &:= \frac{-S}{N_f T_{D7}\mathrm{Vol}} \\ &= \int_{\rho_H}^{\infty} d\rho\ \frac{w^4-w_H^4}{w^4}\sqrt{\frac{(1+(L')^2)}{K}}\left(\frac{w^4+w_H^4}{w^4}\right)^2\rho^6\ , \end{aligned} \tag{3.20}$$

where

$$\bar{\mu} = \int_{\rho_H}^{\infty} d\rho\ \bar{d}\ \frac{w^4-w_H^4}{w^4+w_H^4}\sqrt{\frac{1+(L')^2}{K}}\ , \tag{3.21}$$

$$K = \left(\frac{w^4+w_H^4}{w^4}\right)^2\rho^6+\frac{w^4}{(w^4+w_H^4)}\bar{d}^2\ , \tag{3.22}$$

$$\bar{\mu} := \sqrt{2}^3\pi\alpha' A_t(\infty)\ , \quad \bar{d}:=\frac{\sqrt{2}^3}{N_f T_{D7}2\pi\alpha'}d \tag{3.23}$$

By the same procedures as in the previous sections we get figure 3.9. Compared to figure 3.3, the left column of figure 3.9 is the chiral condensate instead of the embedding configurations. In figure 3.3 there is always a red black hole embedding, which corresponds to the flat embedding at zero quark mass. It is not present at finite quark mass.

At very low temperature the transition is a Minkowski to black hole transition which is second order in the condensate and density (figure 3.9(a)). As the temperature goes up a new black hole to black hole transition pops up by developing a 'swallow tail' in the grand potential — this transition is first order in the condensate and density (figure 3.9(b)). As temperature rises the 'swallow tail' grows continually and eventually 'swallows' the second order Minkowski to black hole transition (figures 3.9(c),(d)). That means that at higher temperature the second order Minkowski to black hole transition enters an unstable regime and plays no role any more. Instead only the first order Minkowski to black hole transition is manifest. Finally the Minkowski embedding becomes unstable compared to the black hole embedding (figure 3.9(e)). At an even higher temperature the Minkowski embedding is not allowed and only a black hole embedding is available, which is not shown in figure 3.9.

These results all match with our work at finite B and increasing mass, confirming

those results and our phase diagrams already presented.

3.7 Comparison to QCD

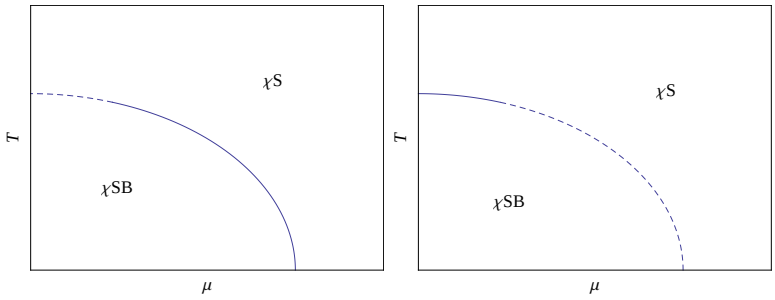

(a) Standard scenario (b) Exotic Scenario

Figure 3.10: *Two possible phase diagrams for QCD with the observed quark masses. (a) is the standard scenario found in most of the literature but a diagram as different as (b) remains potentially possible according to the work in [11]. We have not included any colour superconducting phase here at large chemical potential.*

We have computed the phase diagram for a particular gauge theory using holographic techniques. There are many differences between our theory and QCD: the theory has super partners of the quarks and glue present; it is at large N and small N_f, so quenched (and we have only computed for degenerate quarks to avoid complications involving the non-Abelian DBI action); the theory has deconfined glue for all non-zero temperature; the theory has a distinct meson melting transition. In spite of these differences the phase diagram for the chiral condensate shows many of the aspects of the QCD phase diagram so we will briefly make a comparison here.

The QCD phase diagram is in fact not perfectly mapped out since there have only recently been lattice computations attempting to address finite density [11]. The phase structure also depends on the relative masses of the up, down and strange quarks. The standard theoretical picture [51, 10, 11] for physical QCD is shown in figure 3.10(a). At zero chemical potential the transition with temperature is second order (or a cross over with massive quarks). At zero temperature there is a first order transition with increasing chemical potential (ignoring any superconducting phase). These transitions are joined by a critical point. Comparing to our theory in

figure 3.5 we see that the transitions' orders are reversed and the pictures look rather different.

In fact though as argued in [11] the picture could be very different in QCD. At zero quark mass the finite temperature transition is first order and whether it has changed to second order depends crucially on the precise physical quark masses. Similarly whether the finite density transition is truly first order or second order depends on the exact physical point in the $m_{u,d}$, m_s, μ, T volume. Arguments can even be made for a phase diagram matching that in figure 3.10(b) which then matches the structure of the chiral symmetry restoring phase diagram of the theory we have studied. For the true answer in QCD we must wait on lattice developments. Clearly our model will not match QCD's phase diagram point by point in the $m_{u,d}$, m_s, μ, T volume but it provides an environment in which clear computation is possible for structures that match some points in that phase space.

We found a phase with a quark density but chiral symmetry breaking. Such a phase could potentially exist in QCD. It would be nice also to describe this as a deconfinement transition but firstly the $\mathcal{N} = 4$ background does not induce linear confinement and secondly the presence of any temperature leads to screening of the quarks at the length scale of the inverse temperature. The meson bound states are closer in spirit to atomic bound states than QCD-like mesons. Nevertheless they are being disrupted by the background plasma so the existence of a phase with melted mesons but chiral symmetry breaking at least leads one to speculate on a possible separation of deconfinement and chiral restoration behaviour in the QCD phase plane.

Finally, we note a more general point that seems to emerge from the analysis. The introduction of a chemical potential weakens the first order nature of the transitions in our analysis. This matches with results found in QCD on the lattice. The weakening of the first order phase transition is demonstrated for the chiral transition in the light quark mass regime [75, 76], and is shown for the deconfinement transition in the heavy quark mass regime [77, 78].

Chapter 4

Phase Diagram of the D3/D5 System in a Magnetic Field and a BKT Transition

As seen in the last chapter, the magnetic field induces chiral symmetry breaking in the D3/D7 holographic system. The symmetry breaking and quark confinement are lost at high temperature and density. The rich structure of phase transitions of both first and second order can be seen in figure 3.5. Recently interest has also turned to the D3/D5 system [50, 79, 80, 81, 82, 83, 84] that describes fundamental representation matter fields on a 2+1 dimensional defect within a 3+1 dimensional gauge theory. This system may have some lessons for condensed matter systems. In [85] an analysis of the D3/D5 system at finite density d and at zero temperature T revealed that the chiral symmetry breaking transition with increasing magnetic field B is not second order but similar to a Berezinskii-Kosterlitz-Thouless (BKT) transition [86, 87] (see also the holographic example in [88, 89]). That is order parameters across the transition grow as $\exp(-a/\sqrt{\nu_c - \nu})$ where a is a constant and $\nu = d/B$. (ν_c the critical value for the transition). For small T the authors of [85] showed the BKT transition returns to a second order nature. This difference from the D3/D7 case is surprising so it seems worth fleshing out the entire phase diagram for the theory to see if other surprises are present. In this chapter we

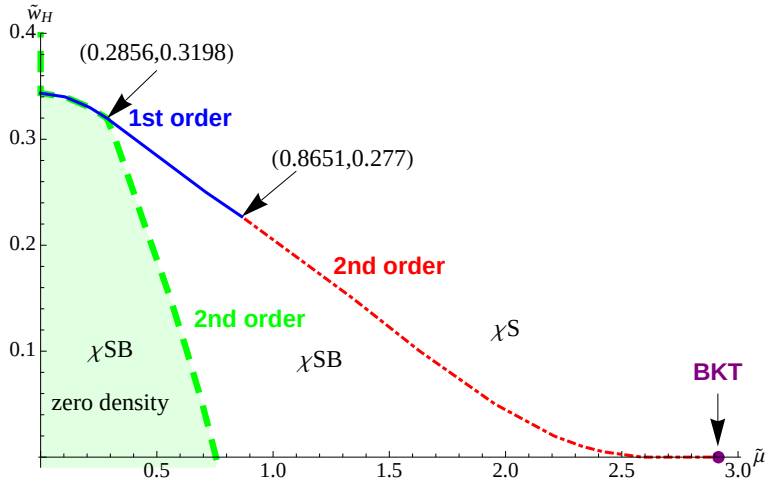

Figure 4.1: *The phase diagrams for D3/D5 system. $\tilde{w}_H$ measure the temperature of the theory whilst $\tilde{\mu}$ is the chemical potential. The dashed line is a second order transition associated with the formation of quark density and meson melting. The dotted line is a second order transition for chiral symmetry restoration. That transition ends at a BKT transition point and its effects on the second order line can be seen. The continuous line is the merged first order transition. The positions of critical points are marked.*

present that analysis — much of the computation matches that in the D3/D7 system which we worked through in chapter 3 so here we very briefly present the formalism and the conclusions. We display the resulting phase diagram for massless matter fields in figure 4.1. Clearly much of the structure is similar to the D3/D7 case but the second order boundary of the chiral symmetry breaking phase is distorted by the presence of the BKT transition.

4.1 The Holographic Description

The $\mathcal{N}$=4 super Yang-Mills gauge theory at finite temperature has a holographic description in terms of an AdS_5 black hole geometry (with N D3 branes at its core)[26, 28, 29]. The geometry can be written as

$$ds^2 = \frac{w^2}{R^2}(-g_t dt^2 + g_x d\vec{x}^2 + g_x dy^2) + \frac{R^2}{w^2}(d\rho^2 + \rho^2 d\Omega_2^2 + dL^2 + L^2 d\bar{\Omega}_2^2) \ , \qquad (4.1)$$

where $\vec{x}$ is two dimensional, y will be the D3 coordinate not shared by our D5, we have split the transverse six plane into two three planes each with a radial

coordinate ρ, L and a two sphere, $R^4 = 4\pi g_s N \alpha'^2$ and

$$g_t := \frac{(w^4 - w_H^4)^2}{2w^4(w^4 + w_H^4)} , \qquad g_x := \frac{w^4 + w_H^4}{2w^4} . \tag{4.2}$$

The temperature of the theory is given by the position of the horizon, $w_H = \pi R^2 T$.

We include our 2+1d defect with fundamental matter fields by placing a probe D5 brane in the D3 geometry. The probe limit corresponds to the quenched limit of the gauge theory. The D5 probe can be described by its DBI action

$$S_{DBI} = -T_{D5} \int d^6\xi \sqrt{-\det(P[G]_{ab} + 2\pi\alpha' F_{ab})} , \tag{4.3}$$

where $P[G]_{ab}$ is the pullback of the metric and F_{ab} is the gauge field living on the D5 worldvolume. We will use F_{ab} to introduce a constant magnetic field (e.g. $F_{12} = -F_{21} = B$) [38] and a chemical potential associated with baryon number $A_t(\rho) \neq 0$ [52, 68, 69, 90] We embed the D5 brane in the $t, \vec{x}, \rho$ and Ω_2 directions of the metric but to allow all possible embeddings must include a profile $L(\rho)$ at constant $y, \bar{\Omega}_2$. The full DBI action we will consider is then

$$S = \int d\xi^6 \mathcal{L}(\rho) = \left(\int_{S^2} \epsilon_2 \int dt d\vec{x} \right) \int d\rho \; \mathcal{L}(\rho) , \tag{4.4}$$

where ϵ_2 is a volume element on the 2-sphere and

$$\begin{aligned} \mathcal{L} \;\; := \;\; & -N_f T_{D5} \frac{\rho^2}{2\sqrt{2}} \left(1 - \frac{w_H^4}{w^4}\right) \times \sqrt{\left(1 + (\partial_\rho L)^2 - \frac{2w^4(w^4 + w_H^4)}{(w^4 - w_H^4)^2} (2\pi\alpha' \partial_\rho A_t)^2\right)} \\ & \times \sqrt{\left(\left(1 + \frac{w_H^4}{w^4}\right) + \frac{4R^4}{w^4 + w_H^4} B^2\right)} . \end{aligned} \tag{4.5}$$

Since the action depends on $\partial_\rho A_t$ and not on A_t, there is a conserved quantity d $\left(:= \frac{\delta S}{\delta F_{\rho t}}\right)$ and we can use the Legendre transformed action

$$\widetilde{S} = S - \int d\xi^6 F_{\rho t} \frac{\delta S}{\delta F_{\rho t}} = \left(\int_{S^2} \epsilon_2 \int dt d\vec{x} \right) \int d\rho \; \widetilde{\mathcal{L}}(\rho) , \tag{4.6}$$

where

$$\widetilde{\mathcal{L}} := -N_f T_{D5} \frac{(w^4 - w_H^4)}{2\sqrt{2}w^4} \sqrt{K(1 + (\partial_\rho L)^2)} \tag{4.7}$$

$$K := \left(\frac{w^4 + w_H^4}{w^4}\right)\rho^4 + \frac{4R^4B^2}{w^4 + w_H^4}\rho^4 + \frac{4w^4}{(w^4 + w_H^4)}\frac{d^2}{(N_f T_{D5} 2\pi\alpha')^2} \ . \tag{4.8}$$

To simplify the analysis we note that we can use the magnetic field value as the intrinsic scale of conformal symmetry breaking in the theory as in chapter 3 — that is we can rescale all quantities in (4.7) by B to give

$$\widetilde{\mathcal{L}} = -N_f T_{D3} (R\sqrt{B})^3 \ \frac{\widetilde{w}^4 - \widetilde{w}_H^4}{\widetilde{w}^4} \sqrt{\widetilde{K}(1 + \widetilde{L}'^2)} \ , \tag{4.9}$$

$$\widetilde{K} = \left(\frac{\widetilde{w}^4 + \widetilde{w}_H^4}{\widetilde{w}^4}\right)\widetilde{\rho}^4 + \frac{1}{\widetilde{w}^4 + \widetilde{w}_H^4}\widetilde{\rho}^4 + \frac{\widetilde{w}^4}{(\widetilde{w}^4 + \widetilde{w}_H^4)}\widetilde{d}^2 \ , \tag{4.10}$$

where the dimensionless variables are defined as

$$(\widetilde{w}, \widetilde{L}, \widetilde{\rho}, \widetilde{d}) := \left(\frac{w}{R\sqrt{2B}}, \frac{L}{R\sqrt{2B}}, \frac{\rho}{R\sqrt{2B}}, \frac{d}{(R\sqrt{B})^2 N_f T_{D5} 2\pi\alpha'}\right) \ . \tag{4.11}$$

In all cases the embeddings become flat at large ρ taking the form

$$\widetilde{L}(\widetilde{\rho}) \sim \widetilde{m} + \frac{\widetilde{c}}{\widetilde{\rho}} \ , \tag{4.12}$$

In the absence of temperature, magnetic field and density the regular embeddings are simply $L(\widetilde{\rho}) = \widetilde{m}$, which is the minimum length of a D3-D5 string, allowing us to identify it with the quark mass as shown in section 1.4.7. $\tilde{c}$ should then be identified with the quark condensate.

We will classify the D5 brane embeddings by their small $\widetilde{\rho}$ behaviour. If the D5 brane touches the black hole horizon, we call it a black hole embedding, otherwise, we call it a Minkowski embedding as in chapter 3. We have used Mathematica to solve the equations of motion for the D5 embeddings resulting from (4.9). Typically, we numerically shoot out from the black hole horizon (for black hole embeddings) or the $\widetilde{\rho} = 0$ axis (for Minkowski embeddings) with Neumann boundary condition for a given $\widetilde{d}$. Then by fitting the embedding function with

(4.12) at large $\widetilde{\rho}$ we can read off $\widetilde{m}$ and $\widetilde{c}$.

Hamilton's equations from (4.6) are $\partial_\rho d = \frac{\delta \widetilde{S}}{\delta A_t}$ and $\partial_\rho A_t = -\frac{\delta \widetilde{S}}{\delta d}$. The first simply means that d is the conserved quantity. The second reads as

$$\partial_{\widetilde{\rho}} \widetilde{A}_t = \widetilde{d}\, \frac{\widetilde{w}^4 - \widetilde{w}_H^4}{\widetilde{w}^4 + \widetilde{w}_H^4} \sqrt{\frac{1 + (\widetilde{L}')^2}{\widetilde{K}}}\ , \tag{4.13}$$

where $\widetilde{A}_t := \frac{\sqrt{2} 2\pi\alpha' A_t}{R\sqrt{2B}}$.

There is a trivial solution of (4.13) with $\widetilde{d} = 0$ and constant $\widetilde{A}_t$ [53]. The embeddings are then the same as those at zero chemical potential. For a finite $\widetilde{d}$ there exist black hole embeddings as in chapter 3. For such an embedding the chemical potential($\widetilde{\mu}$) is defined as

$$\begin{aligned} \widetilde{\mu} &:= \lim_{\widetilde{\rho}\to\infty} \widetilde{A}_t(\widetilde{\rho}) \\ &= \int_{\widetilde{\rho}_H}^{\infty} d\widetilde{\rho}\ \widetilde{d}\ \frac{\widetilde{w}^4 - \widetilde{w}_H^4}{\widetilde{w}^4 + \widetilde{w}_H^4} \frac{\sqrt{1 + (\widetilde{L}')^2}}{\sqrt{\widetilde{K}}}\ , \end{aligned} \tag{4.14}$$

where we fixed $\widetilde{A}_t(\widetilde{\rho}_H) = 0$ for a well defined A_t at the black hole horizon.

The generic analysis below with massless quarks and B, T and μ all switched on involves four types of solution of the Euler-Lagrange equations. All of these approach the $\tilde{\rho}$ axis at large $\tilde{\rho}$ to give a zero quark mass. Firstly, there are Minkowski embeddings that avoid the black hole so have a non-zero condensate $\widetilde{c}$ — these solutions have $\tilde{d} = 0$ so $\tilde{A}_t = \mu$. Secondly, there can be generic black hole solutions with both of $\widetilde{c}$ and $\widetilde{d}$ non-zero. Finally there are solutions that lie entirely along the $\tilde{\rho}$ axis so that $\widetilde{c} = 0$ but with $\widetilde{d}$ either zero or non zero. In fact the flat embeddings with $\widetilde{d} = 0$ are always the energetically least preferred but the other three all play a part in the phase diagram of the theory.

To compare these solutions we compute the relevant thermodynamic potentials. The Euclideanised on-shell bulk action can be interpreted as the thermodynamic potential of the boundary field theory. The grand potential ($\widetilde{\Omega}$) is associated with the action (4.5) while the Helmholtz free energy ($\widetilde{F}$) is associated with the Legendre

transformed action (4.6):

$$\begin{aligned}
\widetilde{F}(\widetilde{w}_H,\widetilde{d}) &:= \frac{-\widetilde{S}}{N_f T_{D5}(R\sqrt{B})^3\mathrm{Vol}} \\
&= \int_{\widetilde{\rho}_H}^{\infty} d\widetilde{\rho}\ \frac{\widetilde{w}^4-\widetilde{w}_H^4}{\widetilde{w}^4}\sqrt{(1+(\widetilde{L}')^2)}\sqrt{\widetilde{K}} \qquad (4.15)\\
\widetilde{\Omega}(\widetilde{w}_H,\widetilde{\mu}) &:= \frac{-S}{N_f T_{D5}(R\sqrt{B})^3\mathrm{Vol}} \\
&= \int_{\widetilde{\rho}_H}^{\infty} d\widetilde{\rho}\ \frac{\widetilde{w}^4-\widetilde{w}_H^4}{\widetilde{w}^4}\sqrt{(1+(\widetilde{L}')^2)}\frac{\widetilde{K}(\widetilde{d}=0)}{\sqrt{\widetilde{K}}} \qquad (4.16)
\end{aligned}$$

where Vol denote the trivial five dimensional volume integral except $\widetilde{\rho}$ space, so the thermodynamic potentials defined above are densities, strictly speaking. Since $\widetilde{K}\sim\widetilde{\rho}^4$, both integrals diverge as $\widetilde{\rho}^2$ at infinity and need to be renormalised with the procedure used in chapter 3.

4.2 Chiral Symmetry Restoration by Temperature

The chiral symmetry restoration transition by temperature is first order [67] (a transition related to the thermal transition for non-zero mass at $B=0$ [35, 70, 71, 72, 41]). The transition on the gravity side is between a Minkowski embedding that avoids the black hole to an embedding that lies along the $\tilde{\rho}$ axis ending on the black hole. Figure 4.2 shows the $(-\widetilde{c},\widetilde{m})$ diagram for some temperatures ($\widetilde{w}_H=0.25, 0.3435, 0.45$ from the bottom). The solid lines are the black hole embeddings and the dotted lines are Minkowski embeddings. Since we are interested in the case $\widetilde{m}=0$, the condensate is the intersection of the curves with the vertical axis. As temperature goes up the condensate moves from the lower dot to the middle curve continuously, then jumps at $\widetilde{w}_H=0.3435$ to the origin (zero condensate), which corresponds to the chiral symmetric phase. It is also the transition from a Minkowski (dotted line) to a black hole embedding (solid line). This jump can be seen by a Maxwell construction: $\widetilde{m}$ and $\widetilde{c}$ are conjugate variables and the two areas between the middle curve and the axis are equal at the transition point. See [67] for more details.

This transition as well as restoring chiral symmetry also corresponds to the melting

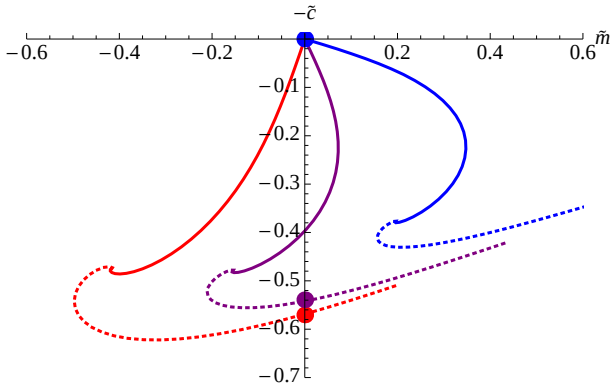

Figure 4.2: *A plot of the condensate vs. the quark mass to show the first order phase transition at zero chemical potential induced by temperature. The solid line corresponds to the black hole embedding and the dotted line to a Minkowski embedding. From bottom to top the curves correspond to temperatures* $\widetilde{w}_H = 0.25, 0.3435, 0.45$.

of bound states of the defect quarks since the Minkowski embedding has stable linearised mesonic fluctuation whilst the black hole embedding has a quasi-normal mode spectrum [59, 58, 60, 61].

4.3 Chiral Symmetry Restoration by Density

At zero temperature we find two phase transitions with increasing chemical potential. At low chemical potentials the preferred embedding is a Minkowski embedding with $\tilde{A}_t = \mu$ so there is no quark density. There is then a transition to a black hole embedding with non-zero quark density, $\widetilde{d}$. This transition, whilst appearing first-order in terms of the brane embeddings, displays second-order behaviour in all field-theory quantities such as the condensate or density (which grows smoothly from zero). The transition also corresponds to the onset of bound state melting since the black hole embedding has quasi-normal modes rather than stable fluctuations.

The chiral symmetry transition induced by density at zero temperature is distinct and also a continuous transition. It has been shown to be of the BKT type for this D3/D5 case [85] as opposed to a mean-field type second order transition as seen in the D3/D7 case [91] and chapter 3.

The chiral symmetric phase corresponds to the trivial embedding, $L = 0$. Chiral

symmetry breaking is signalled by the instability of small fluctuations around the $L = 0$ embedding. The free energy (4.15) with (4.10) at zero T reads

$$\widetilde{F} \sim \sqrt{1+\widetilde{L}'^2}\sqrt{\widetilde{\rho}^4+\frac{\widetilde{\rho}^4}{\widetilde{w}^4}+\widetilde{d}^2}\,, \tag{4.17}$$

which can be expanded up to the quadratic order in $\widetilde{L}$ as

$$\widetilde{F} \sim -\frac{1}{2}\sqrt{1+\widetilde{\rho}^4+\widetilde{d}^2}\widetilde{L}'^2+\frac{\widetilde{L}^2}{\widetilde{\rho}^2\sqrt{1+\widetilde{\rho}^4+\widetilde{d}^2}} \tag{4.18}$$

At $\widetilde{\rho} \gg 1$, $\frac{\widetilde{L}}{\widetilde{\rho}}$ behaves as a scalar with $m^2 = -2$ in AdS_4, while at small $\widetilde{\rho} \ll 1$ and $\widetilde{\rho} \ll \widetilde{d}$ it behaves as a scalar with $m^2 = -\frac{2}{1+\widetilde{d}^2}$ in AdS_2. The Breitenlohner-Freedman (BF) bound of AdS_2 is $-\frac{1}{4}$, so below $\widetilde{d}_c = \sqrt{7}$ the BF bound is violated and the embedding $\widetilde{L} = 0$ is unstable [85]. This critical density corresponds to the critical chemical potential $\widetilde{\mu} \sim 2.9$ as can be computed from (4.14). In [85] it was shown that the condensate scales near this transition as

$$-\widetilde{c} \sim -e^{-\pi\sqrt{\frac{1+\widetilde{d}^2}{\widetilde{d}_c^2-\widetilde{d}^2}}}\,, \tag{4.19}$$

which corresponds to BKT scaling [86, 87]. This transition is an example of the analysis in [88] where it was shown that if a scalar mass in a holographic model could be tuned through the BF bound a BKT transition would be seen at the critical point.

4.4 Phase Diagram in μ-T Plane

To compute the full phase diagram we work on a series of constant-T slices. We have found the four relevant embeddings discussed above and found those that minimise the relevant thermodynamic potential. For more details of the method and relevant analysis we refer to the calculations and analysis in chapter 3. Figure 4.3 shows some example plots of the dependence of the condensate on the chemical potential on fixed T slices. It shows that the Minkowski embedding with $\widetilde{d} = 0$ is preferred at low $\tilde{\mu}$, a black hole embedding with growing $\widetilde{d}$ at intermediate $\tilde{\mu}$, before

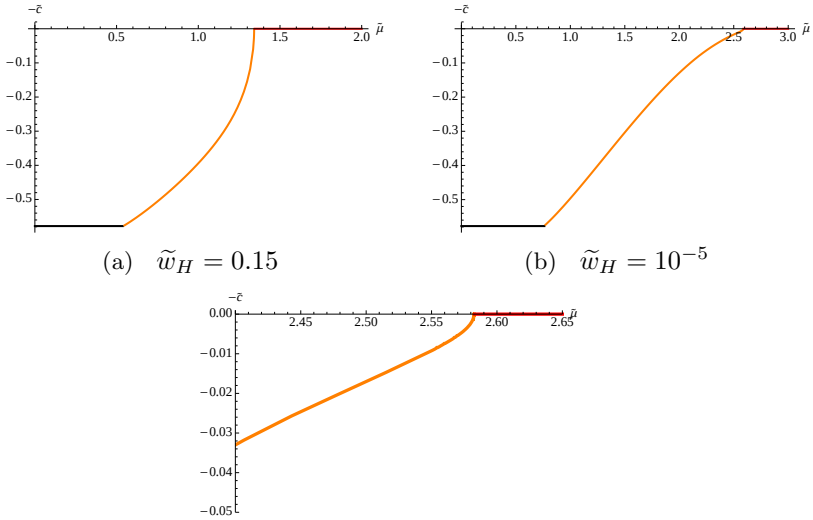

(a) $\widetilde{w}_H = 0.15$

(b) $\widetilde{w}_H = 10^{-5}$

(c) $\widetilde{w}_H = 10^{-5}$ near the critical point

Figure 4.3: *Plots of the condensate vs. chemical potential on fixed temperature slices, showing the phase structure of the theory. The black lines correspond to the Minkowski embedding, the orange lines to chiral symmetry breaking black hole embeddings and the red lines to the flat embedding along the $\widetilde{\rho}$ axis. Figure (b) and (c) show that at low temperature the BKT transition becomes second order.*

finally a transition to a flat embedding occurs at high chemical potential.

Qualitatively the phase diagram, shown in figure 4.1, is almost the same as the D3/D7 case - the two second order transitions at zero temperature converge at two critical points to form the first order transition identified at zero density. The only difference is induced by the chiral phase transition at zero T. Comparing to the D3/D7 case we see there is a long tail near zero T, the end point of which corresponds to the BKT transition. However even infinitesimal temperature turns it into a mean-field type second order transition[85, 89]. In figure 4.3(b),(c) we plot the condensate against μ at a very low temperature ($\widetilde{w}_H = 10^{-5}$) to show the second-order nature.

Chapter 5

E, B, μ, T Phase Structure of the D3/D7 Holographic Dual

In chapter 3 we computed the phase diagram for large N $\mathcal{N}$=4 SYM with quenched $\mathcal{N}$=2 massless quarks in a magnetic field, in the temperature-chemical potential plane (T-μ plane) which we show in figure 5.1(a). It has considerable structure. Whilst the magnetic field favours chiral symmetry breaking, the temperature and chemical potential favour the chirally symmetric phase.

In this chapter we wish to study how robust the phase structure is to changes of parameters. In particular we will introduce the additional parameter of an electric field (E) parallel to the magnetic field. Note this case is simpler than when the E and B fields are perpendicular because no Hall current forms. We do allow for the induced current in the direction of the electric field. The effect on the theory of an electric field has been studied previously for probe branes in [92, 93, 64, 94, 95, 96, 97]. Although the electric field continuously acts on the quarks an equilibrium configuration is nevertheless reached where energy is being dissipated to the bulk $\mathcal{N} = 4$ plasma. The quarks and anti-quarks have opposite charge when interacting with the electric field so the field tends to loosen the binding in mesonic bound states and, if it is strong enough, to dissociate the mesons. With an electric field present in the theory a *singular shell* develops in the gravity description. If the D7 brane passes through this shell its action becomes

imaginary and in order to keep the action real one must turn on the appropriate electric current J. The singular shell plays the role of an effective horizon for worldvolume meson fluctuations [98]. If the probe brane touches the singular shell, one expects that fluctuations of the brane at that point must be in-falling and the spectrum will resemble a quasi-normal mode spectrum describing mesons that have a complex mass. In other words, the electric field has acted to dissociate the meson in a similar fashion to how temperature melts the mesons [58, 59].

The field theory phase structure is determined holographically by comparison of the classical bulk field configurations. In this chapter, we introduce three bulk fields $L(\rho)$ (embedding scalar), $A_t(\rho)$ (gauge field), and $A_z(\rho)$ (gauge field) in the D7 brane worldvolume with given background parameters (E, B, T). By fixing the asymptotic values of fields in the UV (large ρ) with $L \to m$ (quark mass), $A_t \to \mu$ (chemical potential), $A_z \to t\frac{E}{2\pi\alpha'}$, we look for the sub-leading behaviours of fields at large ρ: c (condensate), d (density), and J (current), which are determined by the bulk DBI dynamics. Therefore, our problem is classifying the phases by three quantities (c, d, J) in the five-dimensional space (T, B, E, m, μ). It turns out that, because of a scaling symmetry, we can scale all variables by B, which reduces our phase space to four dimensions. Since we are interested in spontaneous chiral symmetry breaking, we will choose $m = 0$. Our phase space becomes three-dimensional (T, μ, E) and we will classify this space by 8 possible states consisting of the three order parameters (c, d, J) being 'on or off'. Among them, only in the $c \neq 0, d = J = 0$ phase are stable mesons allowed[3]. T, μ, E tend to turn off c $(c = 0)$ and turn on d, J $(d, J \neq 0)$, and so oppose B. Due to these competitions between E, T, μ and B a rich phase structure is constructed.

One of our main results here is that three phases (corresponding to three embedding types) are also present in the T, E plane as we summarise in figure 5.1(b). With a large (small) electric field, the theory becomes a conductor (insulator) and is in a

[3]We should caution that when studying phase diagrams one is always limited by the states allowed in the analysis. We do not study the effects of the parameters on the squark potential, for example, which is likely unstable in the presence of a chemical potential [70]. The electric field could also potentially generate phenomena beyond chiral symmetry restoration, density creation, current induction, and meson melting but our results should stand as a starting point for exploring such extra phases, should they exist.

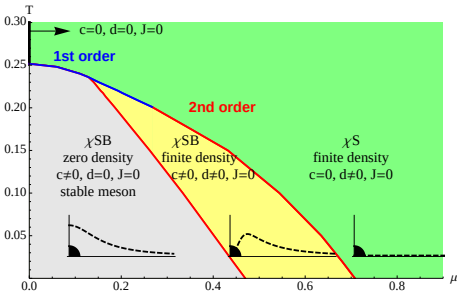

(a) T-μ phase diagram. The inset diagrams are representative probe brane embeddings (dotted lines), where a black disk represents a black hole.

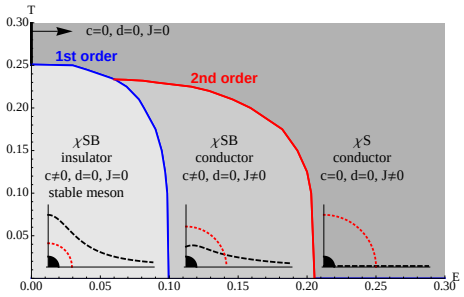

(b) T-E phase diagram. The inset diagrams are representative probe brane embeddings (dotted lines), where a red arc represents a singular shell.

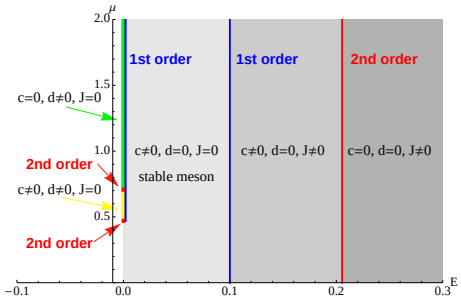

(c) μ-E phase diagram. The $\mu(E)$ axis agrees with the $\mu(E)$ axis of figure 5.1(a) and phases in 5.1(b) are shown by the same colour. Thus embeddings are the same as 5.1(a) and 5.1(b) without the black hole.

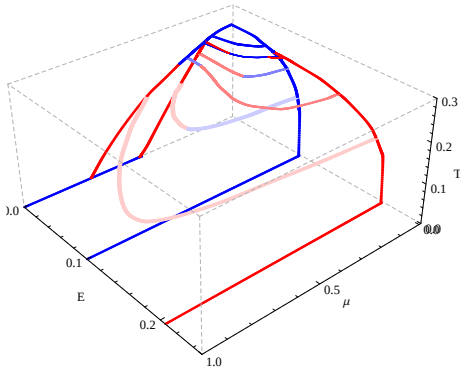

(d) E-μ-T phase diagram. The curves show the phase boundaries at fixed T ($T = 0$, 0.15, 0.21, 0.232, 0.24 from the bottom). See figure 5.6 for more detail.

Figure 5.1: *The phase diagrams of the massless $\mathcal{N} = 2$ gauge theory with a magnetic field. First order transitions are shown in blue, second order transitions in red. The temperature is controlled by the parameter T, chemical potential by μ and electric field by E.*

chirally symmetric χS phase (a χSB phase in which chiral symmetry is broken). At an intermediate electric field strength, the system is a chiral symmetry broken conductor. Note that the orders of the phase transitions and the positions and presence of the critical points vary relative to the T, μ case (figure 5.1(a)).

Interestingly, the μ-E phase diagram (figure 5.1(c)) shows a very different structure from the T-μ or the T-E phase diagram. At zero temperature and finite E and B field, the contribution to the action from the density is cancelled by the contribution from the induced current, which is a function of density. Consequently the free energy of the system is independent of density, which was pointed out in [64] in the zero B field case. Thus the system is essentially a zero density system

and the phase diagram is independent of the chemical potential. At first this may seem at odds with figure 5.1(a) since the μ axis has structure present. In fact there is a first order transition at $T = 0$ between the μ axis and the rest of the E, μ plane. There are two limits approaching the μ axis: (1) $E = 0$ and then $T \to 0$ (2) $T = 0$ and then $E \to 0$. These two limits are different and only the former is a continuous limit to the μ axis.

Indeed by computing the phase structure through the entire T, μ, E volume (e.g. computing the μ-E diagram at various fixed T) we show the smooth evolution through that volume connecting the three surface planes. There are interesting movements of the critical points and phase boundaries. These results are summarised in figure 5.1(d) which we discuss in much more detail in section 5.4. We also see the development of the first order transition between the E-μ plane and the μ axis as $T \to 0$. Two of the missing states from figures 5.1(a)-5.1(c), $(c \neq 0, d \neq 0, J \neq 0)$ and $(c = 0, d \neq 0, J \neq 0)$ from among the 8 possible states, are found in the 3D bulk of figure 5.1(d).

These models with their varied behaviours in the B, T, μ, E volume can hopefully serve as exemplars, or templates from which to find exemplars, for different phase structures in physical theories.

5.1 The Holographic Description

The $\mathcal{N}$=4 gauge theory at finite temperature has a holographic description in terms of an AdS_5 black hole geometry (with N D3 branes at its core) [26, 28, 29]. The geometry is

$$ds^2 = \frac{r^2}{R^2}(-f dt^2 + d\vec{x}^2) + \frac{R^2}{r^2 f} dr^2 + R^2 d\Omega_5^2 \ , \tag{5.1}$$

where $R^4 = 4\pi g_s N \alpha'^2$ and

$$f := 1 - \frac{r_H^4}{r^4} \ , \qquad r_H := \pi R^2 T_{\rm FT} \ . \tag{5.2}$$

Here r_H is the position of the black hole horizon which is linearly related to the dual field theory temperature $T_{\rm FT}$. We will find it useful to make the coordinate transformation

$$\frac{dr^2}{r^2 f} \equiv \frac{dw^2}{w^2} \implies \sqrt{2}w = \sqrt{r^2 + \sqrt{r^4 - r_H^4}} \ , \tag{5.3}$$

with $\sqrt{2}w_H = r_H$. Note that this is a slightly different coordinate transformation to that done in chapter 3. Comparing equations from this chapter to ones in chapter 3 will give differing factors of 2 in some of the equations. This change makes the presence of a flat 6-plane perpendicular to the horizon manifest. We will then write the coordinates in that plane as ρ and L according to

$$w = \sqrt{\rho^2 + L^2} \ , \quad \rho := w \sin\theta \ , \quad L := w\cos\theta \ , \tag{5.4}$$

The metric is then

$$ds^2 = \frac{w^2}{R^2}(-g_t dt^2 + g_x d\vec{x}^2) + \frac{R^2}{w^2}(d\rho^2 + \rho^2 d\Omega_3^2 + dL^2 + L^2 d\Omega_1^2) \ , \tag{5.5}$$

where

$$g_t = \frac{(w^4 - w_H^4)^2}{w^4(w^4 + w_H^4)} \ , \qquad g_x = \frac{w^4 + w_H^4}{w^4} \ . \tag{5.6}$$

Quenched ($N_f \ll N$) $\mathcal{N}$=2 quark superfields can be included in the $\mathcal{N}$=4 gauge theory through probe D7 branes in the geometry. The D7 probe can be described by its DBI action

$$S_{DBI} = -T_{D7}\int d^8\xi \sqrt{-\det(P[G]_{ab} + 2\pi\alpha' F_{ab})} \ , \tag{5.7}$$

where $P[G]_{ab}$ is the pullback of the metric and F_{ab} is the gauge field living on the D7 worldvolume. We will use F_{ab} to introduce a constant magnetic field (e.g. $F_{12} = -F_{21} = B/(2\pi\alpha')$), a chemical potential associated with baryon number $A_t(\rho) \neq 0$ and our crucial extra ingredient here is an electric field parallel to the magnetic field ($F_{03} = -F_{30} = E/(2\pi\alpha')$)[92, 93, 64, 94]. We will also allow for the

possibility that the electric field induces a current in the z direction by including A_z.

We embed the D7 brane in the t, $\vec{x}$, ρ and Ω_3 directions of the metric but to allow all possible embeddings must include a profile $L(\rho)$ at constant Ω_1. The full DBI action we will consider is then

$$S = \int d\xi^8 \mathcal{L}(\rho) = \left(\int_{S^3} \epsilon_3 \int dt d\vec{x}\right) \int d\rho \; \mathcal{L}(\rho) \; , \tag{5.8}$$

where ϵ_3 is a volume form on the 3-sphere. Here

$$\begin{aligned} \mathcal{L} = &-\mathcal{N}\rho^3 \left(1 - \frac{w_H^4}{w^4}\right) \sqrt{\left(\left(1 + \frac{w_H^4}{w^4}\right)^2 + \frac{R^4}{w^4} B^2\right)} \\ &\times \sqrt{\left(1 - \frac{E^2 R^4 w^4}{(w^4 - w_H^4)^2}\right)(1 + L'^2) - \frac{w^4(w^4 + w_H^4)}{(w^4 - w_H^4)^2}(2\pi\alpha' A_t')^2 + \frac{w^4 (2\pi\alpha' A_z')^2}{w^4 + w_H^4}} \; , \end{aligned} \tag{5.9}$$

and $\mathcal{N} = N_f T_{D7}$. Here A_t' denotes the derivative of A_t with respect to ρ. At large ρ, for fixed E and B, the fields behave as

$$L \sim m + \frac{c}{\rho^2} + ..., \qquad A_t \sim \mu + \frac{d}{\rho^2} + ..., \qquad A_z \sim t\frac{E}{2\pi\alpha'} + \frac{J}{\rho^2} \; , \tag{5.10}$$

where m is proportional to the quark mass, c the quark condensate, μ the chemical potential, d the quark density and J the current. For more physical identifications we refer to [55, 52, 56, 53, 92]. Since the action is independent of A_t and A_z, there are conserved quantities $d \left(:= \frac{\delta S}{\delta F_{\rho t}}\right)$ and $J \left(:= \frac{\delta S}{\delta F_{\rho z}}\right)$. These relations can be inverted to express A_t' and A_z' in terms of d and J as

$$\begin{aligned} &2\pi\alpha' A_t' = \frac{d}{2\pi\alpha'\mathcal{N}} \frac{w^4 - w_H^4}{w^4 + w_H^4} Q \; , \qquad 2\pi\alpha' A_z' = \frac{J}{2\pi\alpha'\mathcal{N}} \frac{w^4 + w_H^4}{w^4 - w_H^4} Q \; , \\ &Q = \sqrt{\frac{\left(1 - E^2 R^4 \frac{w^4}{(w^4 - w_H^4)^2}\right)(1 + L'^2)}{\left(\frac{d}{2\pi\alpha'\mathcal{N}}\right)^2 \frac{w^4}{(w^4 + w_H^4)} - \left(\frac{J}{2\pi\alpha'\mathcal{N}}\right)^2 \frac{w^4(w^4 + w_H^4)}{(w^4 - w_H^4)^2} + \left(\frac{B^2 R^4}{w^4} + \left(1 + \frac{w_H^4}{w^4}\right)^2\right)\rho^6}} \; . \end{aligned} \tag{5.11}$$

This is used to express the Legendre transformed action in terms of d and J:

$$\begin{aligned} S_{LT} &= S - \int d\xi^8 F_{\rho t}\frac{\delta S}{\delta F_{\rho t}} - \int d\xi^8 F_{\rho z}\frac{\delta S}{\delta F_{\rho z}} \\ &= \left(\int_{S^3}\epsilon_3 \int dt d\vec{x}\right)\int d\rho\ \mathcal{L}_{LT}(\rho)\ , \end{aligned} \tag{5.12}$$

where

$$\mathcal{L}_{LT} = -\mathcal{N}\frac{(w^4-w_H^4)}{w^4}\sqrt{K(1+L'^2)}\ , \tag{5.13}$$

$$\begin{aligned} K &= \left(1-\frac{E^2R^4w^4}{(w^4-w_H^4)^2}\right)\left[\left(\frac{w^4+w_H^4}{w^4}\right)^2\rho^6 + \frac{R^4B^2}{w^4}\rho^6\right. \\ &\left. + \frac{w^4}{(w^4+w_H^4)}\frac{d^2}{(N_fT_{D7}2\pi\alpha')^2} - \frac{w^4(w^4+w_H^4)}{(w^4-w_H^4)^2}\frac{J^2}{(N_fT_{D7}2\pi\alpha')^2}\right]. \end{aligned} \tag{5.14}$$

Note that the first factor of K changes sign at w_s,

$$w_s = \sqrt{\frac{ER^2}{2} + \frac{\sqrt{E^2R^4+4w_H^4}}{2}}\ , \tag{5.15}$$

which defines a *singular shell* with a radius w_s. At zero temperature ($w_H = 0$) the singular shell forms at $\sqrt{E}R$, and at zero E it disappears. Note that the singular shell does not depend on density. In order to make the action regular, the second term of K should change sign at the singular shell. This condition determines the current J and conductivity σ by Ohm's law:

$$\begin{aligned} &J = \sigma E\ , \\ &\sigma = \mathcal{N}(2\pi\alpha')R^2\sqrt{\frac{w_s^4}{(w_s^4+w_H^4)^2}\frac{d^2}{N^2(2\pi\alpha')^2} + \left[\frac{R^4B^2}{w_s^4(w_s^4+w_H^4)} + \frac{(w_s^4+w_H^4)}{w_s^8}\right]\rho_s^6}\ , \end{aligned} \tag{5.16}$$

where ρ_s is the ρ coordinate where an embedding touches the singular shell. This is still a function of quark mass m after all other parameters are fixed. In spite of the way we write (5.16) the current is non-linear in E since w_s and ρ_s are functions of E. σ has two contributions. The first term is from net charge carrier density, d, and the second term is from pair-produced virtual charges. Interestingly, the conductivity from pair-produced charges is enhanced by B. The more general

conductivity for arbitrarily angled constant E and B was obtained in [93, 97] in a different coordinate system[4]. By plugging (5.16) into (5.13) and rescaling we have a dimensionless Lagrangian $\widetilde{\mathcal{L}}_{LT}$:

$$\widetilde{\mathcal{L}}_{LT} = -\frac{\mathcal{L}_{LT}}{R^4 B^2 \mathcal{N}} = \frac{(w^4 - T^4)}{w^4}\sqrt{\widetilde{K}(1+L'^2)}\ , \tag{5.17}$$

$$\begin{aligned}\widetilde{K} = &\left(1 - \frac{E^2 w^4}{(w^4-T^4)^2}\right)\left[\left(\frac{w^4+T^4}{w^4}\right)^2 \rho^6 + \frac{1}{w^4}\rho^6 + d^2\frac{w^4}{(w^4+T^4)}\right.\\ &\left. -E^2\frac{w^4(w^4+T^4)(w_s^4+(w_s^4+T^4)^2)}{(w^4-T^4)^2(w_s^4+T^4)w_s^8}\rho_s^6 - d^2E^2\frac{w^4(w^4+T^4)w_s^4}{(w^4-T^4)^2(T^4+w_s^4)^2}\right]\ ,\end{aligned} \tag{5.18}$$

where we rescaled

$$(\omega, L, \rho) \to R\sqrt{B}\ (\omega, L, \rho)\ , \quad (d, J) \to (R\sqrt{B})^3 \mathcal{N} 2\pi\alpha'\ (d, J)\ , \quad E \to BE\ , \tag{5.19}$$

and define $T \equiv w_H$ for notational clarity. The Lagrangian $\widetilde{\mathcal{L}}_{LT}$ will be our starting point for the numerical analysis in the following sections.

The chemical potential is obtained by integrating A_t' (5.11) from the horizon to the boundary

$$\mu = \int_{\rho_H}^{\infty} d\rho\, d\frac{w^4 - T^4}{w^4 + T^4}\sqrt{\frac{\left(1 - E^2\frac{w^4}{(w^4-T^4)^2}\right)(1+L'^2)}{d^2\frac{w^4}{(w^4+T^4)} - J^2\frac{w^4(w^4+T^4)}{(w^4-T^4)^2} + \left(\frac{1}{w^4} + \left(1+\frac{T^4}{w^4}\right)^2\right)\rho^6}}\ , \tag{5.20}$$

where $A_t(\rho_H) = 0$.

In the following sections we will present our results on various aspects of the phase structure of this theory. Until the final section of this chapter we will concentrate on the case of massless quarks where the $U(1)$ symmetry in the $d\Omega_1$ direction is a good UV symmetry of the theory. Also here and below we will express all our dimensionful parameters in units of the magnetic field B to the appropriate power (see (5.19)) — in other words we will use the magnetic field as the intrinsic scale in the theory.

[4]The conductivity of other models have been obtained by the same method. See for example [99, 100] and references therein.

5.2 B, T, E Phase Diagram

The rich structure of the B, μ, T phase diagram (figure 5.1(a)) leads one to ask how generic it is. The main goal of this chapter is to introduce an additional parameter that favours chiral symmetry preservation to see how sensitive the phase diagram is to a change of parameter. We will use electric field (E) as that new parameter.

5.2.1 B, E at Zero Temperature

As a first example let us consider the system with E and B but no T or μ. The Legendre transformed Lagrangian is

$$\widetilde{\mathcal{L}}_{LT} = \sqrt{(1+L'^2)}\sqrt{\left(1-\frac{E^2}{w^4}\right)\left[\rho^6+\frac{\rho^6}{w^4}-J^2\right]}\ . \tag{5.21}$$

As has been discussed in (5.15) and (5.16), there is a singular shell at $w_s = \sqrt{E}$ and the current is given by

$$J = E\frac{\sqrt{1+w_s^4}\rho_s^3}{w_s^4} = \sqrt{(1+E^2)E\cos^6\theta_s}\ . \tag{5.22}$$

One can therefore find the embeddings that end on the singular shell by shooting out (in) from the singular shell with J determined by the point on the shell one is shooting from. We then seek amongst such solutions for those that satisfy $L \to 0$ ($m \to 0$) as $\rho \to \infty$ to find the massless (mass m) embeddings. Generically we again find three types of solutions: (1) embeddings that curve off axis and reach $\rho = 0$ missing the singular shell (when $E \ll B$); (2) embeddings that curve off axis and pass through the singular shell (when $E \sim B$); (3) the flat embedding $L = 0$. The schematic plots of these three cases are shown in the inset of figure 5.1(b), where the black disk should be ignored at zero T. In figure 5.2(a) we show some sample numerical embeddings ending on (2) and off (1) the singular shell.

All non-flat embeddings that pass through the singular shell have a conical singularity at $\rho = 0$, whose precise interpretation is unclear and discussed in [64, 94]. The conical singularity is most likely a reflection of the energy being

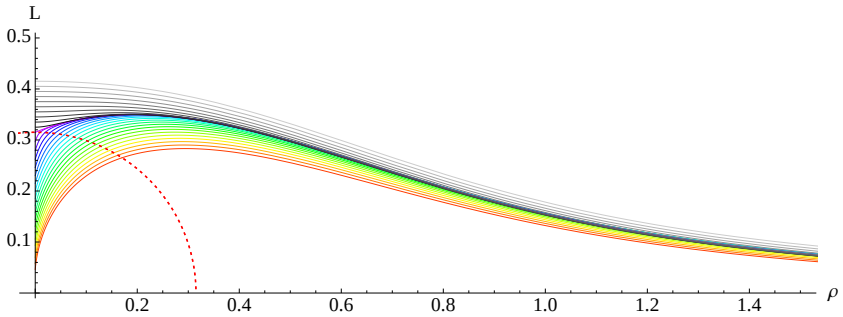

(a) Embeddings ending on and off the singular shell ($E = 0.1, m = 0$).

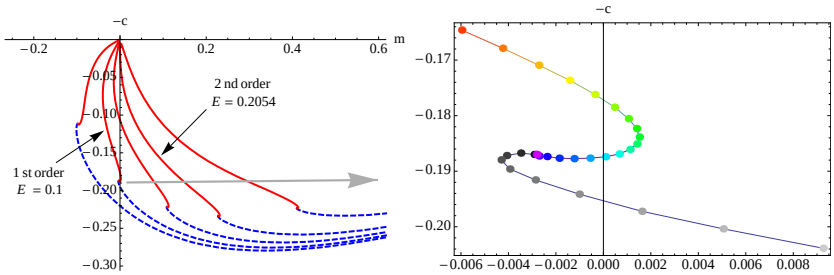

(b) The condensate, c vs. mass, m for given E values. Curves shift to left as E decreases. The red (blue) part corresponds to the embedding touching (missing) the singular shell. The inset on the right is a zoom-in around the first order phase transition. The coloured points correspond to the coloured embeddings in figure 5.2(a).

Figure 5.2: *Embeddings and c-m diagram at finite E parallel to finite B, but no density and temperature.*

injected by the electric field being sunk into the gauge background through stringy physics representing the quark interactions with the $\mathcal{N} = 4$ Yang-Mills fields.

The figure 5.2(b) shows the condensate, c, vs. mass, m, plot for given Es. One point (c,m) in the plot corresponds to one embedding since it gives a complete initial condition for the embedding equation (a second order differential equation). For example, the coloured points in the inset of figure 5.2(b) correspond to the embedding in figure 5.2(a) of the same colour.

From figure 5.2(b) we can determine the phase structure as follows. For a larger E (relative to B), the c-m curves tend to be pushed to the right. So if we focus on $m = 0$ case, the only available point at large E is $(m, c) = (0, 0)$, which corresponds to the flat embedding. The flat embedding preserves the $U(1)$ chiral symmetry, so the system is chiral symmetric (χS). Since the flat embedding necessarily crosses the singular shell, there is no stable meson but there is a current (5.22) with $\theta_s = 0$: $J = \sqrt{(1 + E^2)E}$, which is the maximal current for a given E. i.e. the system is a

conductor.

As E is lowered the c-m curve shifts to the left. At $E \sim 0.2054$ a new solution for $m = 0$ appears, whose c is finite and the ground state corresponds to this new solution. This is a second order transition because the second solution for c at $m = 0$ moves smoothly away from the $c = 0$ embedding. Because of the finite c, the embedding is curved and breaks the $U(1)$ symmetry, so the system is in a chiral symmetry broken (χSB) phase. However the embedding still passes through the singular shell, so it is a conductor with no stable meson.

Finally, around $E \sim 0.1$ the small 'S' shape structure connecting the red part (singular shell touching embedding) and blue part (a singular shell missing Minkowski embedding), meets the $m = 0$ line, which is zoomed in, in the inset of figure 5.2(b). It shows a typical first order phase transition structure and by a Maxwell construction we can pin down the transition point. So as E decreases, the green point should move to the grey point with a discontinuous condensate jump (see the zoomed in inset). The blue part (or the grey points in the inset) corresponds to the Minkowski embedding and the system is a χSB insulator with stable mesons.

One would like to match this picture to a computation of the free energy. Naively it seems one should just compute the original action (before Legendre transforming) evaluated on these solutions. However, there is a subtle point related to the conical singularity[5] of the embedding at $\rho = 0$ and also a log divergence of A_x [92, 95, 97] at the horizon. We cannot cure this behaviour in out theory. A possible way of dealing with this behaviour is to add a boundary term to take care of the singularity at $\rho = 0$ or at the horizon. This boundary term will also contribute to the free energy so must be taken into account. Of course, one should be careful when changing the infra-red region of the model or effective theory, because this is affecting precisely the physics that one is trying to describe. This is in contrast to changes in the UV where one can simply add counterterms in the effective theory to match up with the full theory.

[5]If we consider the finite density system this conical singularity disappears. However another singularity seems to appear for A_t as discussed in section 5.3.

However, this surface term does not change the equation of motion. Furthermore, as far as the embedding dynamics is concerned, the singular shell position has the same singular structure as a black hole horizon and the embedding outside a singular shell is independent of the ones inside the shell. So the c-m plots, based on the classical embedding outside the shell, are valid regardless of the additional boundary terms at the IR boundary.

These solutions correctly show us the maxima and minima of the free energy as a function of E. The discussion above is the only consistent picture with the c-m plots so we can be confident of its validity. For this reason in what follows we will focus on the c-m plots (and also when chemical potential is present we will track the quark density) to determine the phase structure. A similar philosophy was used in [64, 94].

However, it would be interesting to identify the correct boundary term and compute the consistent free energy graph for our c-m plot (we have not been able to so far). To identify it, in principle, one should start with the time-dependent backreacted system, since the singularities are related to time-dependent energy loss of the system and its effect on the background adjoint matters. However one may also be able to introduce an 'effective' boundary term. Our c-m diagram would be a good guide to figure out the correct boundary term and free energy or could even be used as a rule to determine it, since sometimes thermodynamic consistency plays a complementary role in AdS/CFT applications.

5.2.2 B, E at Finite Temperature

We can now extend our analysis to include temperature straightforwardly. From (5.17) with $d = 0$

$$\widetilde{\mathcal{L}}_{LT} = \frac{(w^4 - T^4)}{w^4}\sqrt{\widetilde{K}(1 + L'^2)}, \tag{5.23}$$

$$\widetilde{K} = \left(1 - \frac{E^2 w^4}{(w^4 - T^4)^2}\right)\left[\left(\frac{w^4 + T^4}{w^4}\right)^2 \rho^6 + \frac{1}{w^4}\rho^6 - J^2 \frac{w^4(w^4 + T^4)}{(w^4 - T^4)^2}\right] \tag{5.24}$$

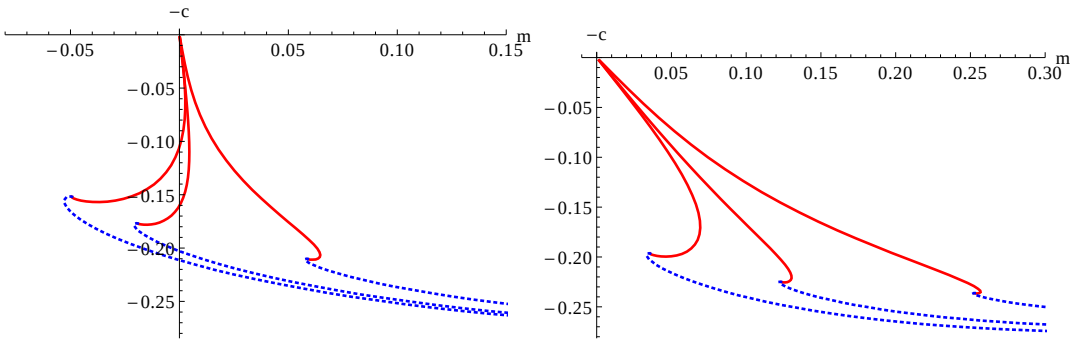

(a) $T = 0.24$. $E = 0.0001, 0.049, 0.1$ from left. (b) $T = 0.30$. $E = 0.0001, 0.100, 0.180$ from left.

Figure 5.3: *c-m diagram at finite E parallel to finite B at finite (high) temperature.*

and

$$w_s = \sqrt{\frac{E}{2} + \frac{\sqrt{E^2 + 4T^4}}{2}}\ , \qquad J = E\sqrt{\frac{w_s^4 + (w_s^4 + T^4)^2}{(w_s^4 + T^4)w_s^8}}\rho_s^3\ . \tag{5.25}$$

It is apparent that even with non-zero T there remains a singular shell - it always lies outside the horizon for any T (5.15). Requiring regularity of the on-shell action allows us to fix the current J (5.16). If the embedding does not touch the singular shell $\rho_s = 0$, then there is no current.

We shoot out to obtain the embeddings as a function of E and T at fixed B. The process is laborious — we plot the evolution of the c-m plot on fixed T trajectories. There are three types of c-m plot. At low temperature, it is similar to figure 5.2(b). At high temperature two qualitatively different structures appear as shown in figure 5.3. As the temperature increases, the T effect dominates the E effect, which is visualised in the c-m diagram as follows. The curve near $(m, c) = (0, 0)$ is curved to the left (figure 5.2(b)) at low T but curved to the right (figure 5.3(a)) at high T, showing competition between E and T. Both are an attractive effect from the embedding dynamic's point of view, but the T-driven first order attraction is so strong that the E-driven second order smooth attractive effect cannot be realised. At very high T the repulsive effect of B is completely suppressed and the only allowed embedding is a flat one (figure 5.3(b)).

The resulting phase diagram is shown in figure 5.1(b). For $T \lesssim 0.233$, three regions, as at zero T, exist: as E increases, the phases change from a χSB insulator (stable

meson) phase to a χSB conductor at a first order transition. There is then a second order transition to a χS conductor. Above $T \sim 0.233$ the intermediate region χSB and conductor phase disappears and the chiral symmetry restoration and insulator-conductor transition happen at the same time. It is a first order transition and exists in the temperature range $0.233 \lesssim T \lesssim 0.25$. Finally for higher temperatures $T \gtrsim 0.25$, the system becomes a chiral symmetric conductor for any finite E.

There are distinct features of the phase diagram though from the T, μ phase diagram in figure 5.1(a). The insulator-conductor transition is first order along its whole length. At finite mass and zero magnetic field, this insulator-conductor transition was also shown to be first order in [94, 64]. The chiral symmetry restoration phase transition is second order along all its length from the critical point where it joins the insulator-conductor transition. The ability to reproduce different phase structures is interesting and potentially useful if one wanted to use these models as effective descriptions of more complex gauge theories or condensed matter systems.

5.3 B, μ, E at Zero Temperature

We now turn to the E, μ plane at fixed B and zero T where the behaviour appears somewhat different from those of the planes so far discussed.

From (5.17) with $T = 0$

$$\widetilde{\mathcal{L}}_{LT} = \sqrt{(1+L'^2)}\sqrt{\left(1-\frac{E^2}{w^4}\right)\left[\rho^6 + \frac{\rho^6}{w^4} + d^2 - J^2\right]}\,, \tag{5.26}$$

and

$$J = \frac{\sqrt{d^2 w_s^4 + (1+w_s^4)\rho_s^6}}{w_s^2} = \sqrt{d^2 + (1+E^2)E\cos^6\theta_s}\,, \tag{5.27}$$

where $w_s = \sqrt{E}$. Note that this formula for J is only valid for finite E, because the current J is introduced to make a sign change when $\left(1 - \frac{E^2}{w^4}\right)$ changes sign. If

$E = 0$ we would not have any reason to introduce J.

If we now substitute J back into $\widetilde{\mathcal{L}}_{LT}$ then the d dependence explicitly vanishes, as also observed in [64] for the zero B case:

$$\widetilde{\mathcal{L}}_{LT} = \sqrt{(1+L'^2)}\sqrt{\left(1-\frac{E^2}{w^4}\right)\left[\rho^6+\frac{\rho^6}{w^4}-(1+E^2)E\cos^6\theta_s\right]}\ . \tag{5.28}$$

It is the same action as (5.21), but the physics could still be different because at finite density the boundary condition for the embedding is the Dirichlet condition ($L(0) = 0$), which is different from the zero density Neumann condition ($L'(0) = 0$). Furthermore the current (5.27) looks different from the $d = 0$ case (5.22) through its d dependence (explicitly and implicitly through θ_s). However, at zero temperature and finite E, it turns out that the density is always zero, which can be shown as follows. From (5.11) or (5.20), at zero T,

$$A_t' = d\sqrt{\frac{(w^4-E^2)(1+L'^2)}{d^2w^4+\left[-d^2-\left(1+\frac{1}{w_s^4}\right)\rho_s^6\right]_{E\neq 0}w^4+(1+w^4)\rho^6}}\ , \tag{5.29}$$

where $w = \sqrt{L^2+\rho^2}$ and the square bracket is the current which must be zero at $E = 0$. So, for non-zero E, the density cancels in the denominator. Let us first consider a fixed non-zero E and the flat embedding and take the limit $\rho \to 0$:

$$A_t' \sim \frac{d}{E+1/E}\frac{1}{\rho^2}\ . \tag{5.30}$$

Thus $\mu \sim d \times$ a d-independent integral that diverges near $\rho = 0$. There is, therefore, no way to get a finite μ from a finite d. The only available density is exactly zero and if density is zero we should not use the relation (5.29). Any constant A_t is an available solution so any constant μ is allowed.

To confirm this analysis, we numerically evaluate density at small temperatures for four sample points, $(E, \mu) = (3, 10), (0.3, 10), (3, 1), (0.3, 1)$, in figure 5.4. The density indeed vanishes as T goes to zero. Turning on larger chemical potential does not change the tendency: a 10 times larger chemical potential vanishes 10 times faster (compare $\mu = 10$ and $\mu = 1$). Electric field does not affect this much:

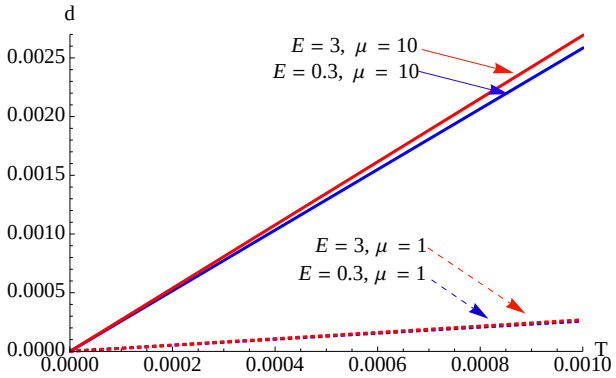

Figure 5.4: *d vs. T for four points $(E, \mu) = (3, 10)$, $(0.3, 10)$, $(3, 1)$, $(0.3, 1)$. $d \to 0$ as $T \to 0$.*

$E = 3$ and $E = 0.3$ at $\mu = 1$ are indistinguishable in figure 5.4. Thus we find that vanishing density at $T = 0$ is consistent with the limit $T \to 0$.

Given this argument it is worth checking how non-trivial results come from the same expression on the μ axis in figure 5.1(a), where $T = E = 0$. Let us consider $E = 0$ not $E \to 0$.

$$A_t' = d\sqrt{\frac{w^4(1 + L'^2)}{d^2 w^4 + (1 + w^4)\rho^6}} \ . \tag{5.31}$$

For a flat embedding and near $\rho = 0$

$$A_t' \sim 1 - \frac{\rho^2}{2d^2} \ . \tag{5.32}$$

We learn that $\mu \sim d$ times a d-dependent regular integral. So here there is a non-trivial μ, d relation. We should be careful with the $d \to 0$ limit. Then the d-dependent integral diverges as d gets smaller. However it turns out that it is less divergent than $1/d$ so we get $\mu = 0$ as expected. If we consider the spiky embedding then the singular integral will fall as $\sim 1/d$ due to the divergence in L'. Here we can have a non-zero chemical potential when $d \to 0$. This occurs at the first transition point (from the solution lying outside the singular shell to the spiky embedding) shown on the μ axis (zero T) in figure 5.1(a).

Notice that the $T = E = 0$ theory and the $T = 0$, $E \to 0$ limit are distinct. The $T = 0$, E, μ plane for any finite E has zero density. However, the strict $E = 0$ axis does have density present for the spike and flat embeddings; we show this with the

yellow and green lines respectively on the $E = 0$ axis in figure 5.1(c). Since there is a jump in the density off the $E = 0$ axis at $T = 0$ there is formally a first order transition with increasing E, which is expressed by the blue line near $E = 0$ in figure 5.1(c). (note the transitions on the $E = 0$ axis are second order though - two red dots in figure 5.1(c)). In the next section we will approach the $T = 0$ plane from positive T to confirm this picture.

The surprising aspect of this result is that, at zero T, and with even an infinitesimal E present, density is not generated no matter how large the chemical potential μ is. Therefore the flat, chirally symmetric configuration is not favoured for very large μ when a small E is present.

These conclusions are certainly correct within the DBI analysis presented here. If the reader wishes to seek additional physics that might generate density at $T = 0, E \neq 0$ and more simply connect the phases at zero and infinitesimal E, then one might be able to do that through additional boundary terms at the origin (this is where singular behaviour also enters in the μ, d relation). Again, we note that one has to be very careful when making changes to the infra-red region, as discussed above. Presumably at this point the physics associated with the sink of the energy being injected by the E field should be better understood. Equally, the DBI action may not be valid for this system due to a divergent gauge field near the origin [98]. Resolving this issue is beyond our DBI analysis here.

5.4 The Full B, T, E, μ Phase Structure

Our final task is to complete the phase structure analysis by extending it to the full E, μ, T volume at fixed B. The number of embeddings that must be analysed on any fixed plane through this space is already large so we restrict ourselves to looking at some representative slices that will be sufficient to reveal the structures present.

In particular we will study fixed-T slices and draw the phase structure in the E, μ plane. The embedding equations are now given by the full form of (5.17). To determine the presence and nature of a transition it is sufficient to track any

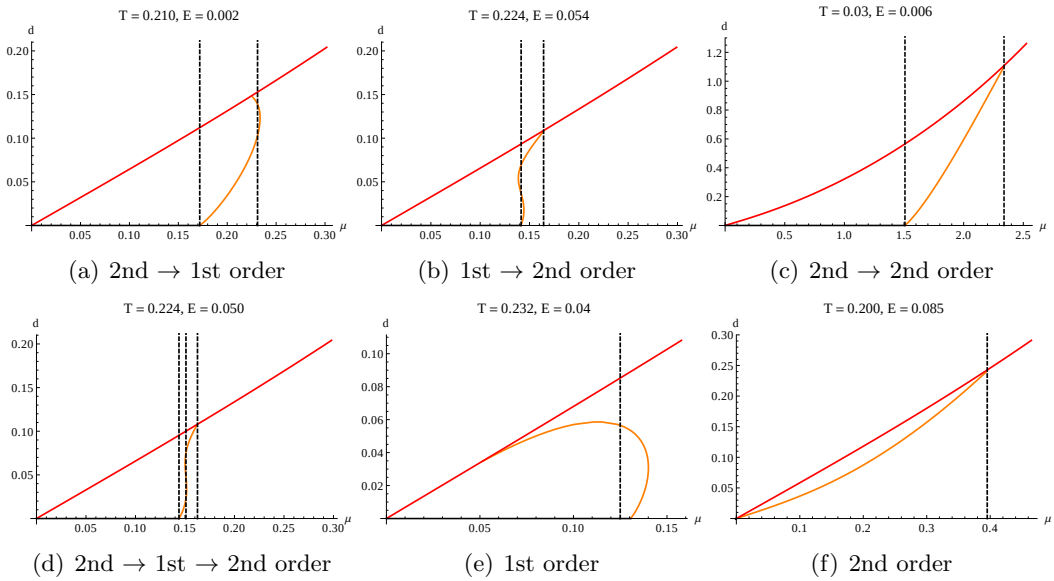

(a) 2nd → 1st order (b) 1st → 2nd order (c) 2nd → 2nd order

(d) 2nd → 1st → 2nd order (e) 1st order (f) 2nd order

Figure 5.5: *Representative μ-d plots. The black line on the μ axis corresponds to an embedding that misses the singular shell; the orange curve to a spike embedding that ends on the singular shell; and the red curve to a flat embedding. The transition points are shown by the vertical dotted lines. Subcaptions are the order of transition as μ increases.*

operator of the theory. We have found it easiest on these planes to plot the density d against the chemical potential μ. i.e. we use d as our order parameter.

In figure 5.5 we show sample plots from which each of a first and second order transition can be identified. There are in total six types of d-μ plots. In each of the figures the black line on the μ axis corresponds to a chiral symmetry breaking embedding that misses the singular shell; the orange curve to a spike embedding that ends on the singular shell; and the red curve to a flat embedding. It can be seen from the plots whether each transition between embeddings is smooth and hence second order, or whether there is an 'S' shaped structure so that one expects a first order transition. The transition points are shown by the vertical dotted lines. We have used these techniques on constant E lines on each constant T plane to determine the transition places and orders. Figure 5.6 is constructed from sequences of d-μ plots (figure 5.5). For example, figure 5.6 shows the following evolution of the d-μ plot as E increases (table 5.1).

In figure 5.6 we show six slices through the volume at varying T. Starting at high temperature the theory lives in the chirally symmetric phase with unstable mesons

figure 5.6	d-μ plot evolution (figure 5.5)
(a)	(a)→(e)→(b)→(f)
(b)	(a)→(d)→(b)→(f)
(c)	(a)→(c)→(d)→(b)→(f)
(d)	(a)→(c)→(b)→(f)
(e),(f)	(c)→(b)→(f)

Table 5.1: *The evolution of the d-μ plot for increasing electric field E for each plot in figure 5.6.*

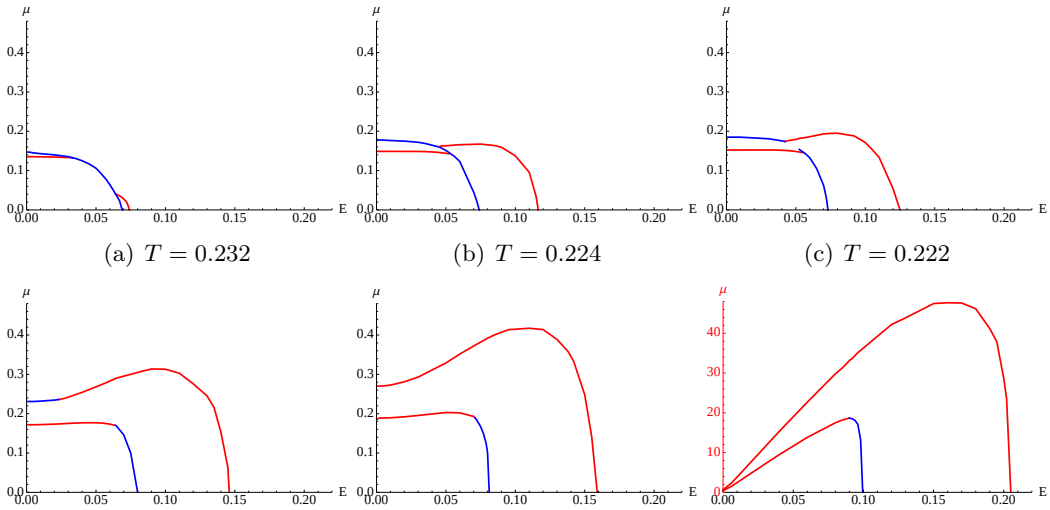

(a) $T = 0.232$ (b) $T = 0.224$ (c) $T = 0.222$

(d) $T = 0.210$ (e) $T = 0.200$ (f) $T = 0.003$ (Notice that the scale of μ is 100 times larger)

Figure 5.6: *Phase diagrams in the $\mu - E$ plane at various values of temperature showing the phase structure. The solid blue lines are first order transitions, the red lines are second order.*

and the material is a conductor. As the temperature falls to $T \simeq 0.25$ the first order transition to the chiral symmetry breaking, stable meson, insulator regime begins to appear in the μ-E plane around $\mu = E = 0$. That transition then expands away from the origin and remains briefly first order.

Our plot for $T = 0.232$ shows the first interesting structure. Two areas in the plane grow out from the first order line bordered by additional second order transitions. In these areas the theory is in a chiral symmetry breaking but conducting phase. The critical points where the first and second order transitions meet migrate inwards along the first order boundary from each axis as the temperature falls and eventually pass each other as shown for $T = 0.224$. At temperatures below that point there are constant E trajectories across which there are three transitions. A second order transition from conductor to insulator, a first order transition between

two spike embeddings and finally a second order chiral symmetry restoration transition. An example of the relevant density chemical potential plot for this case is in figure 5.5(d).

Our plot for $T = 0.222$ shows the next key transition. The first order line between the two spike embeddings breaks, making the spike embedding phase continuously connected, although there is a remnant of the first order transition line ending at a critical point.

The first order transition near the $E = 0$ phase boundary then diminishes as temperature is further reduced, retreating towards the axes — see the plot for $T = 0.21$. It has totally disappeared by $T = 0.2$. However the first order transition element on the conductor insulator transition grows from the E axis as temperature decreases.

The final interesting feature begins to appear in the plot at $T = 0.21$ where the phase boundaries have begun to deform. They expand out to large μ very rapidly. Note that the scale of the μ axis at $T = 0.03$ is 100 times larger than the others. If we drew it on the same scale as the others it would look like figure 5.1(c): the μ-independence of the $T = 0$ limit is starting to be seen. At zero T (figure 5.1(c)) there is a first order transition between the μ axis and the rest of the μ, E plane - here we see that that forms as the second order boundaries are pressed onto the μ axis.

These results have been incorporated into the 3D plot in figure 5.1(d) which summarises the full and rich phase structure.

5.5 Quark Mass

The analysis above has been purely for zero quark mass. We have not performed an analysis of the introduction of a quark mass. However, we note here that an immediate consequence of introducing a small quark mass is that the second-order chiral-symmetry restoration transitions (the outer red lines in our figures) become cross overs. We would expect some remnant of the first order segment of this

transition to remain associated with a transition at which there is a discontinuity in the quark condensate even in the infinite mass limit where the theory becomes the massive $\mathcal{N} = 2$ theory (we observed this in the $E = 0$ limit in section 3.6). The insulator conductor transition remains with quark mass and will again become that of the $\mathcal{N} = 2$ theory at large mass. At finite mass and temperature but without magnetic field, the insulator-conductor transition was shown to be first order in [94, 64].

5.6 Summary

We have explored the phase structure of the $\mathcal{N} = 2$ gauge theory whose dual is the D3/D7 system. A magnetic field, B, tries to induce chiral symmetry breaking. An electric field, E, tries to dissociate the mesons of the theory and makes it a conductor. Finite density, d, (or chemical potential μ) and temperature, T, each favour melting of the mesons. The competition between these effects leads to a rich phase structure.

In figure 5.1(a) we display the (T, μ)- phase plane for the massless theory at fixed magnetic field. There are three phases: at low (T, μ) a chiral symmetry breaking phase with stable mesons, at intermediate values a chiral symmetry breaking phase with unstable mesons, and at large T, μ a chirally symmetric phase with unstable mesons. The transitions between these are a mix of first and second order transitions linked at two critical points.

In figure 5.1(b) we show the (T, E) phase plane for the massless theory at fixed magnetic field. There are again three phases: at low T, E a chiral symmetry breaking phase with stable mesons which acts as an insulator in the presence of a small electric field; at intermediate values a chiral symmetry breaking phase with unstable mesons which is a conductor and sustains a current in the presence of an electric field; and at high T, E a conducting chirally symmetric phase with unstable mesons. The transitions between these are again a mix of first and second order transitions linked at one critical point.

The E, μ phase plane has rather different structure (figure 5.1(c)). In particular for any finite E the plane is μ independent and density is zero. At low E we have a chiral symmetry breaking, insulator phase; at intermediate E a chiral symmetry breaking but conducting phase; at large E a conducting and chirally symmetric phase. That the presence of infinitesimal electric field does not allow density even with a very large chemical potential and stops the restoration of chiral symmetry is rather surprising. The conclusion is certainly correct within the analysis that we have performed. It is possible though that additional stringy physics should be present near the IR boundary in this limit to explain the sink for the energy the E field is injecting. Such physics could potentially change the phase structure at low T.

Finally we have explored the full (E, μ, T)-volume at fixed B to show how these phases are linked. The phase diagram is summarised in figure 5.1(d) with the transition boundaries marked.

The variety of phase structure and transition type in such a simple theory is remarkable. Whether these results can serve as an exemplar for other gauge theories either qualitatively or quantitatively remains to be seen but they certainly suggest a rich structure of phases will be present in many gauge theories.

We would like to add that since we conducted this research there has been development in the field. The authors of [101, 102] pointed out that there may be an instability in figure 5.1(b) due to the WZ term contribution. The authors of [101] followed up the analysis presented in this chapter to consider the case of mutually perpendicular electric and magnetic fields — they found the chiral transition to be first order in nature throughout the full (T-E) plane.

Chapter 6

Towards a Holographic Model of the QCD Phase Diagram

The QCD phase diagram is notoriously difficult to compute. Firstly the physics associated with deconfinement or chiral symmetry restoration is strongly coupled. In the strongly coupling regime we traditionally do not know how to compute physical quantities, as perturbation theory breaks down. Secondly at finite density lattice gauge theory, the first principles simulation of the theory on supercomputers, suffers from a 'sign problem' that means Monte Carlo methods break down. In fact with light quarks there is no clear order parameter for deconfinement so we will concentrate on the chiral transition. Progress has been made by identifying effective theories of the transitions and through lattice computations at low density. Section 1.2.3 provides a review of the standard picture. It is believed for QCD, with the physical quark masses, that the phase transition with temperature is a smooth cross over (becoming a second order transition as the up and down quark masses go to zero). At zero temperature the transition with density is believed to be first order. There must therefore be a tri-critical point where the first order line ends in the temperature density plane.

In the previous chapter we have used holographic techniques to study phase diagrams of strongly coupled physics. In this chapter we want to ask whether these holographic models can in principle describe a phase diagram like that of real QCD.

We can not of course describe true QCD holographically because the dual, if it exists, is not known and is probably very complicated (and strongly coupled, at least, in the UV). Our analysis is therefore in the spirit of AdS/QCD [103, 104], a phenomenological modelling of the QCD phase diagram. If one could model the phase diagram correctly one might hope to then predict other features of the theory such as time dependent dynamics during transitions and so forth.

Our models will be in the context of the simplest brane construction of a 3+1-dimensional gauge theory with quarks which is the D3/D7 system used in chapters 2, 3 and 5. The basic gauge theory is large N, $\mathcal{N} = 4$ super Yang-Mills with N_f quark fields. We will work in the quenched approximation where we neglect quark loops. On the gauge theory side we do not backreact the D7 branes, that provide the quarks, on the geometry but instead work in the probe approximation.

So called top-down models of this type exist with chiral symmetry breaking. Supergravity solutions exist that correspond to the AdS space being deformed in reaction to a running coupling introduced by a non-trivial dilaton profile as used in chapter 2. In cases where the coupling grows in the infrared (IR), breaking the conformal symmetry, chiral symmetry breaking is induced. These models have very specific forms for the running coupling and are typically singular somewhere in the interior. At the string theory level a full interpretation is lacking.

In chapters 3 and 4 we have explored the phase structure of the theory with a magnetic field breaking chiral symmetry. It can be seen in figure 5.1(a). Temperature can be introduced through an AdS Schwarzschild black hole in the geometry. Density and chemical potential can be added through the temporal component of the $U(1)$ baryon number gauge field. How generic to the holographic description is this phase structure? Keeping within the top-down analysis one can change parameters and see what effect they have on the phase diagram. For example in chapter 5 we traded density for an electric field parallel to the magnetic field. The electric field tries to dissociates mesons by accelerating the quark and anti-quark in opposite directions and so opposes the formation of a chiral condensate.

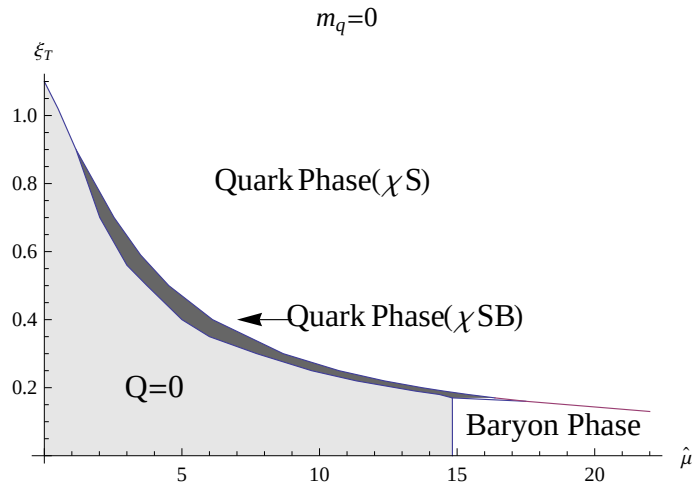

Figure 6.1: *The phase diagram of the massless axion/dilaton gauge theory in [105]. Here Q is the density, ξ_T the temperature and $\hat{\mu}$ the chemical potential.*

A recent paper [105] performed a similar analysis with a running dilaton geometry. The geometry is that of [106] in which there is a non-zero profile for both the dilaton and axion fields in AdS. The field theory is the $\mathcal{N} = 4$ gauge theory with a vev for both $\mathrm{Tr}F^2$ and $\mathrm{Tr}F\tilde{F}$ which preserves supersymmetry at zero temperature but displays confinement. A D7 was introduced in a supersymmetry breaking fashion and chiral symmetry breaking is observed. The temperature density chiral transformation was first order throughout the plane and is shown in figure 6.1. It shows the same three phases as the magnetic field case. An extra component of the analysis in [105] was to note that in the confining geometry with a running dilaton a baryonic phase was also present. A baryon vertex is described by a D5 brane wrapped on the S^5 of the $\mathrm{AdS}_5 \times S^5$ space. In the pure $\mathcal{N} = 4$ theory such vertices shrink to zero. However in the running dilaton geometry the large IR value of the dilaton stabilises the D5 embedding. Solutions exist that link the D5 to the D7 brane embedding with a balancing force condition. These configurations describe the gauge theory with finite baryon density rather than finite quark density. This phase sets in at finite chemical potential and then persists to infinite chemical potential (as shown in figure 6.1) which is certainly unlike QCD. We will not focus on this phase in this chapter but it would be interesting to study it in future work to find models that have a baryonic phase in some intermediate range of chemical potential like QCD.

These phase structures are very interesting and surprisingly complex but do not match the expectations in QCD. In QCD we need a second order transition with temperature and a first order transition with density to the chirally symmetric phase.

Here we want to work in a much more generic framework to ask what phase structures it is possible to get in the holographic description and to try to force ourselves onto a representation of the QCD phase diagram. We will therefore take a bottom-up approach within the model and allow ourselves to dial the running of the gauge coupling by hand. We will have a dilaton profile that smoothly transitions from a UV conformal regime to an IR conformal regime through a step of variable height and width. Such an ansatz allows one to consider runnings that range from precocious growth in the IR to walking dynamics [18]. We used a similar ansatz in chapter 2 to study the impact of walking on meson physics. Here we find that with the simple step ansatz we can move from a totally first order transition in the phase plane to a configuration similar to the one we obtained with a B field (a first order transition with temperature but second order with density). With this ansatz we cannot achieve a second order transition with temperature.

The model directly suggests other phenomenological generalisations though. In particular, if we think of the running dilaton profile as a short cut for including the backreaction due to the quark fields/D7 brane, then it is natural to break the $SO(6)$ symmetry of AdS_5 in the dilaton in the same fashion as the D3/D7 system's geometry. This allows us an extra phenomenological freedom to distort the dilaton or black hole horizon. These simple changes do allow us to reproduce a wide range of phase diagrams including QCD-like ones as we will show below. We will discuss the simple geometric reasons for the emergence of first or second order transitions in these different scenarios.

Our conclusion therefore is that the holographic model has no intrinsic problem with mimicking the QCD phase diagram and these systems may therefore be phenomenologically useful in the future.

6.1 The Model

First let us briefly review the gravity dual description of the symmetry breaking behaviour of our strongly coupled gauge theory.

The set-up in this chapter is similar to that in chapter 2. We will consider a gauge theory with a holographic dual described by the Einstein frame geometry $\mathrm{AdS}_5 \times S^5$

$$ds^2 = \frac{1}{g_{\mathrm{UV}}}\left[\frac{r^2}{R^2}dx_4^2 + \frac{R^2}{r^2}\left(d\varrho^2 + \varrho^2 d\Omega_3^2 + dw_5^2 + dw_6^2\right)\right], \tag{6.1}$$

where we have split the coordinates into the x_{3+1} of the gauge theory, the ϱ and Ω_3 which will be on the D7 brane worldvolume and two directions transverse to the D7, w_5, w_6. The radial coordinate, $r^2 = \varrho^2 + w_5^2 + w_6^2$, corresponds to the energy scale of the gauge theory. The radius of curvature is given by $R^4 = 4\pi g_{\mathrm{UV}}^2 N \alpha'^2$ with N the number of colours. g_{UV}^2 is the $r \to \infty$ value of the dilaton. In addition we will allow ourselves to choose the profile of the dilaton as $r \to 0$ to represent the running of the gauge theory coupling

$$e^{\phi} = g_{YM}^2(r) = g_{\mathrm{UV}}^2\ \beta(r)\,, \tag{6.2}$$

where the function $\beta \to 1$ as $r \to \infty$. The $r \to \infty$ limit of this theory is dual to the $\mathcal{N} = 4$ super Yang-Mills theory where g_{UV}^2 is the constant large r asymptotic value of the gauge coupling.

An interesting phenomenological case is to consider a gauge coupling running with a step of the form

$$\beta(r) = A + 1 - A\tanh\left[\Gamma(r-\lambda)\right]. \tag{6.3}$$

Of course in this case the geometry is not backreacted to the dilaton and the model is a phenomenological one in the spirit of AdS/QCD [103, 104]. This form introduces conformal symmetry breaking at the scale $\Lambda = \lambda/2\pi\alpha'$ which triggers chiral symmetry breaking. The parameter A determines the increase in the coupling across the step.

We will introduce a single D7 brane probe into the geometry to include quarks.

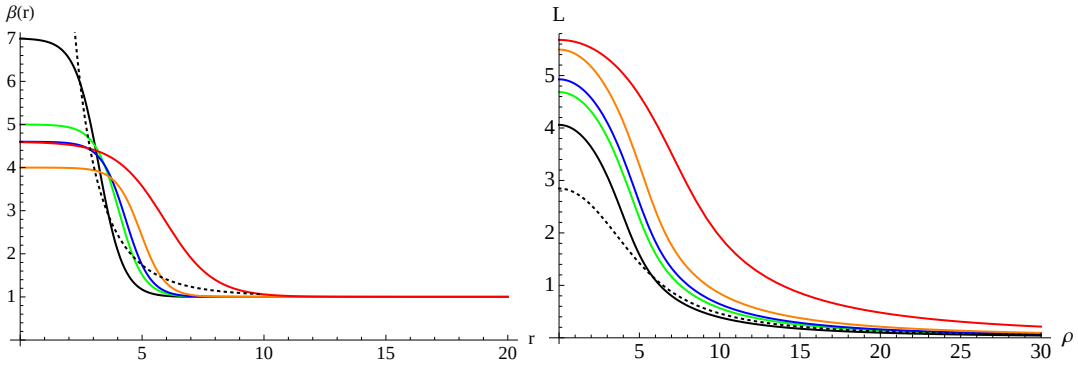

	Γ	A	λ
Black	1	3	3.240
Green	1	2	4.045
Blue	1	1.8	4.325
Orange	1	1.5	4.940
Red	0.5	1.8	5.882
Black(Dotted)	$B = 35.6$	-	-

Figure 6.2: *Example coupling flows (6.3) (left) and the induced D7 brane embeddings/quark self-energy L (right) as defined in (6.9) and calculated using the Lagrangian (6.17) with the parameter choices shown in the table. We also includ an embedding with chiral symmetry breaking induced by a magnetic field B (see chapter 3).*

This system has a $U(1)$ axial symmetry on the quarks, corresponding to rotations in the w_5-w_6 plane, which will be broken by the formation of a quark condensate. In chapter 2 was discussed how a non-trivial β introduces chiral symmetry breaking.

If the coupling is larger near the origin then the D7 brane will be repelled from the origin[6]. The parameter Γ spreads the increase in the coupling over a region in r of order Γ^{-1} in size.

We display the embeddings for some particular cases in figure 6.2. Note that we have chosen parameters here that make the vacuum energy of the theory the same in each case. The vacuum energy is given by minus the DBI action evaluated on the solution. In fact this energy is formally divergent corresponding to the usual cosmological constant problem in field theory. As usual we will subtract the UV component of the energy to renormalise.

[6]In fact there is a competition between the increased action from the D7 entering the region with larger dilaton and the derivative cost of the D7 bending to avoid it. This leads to a critical value of A to trigger chiral symmetry breaking. For example for $\lambda = 1.7$ and $\Gamma = 1$ $A_c = 2.1$. In this chapter we will consider only super-critical values of A.

The symmetry breaking of these solutions is visible directly [35]. The $U(1)$ symmetry corresponds to rotations of the solution in the w_5-w_6 plane. An embedding along the ϱ axis corresponds to a massless quark with the symmetry unbroken (this is the configuration that is preferred at high temperature and it has zero condensate c). The symmetry breaking configurations though map onto the flat case at large ϱ (the UV of the theory) but bend off axis breaking the symmetry in the IR.

6.1.1 Temperature

Temperature can be included in the theory by using the AdS Schwarzschild black hole metric. In the Einstein frame we have

$$ds^2 = \frac{1}{g_{\rm UV}}\left[\frac{-K(r)}{R^2}dt^2 + \frac{R^2}{K(r)}dr^2 + \frac{r^2}{R^2}d\vec{x}_3^2 + R^2 d\Omega_5^2\right], \tag{6.4}$$

where

$$K(r) = r^2 - \frac{r_H^4}{r^2}\,, \qquad r_H = \pi R^2 T\,. \tag{6.5}$$

The parameter r_H is identified with the temperature T. We make the coordinate transformation also used in chapter 5

$$\frac{rdr}{(r^4 - r_H^4)^{1/2}} \equiv \frac{dw}{w}\,, \quad 2w^2 = r^2 + \sqrt{r^4 - r_H^4}\,, \tag{6.6}$$

with $\sqrt{2}w_H = r_H$, such that the metric becomes

$$ds^2 = \frac{1}{g_{\rm UV}}\left[\frac{w^2}{R^2}(-g_t dt^2 + g_x d\vec{x}^2) + \frac{R^2}{w^2}(d\rho^2 + \rho^2 d\Omega_3^2 + dL^2 + L^2 d\Omega_1^2)\right], \tag{6.7}$$

where

$$g_t = \frac{(w^4 - w_H^4)^2}{w^4(w^4 + w_H^4)}\,, \quad g_x = \frac{w^4 + w_H^4}{w^4}\,, \tag{6.8}$$

and

$$w = \sqrt{\rho^2 + L^2}\,, \quad \rho = w\sin\theta\,, \quad L = w\cos\theta\,. \tag{6.9}$$

Now we have to transform β also:

$$e^{\phi} = g^2_{YM}(r^2) = g^2_{\rm UV}\ \beta\left(\frac{w^4+w_H^4}{w^2}\right) = g^2_{\rm UV}\ \beta\left(\frac{(\rho^2+L^2)^2+w_H^4}{\rho^2+L^2}\right), \tag{6.10}$$

and therefore

$$\beta = A + 1 - A\tanh\left[\Gamma\left(\sqrt{\frac{(\rho^2+L^2)^2+w_H^4}{\rho^2+L^2}} - \lambda\right)\right]. \tag{6.11}$$

Note that for $w_H \to 0$: $w \to r$, $\rho \to \varrho$ and $L \to w_5$, if we set $w_6 = 0$.

6.1.2 Chemical Potential

We introduce a chemical potential through the $U(1)$ baryon number gauge field which enters the DBI action in Einstein frame as

$$S_{D7} = -T_7 \int d^8\xi e^{\phi}\sqrt{-\det\left(P[G]_{ab} + (2\pi\alpha')F_{ab}\right)}, \tag{6.12}$$

where $T_7 = 1/(2\pi)^7\alpha'^4$ and $\overline{T}_7 = 2\pi^2 T_7/g^2_{\rm UV}$ when we have integrated over the 3-sphere on the D7. We allow a chemical potential through $A_t(\rho) \neq 0$. So the action becomes

$$\begin{aligned} S_{D7} &= \int d^4x\ d\rho\ \mathcal{L} \\ &= -\overline{T}_7 \int d^4x\ d\rho\ \beta(\rho)\rho^3\ \sqrt{g_t g_x^3\left(1+L'^2\right) - (2\pi\alpha' g_{\rm UV})^2 A_t'^2 \frac{g_x^3}{\beta(\rho)}}\,. \end{aligned} \tag{6.13}$$

In our convention for the metric this is

$$\begin{aligned} \mathcal{L} &= -\overline{T}_7\ \beta(\rho)\rho^3\ \left(1-\frac{w_H^4}{w^4}\right)\left(1+\frac{w_H^4}{w^4}\right) \\ &\times \sqrt{\left(1+L'^2\right) - \frac{w^4\left(w^4+w_H^4\right)}{\left(w^4-w_H^4\right)^2}\frac{1}{\beta(\rho)}(2\pi\alpha' g_{\rm UV})^2 A_t'^2}\,. \end{aligned} \tag{6.14}$$

Now we can Legendre transform the action as we have a conserved quantity, the density, $d\left(=g_{\rm UV}^2\frac{\delta S_{D7}}{\delta A_t'}\right)$.

$$\tilde{S}_{D7} \;=\; S_{D7}-\int d^8\xi A_t'\frac{\delta S_{D7}}{\delta A_t'} \;=\; \left(\int_{S3}\epsilon_3\int d^4x\right)\int d\rho\;\tilde{\mathcal{L}}\,, \tag{6.15}$$

where

$$\begin{aligned}\tilde{\mathcal{L}} &= -\overline{T}_7\frac{\left(w^4-w_H^4\right)}{\left(w^4\right)}\sqrt{1+L'^2}\\ &\times \sqrt{\left(\frac{w^4d^2\beta(\rho)}{\left((2\pi\alpha' g_{\rm UV})^2N^2\left(w^4+w_H^4\right)\right)}+\frac{\rho^6\left(w^4+w_H^4\right)^2}{w^8}\beta(\rho)^2\right)}.\end{aligned} \tag{6.16}$$

We can redefine $d=(2\pi\alpha' g_{\rm UV})\overline{T}_7\tilde{d}$ to give the simpler expression

$$\tilde{\mathcal{L}}=-\overline{T}_7\frac{\left(w^4-w_H^4\right)}{\left(w^4\right)}\sqrt{1+L'^2}\sqrt{\left(\frac{w^4\tilde{d}^2\beta(\rho)}{\left(w^4+w_H^4\right)\right)}+\frac{\rho^6\left(w^4+w_H^4\right)^2}{w^8}\beta(\rho)^2\right)}. \tag{6.17}$$

By varying the Lagrangian with respect to A_t', we get an expression for $d(A_t')$ which we can invert for an expression for $A_t'(d)$

$$(2\pi\alpha' g_{\rm UV})A_t'=\tilde{d}\frac{\left(w^4-w_H^4\right)}{\left(w^4+w_H^4\right)}\sqrt{1+L'^2}\sqrt{\frac{1}{\frac{\tilde{d}^2}{\beta(\rho)}\frac{w^4}{\left(w^4+w_H^4\right)}+\rho^6\left(\frac{w^4+w_H^4}{w^4}\right)^2}}\,. \tag{6.18}$$

This can be used to find the chemical potential $\mu=\frac{\tilde{\mu}}{(2\pi\alpha' g_{\rm UV})}$

$$\tilde{\mu}=\int_{\rho_H}^{\infty}d\rho\;\tilde{d}\frac{\left(w^4-w_H^4\right)}{\left(w^4+w_H^4\right)}\sqrt{\frac{(1+L'^2)}{\frac{\tilde{d}^2}{\beta(\rho)}\frac{w^4}{\left(w^4+w_H^4\right)}+\rho^6\left(\frac{w^4+w_H^4}{w^4}\right)^2}}\,, \tag{6.19}$$

where $\tilde{\mu}(\rho\to\rho_H)=0$.

The free energy can be found by integrating the Legendre transformed Lagrangian and the grand potential by integrating the original Lagrangian, where we replace

$A_t'(d)$:

$$F = -\frac{\tilde{S}_{D7}}{\overline{T}_7} = \int_{\rho_H}^{\infty} d\rho \, \frac{\left(w^4 - w_H^4\right)}{\left(w^4\right)} \sqrt{1 + L'^2} \times \sqrt{\left(\frac{w^4 \tilde{d}^2 \beta(\rho)}{\left(w^4 + w_H^4\right)} + \frac{\rho^6 \left(w^4 + w_H^4\right)^2}{w^8} \beta(\rho)^2 \right)}. \tag{6.20}$$

The grand potential is

$$\Omega = -\frac{S_{D7}}{\overline{T}_7} = \int_{\rho_H}^{\infty} d\rho \, \beta(\rho)^2 \frac{w^4 - w_H^4}{w^4} \rho^6 \left(\frac{w^4 + w_H^4}{w^4} \right)^2 \times \sqrt{\frac{(1 + L'^2)}{\tilde{d}^2 \beta(\rho) \left(\frac{w^4}{w^4 + w_H^4} \right) + \rho^6 \left(\frac{w^4 + w_H^4}{w^4} \right)^2 \beta(\rho)^2}}, \tag{6.21}$$

where we need to note that $F(\rho \to \infty) = \Omega(\rho \to \infty) = \rho^3$, so we need to subtract $\frac{1}{4}(\Lambda_{UV})^4$ from both integrals to renormalise them. Note, that from now on we will only be using the redefined variables $\tilde{d}$ and $\tilde{\mu}$. For convenience, we will refer to them as density d and chemical potential μ respectively in the remainder of this chapter. To make clear the role of w_H as the scaled temperature, we will refer to it as the temperature T in the remainder of this chapter.

6.2 Analysis and Results

The methodology to study the phase diagram of our model is straightforward if laborious. We will work throughout in the massless quark limit. We can think of the scale λ in the dilaton ansatz as our intrinsic scale of the theory and so we will leave that fixed. Then for each choice of parameters in the dilaton profile (A, Γ) we analyse the theory on a grid in T and μ space.

For each point on the T-μ grid we seek three sorts of embedding. The flat embedding $L = 0$ exists in all cases and describes the theory with $m = 0$ and $c = 0$. The values of m and c can be read off from the large ρ asymptotic solutions of L (or w_5) described in (2.5). We use (6.19) to compute the d-μ relation for these embeddings.

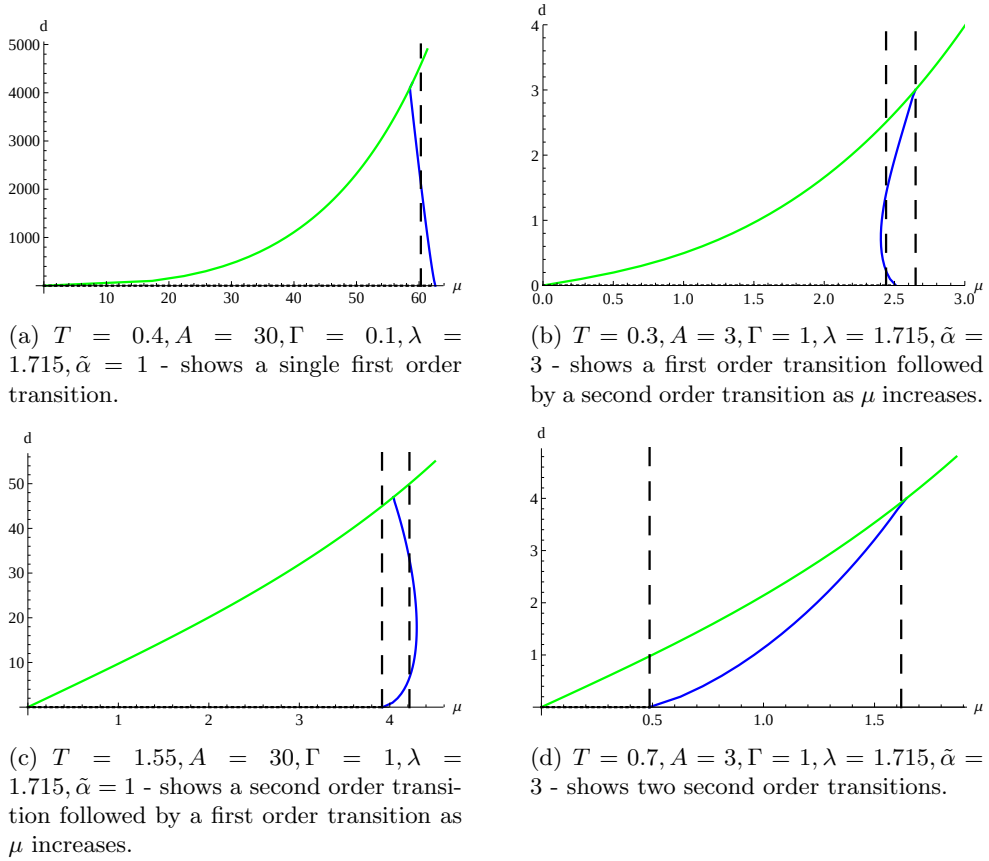

(a) $T = 0.4, A = 30, \Gamma = 0.1, \lambda = 1.715, \tilde{\alpha} = 1$ - shows a single first order transition.

(b) $T = 0.3, A = 3, \Gamma = 1, \lambda = 1.715, \tilde{\alpha} = 3$ - shows a first order transition followed by a second order transition as μ increases.

(c) $T = 1.55, A = 30, \Gamma = 1, \lambda = 1.715, \tilde{\alpha} = 1$ - shows a second order transition followed by a first order transition as μ increases.

(d) $T = 0.7, A = 3, \Gamma = 1, \lambda = 1.715, \tilde{\alpha} = 3$ - shows two second order transitions.

Figure 6.3: *Plots of density d versus chemical potential μ. Transition points are shown by the dotted vertical lines.*

We can also seek curved embeddings that miss the black hole. These solutions must have $d = 0$ but are consistent for any value of μ. Here we use the equation of motion for L from (6.17) and numerically shoot from an initial condition at $\rho = 0$ with vanishing ρ derivative, $L'(0) = 0$. We seek solutions that approach $L = 0$ at large ρ. These configurations have a non-zero condensate parameter c.

Finally we can look for solutions that end on the black hole horizon. To find these we fix the density d and shoot out from all points along the horizon seeking a solution that approaches $L = 0$ at large ρ. We then use (6.19) to compute μ from the solution. In this way we can fill out the T-μ grid. The condensate can again be extracted from the large ρ asymptotics of the embedding.

After finding as many such solutions as exist at each point the easiest method to identify the transition points is to plot the density against μ on fixed-T lines. The transitions and their order are then manifest. We display four sample plots in figure

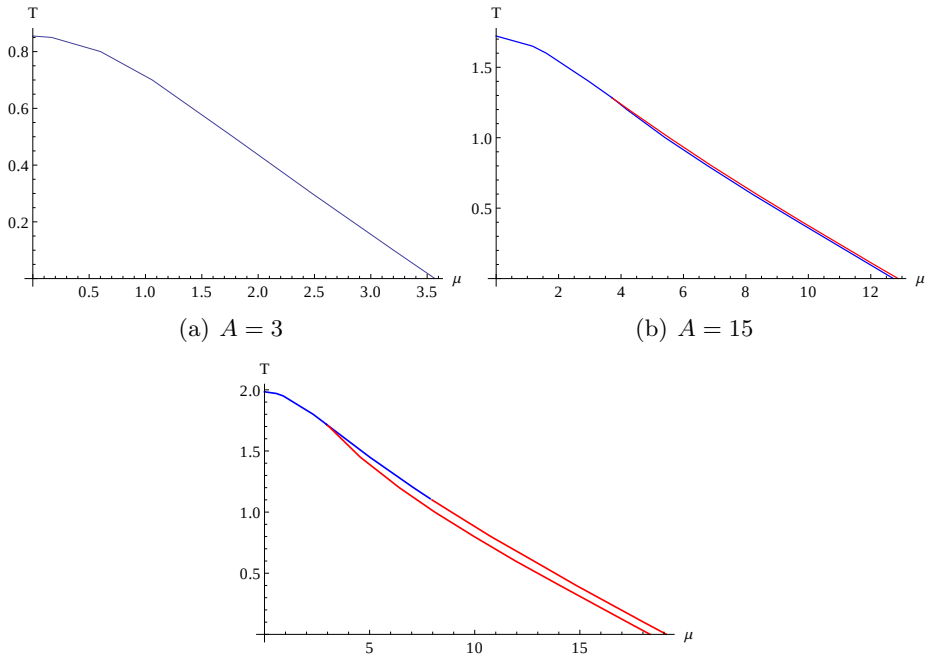

(a) $A = 3$ (b) $A = 15$

(c) $A = 30$

Figure 6.4: *Plots for three possible phase diagrams for the choices* $A = 3, 15, 30$. *Large (small)* A *gives second (first) order transition at low* T. $\Gamma = 1, \lambda = 1.715$.

6.3 taken from scenarios below showing the four cases of the chiral transition and the meson melting transition being respectively first or second order in all combinations.

6.2.1 Dependence on the Change in Coupling

Let us first consider how the phase diagram depends on the height of the step in the gauge coupling function β. We fix λ (the intrinsic scale of the theory) and also $\Gamma = 1$ and explore the phase structure as a function of A. We display the results for three choices of A in figure 6.4.

In these and all our future phase diagrams the regions shown are similar to those in figure 5.1(a) we will simply display the phase boundaries and their order henceforth.

As mentioned in the footnote in section 6.1 there is a critical value of A for chiral symmetry breaking to occur. A conformal theory can not break a symmetry since it offers no scale for that symmetry breaking to occur at. In fact some finite departure from conformality is needed to break the chiral symmetry. For these choices of λ, Γ

the critical A is $A_c = 2.1$. We work above this value throughout.

At low A there is a single transition for chiral symmetry restoration and meson melting which is first order for all T and μ. On the gravity side this is a transition between the curved embedding that misses the black hole and the flat embedding. In this case an embedding ending on the black hole never plays a role.

For larger A, a new phase with chiral symmetry breaking but melted mesons develops. There is a regime now in which the curved embedding ending on the black hole is energetically favoured. The transition from the chiral symmetry breaking phase to this new phase is second order. The chiral symmetry restoration phase remains first order.

At very large A the chiral restoration transition becomes second order at high density. This latter phase resembles that of the theory with chiral symmetry breaking induced by a magnetic field. In fact the B field case can be thought of as our case but with a choice of β given by

$$\beta = \frac{1}{g_{\rm UV}}\sqrt{1+\frac{B^2w^4}{(w^4+T^4)^2}}\,. \tag{6.22}$$

It is the black dotted curve ($T = 0$) in figure 6.2 — it is not surprising therefore that we see similar phase structure here (and indeed that we do provides strength to our analysis which is capturing the behaviour of top-down models).

For very large A the step becomes very sharp and there is little change relative to our phase diagram in figure 6.4(c). In particular the thermal transition always remains first order.

The behaviour we are seeing here can be readily explained from the D7 perspective. First of all the zero density transition with temperature is first order for a simple reason. The D7 embedding breaks chiral symmetry at zero temperature because it prefers to avoid the action cost of entering the region in which the dilaton is large. As temperature is introduced through a small horizon the interior of the space is 'eaten' but the D7 embedding remains oblivious to this change since it never reaches down to small r. As temperature rises the point of transition is when the

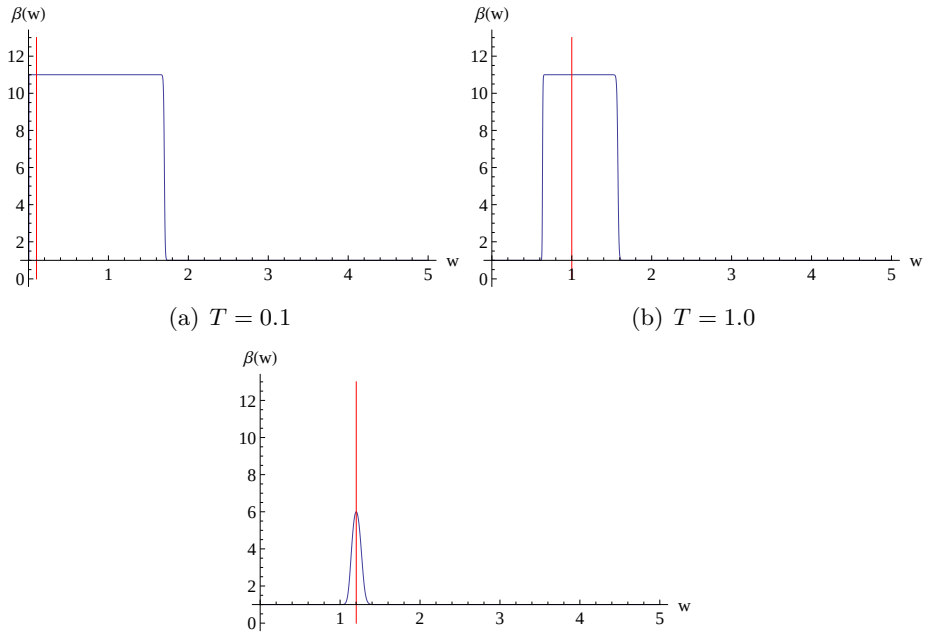

(a) $T = 0.1$

(b) $T = 1.0$

(c) $T = 1.20208 = \frac{\lambda}{\sqrt{2}}$. Dilaton is almost screened. The residual effect is due to finite Γ effect.

Figure 6.5: *Plots for parameter choices $A = 5, \Gamma = 100, \lambda = 1.7$. The blue lines show the value of the coupling β. The red line shows the position of the horizon. The final plot corresponds to the point of the first order transition.*

horizon moves through the scale λ where the dilaton step is. Once the region with a large dilaton is eaten by the black hole the preferred D7 embedding is the flat one.

In figure 6.5 we show an extreme case of this behaviour explicitly. Here we have taken Γ very large so that the transition in the dilaton between the low and high value is very sharp. We plot the β profile against our radial parameter w and mark in red the position of the black hole horizon. Note that in the w coordinates the region where β is large depends on the temperature (it does not in the original r coordinate). The dilaton effective radius λ_* is

$$\lambda_* = \sqrt{\frac{\lambda^2 + \sqrt{\lambda^4 - 4T^4}}{2}}\,, \tag{6.23}$$

where the argument of tanh in (6.11) vanishes. So, as T increases λ_* decreases. When T becomes $T_c = \frac{\lambda}{\sqrt{2}}$, $\lambda_* = T_c$ the dilaton is perfectly screened by the black hole horizon. (i.e. If $T = 0$, $\lambda_* = \lambda$. If $T = \frac{\lambda}{\sqrt{2}}$, $\lambda_* = \frac{\lambda}{\sqrt{2}}$). The point of the first order transition is where the horizon screens the dilaton.

When density is introduced the story can become more complex. The Lagrangian is (6.17) where it can be seen from the first of the two terms in the square root that including d increases the action. This increase can be beneficial though if the second term with β can be reduced. It is possible to reduce the β term if the D7 enters the region where β is large at small ρ. This means that the situation can arise where curving off the axis and then spiking on to the axis can be the lowest action state. This is typically more likely where β is largest in the interior space and the most savings can be made entering that region at low ρ. As we have seen at large values of A, embeddings that spike onto the horizon do play a role introducing an extra phase.

It is only possible to have second order transitions if all three phases we have described are present. In the D7 description the D7 must move from a curved embedding that avoids the black hole to a configuration that spikes onto the black hole to a flat embedding smoothly.

6.2.2 Dependence on the Speed of Running

The parameter Γ controls the period in ρ or RG scale over which the change in the coupling A occurs. It allows us to naively go from a precociously running theory to a walking theory (although the change in the parameter A over that period may enter into what is meant by walking versus running too).

In figure 6.6 we show the phase diagram as a function of Γ at fixed λ and A. We start at $\Gamma = 1$ with a configuration already discussed that has all three phases present and second order transitions at high density. As Γ is reduced so that the step function in the dilaton becomes broader the first order nature of the transitions reasserts itself. By $\Gamma = 0.2$ the mixed phase with chiral symmetry breaking but melted mesons is no longer preferred at any temperature or chemical potential value — there is a single first order transition.

In conclusion, moving towards a walking theory by either increasing the width of the running or decreasing the magnitude of the increase in the coupling both move us towards a first order chiral transition. Stronger or quicker running favours a

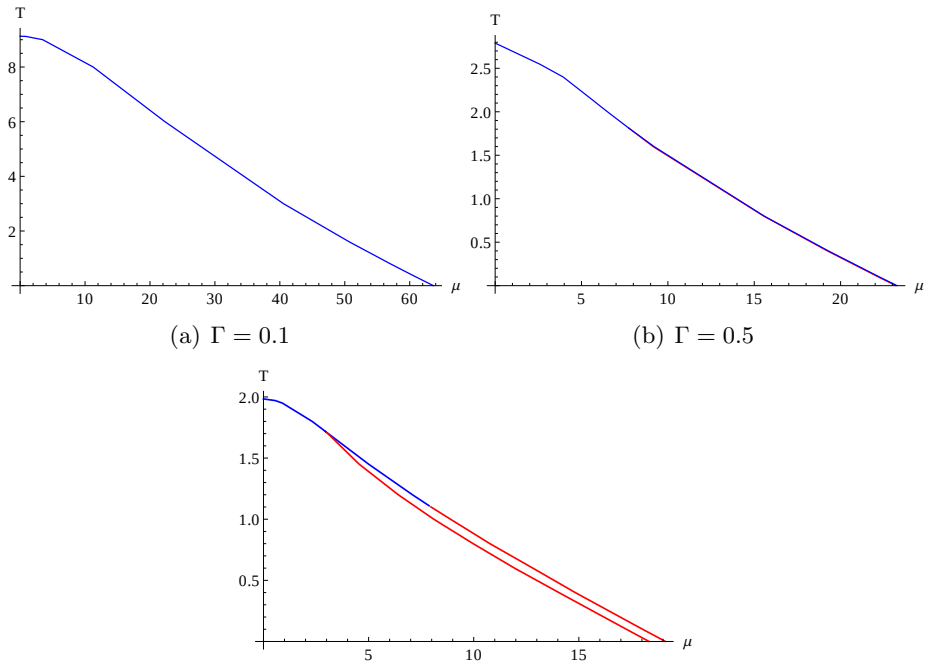

(a) $\Gamma = 0.1$ (b) $\Gamma = 0.5$

(c) $\Gamma = 1$

Figure 6.6: *Example plots of three possible phase structures for* $A = 30, \lambda = 1.715$ *and varying* Γ*. Large (small)* Γ *gives a second (first) order transition at low* T*.*

second order transition at low temperature, high density.

6.3 Breaking the ρ-L Symmetry

Our goal is to attempt to reproduce a phase diagram comparable to that of QCD in our holographic model. So far we have failed to generate a second order transition with temperature at zero density which is a key part of the QCD picture.

6.3.1 Elliptic Dilaton Profile

We have a further natural freedom within our holographic model to exploit. Our running dilaton is in some way supposed to represent the backreaction of the quark fields on the strongly interacting gauge dynamics to allow us to model theories with more interesting dynamics than the conformal $\mathcal{N} = 4$ gauge fields. We introduce quarks through D7 branes that break the $SO(6)$ symmetry of the five sphere of the original AdS/CFT Correspondence down to $SO(4) \times SO(2)$. Our ansatz for the

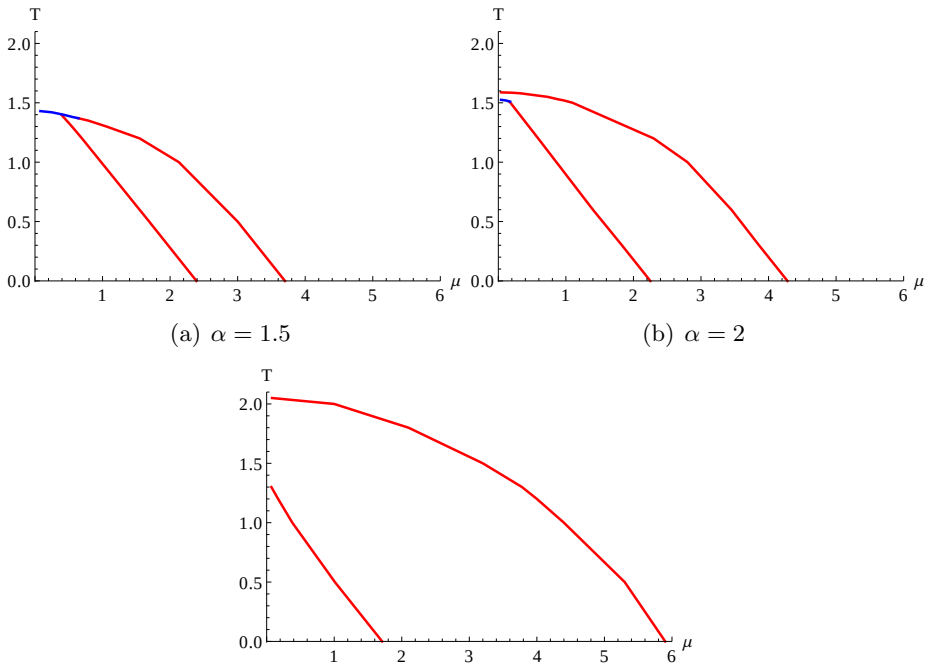

(a) $\alpha = 1.5$ (b) $\alpha = 2$

(c) $\alpha = 5$

Figure 6.7: *Phase diagrams for $A = 5, \lambda = 1.7, \Gamma = 1$ with varying α. Large (small) α gives second (first) order transition at small μ.*

running coupling (6.3) though respected the full $SO(6)$ symmetry. It seems reasonable to make use of the broken symmetry to introduce a further free parameter into our dilaton ansatz. We propose

$$\beta = A + 1 - A \tanh\left[\Gamma\left(\sqrt{\frac{(\rho^2 + \alpha L^2)^2 + T^4}{\rho^2 + \alpha L^2}} - \lambda\right)\right]. \tag{6.24}$$

where α measures the symmetry breaking between the L and ρ directions of the space. We will again not seek to backreact this dilaton on the background — to do so would be very hard.

We show some example phase diagrams we have found by changing α in figure 6.7. In particular we have chosen a case where with $\alpha = 1$ much of the phase diagram has second order transitions. Increasing α then encourages the transition with temperature at zero density to become second order until the full transition space is second order.

The reason for the onset of second order transitions with just temperature is simply understood. We have deformed the dilaton into an ellipse whose major axis is along

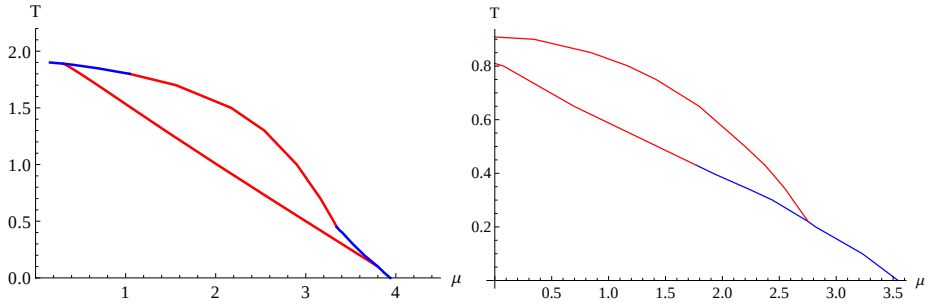

(a) $\tilde{\alpha} = 2, A = 3, \Gamma = 0.9, \lambda = 3.2$ (b) $\tilde{\alpha} = 3, A = 3, \Gamma = 1, \lambda = 1.715$

Figure 6.8: *Sample phase diagrams for theories with non-zero* $\tilde{\alpha}$*.*

the ρ axis. The black hole horizon remains circular in the ρ-L plane. Thus there are temperature periods in which the area of the ρ-L plane with a large dilaton is covered except for a small piece that emerges from the horizon near the ρ axis. If the value of the dilaton is sufficiently large in that uncovered area to encourage the D7 to avoid it, but the horizon on the L axis has met the zero temperature D7 embedding, then a second order transition to a black hole embedding is likely. Since in the absence of the rise in the dilaton the flat embedding would now be preferred the D7 settles on the horizon so it just misses the raised dilaton area. As the black hole grows further the embedding is likely to track down onto the axis smoothly as the raised dilaton area is finally eaten. This intuition is indeed matched by the solutions as shown in figure 6.7.

Thus we have realised a second order thermal chiral restoration transition in a plausible fashion within a bottom-up model.

6.3.2 Elliptic Black Hole Horizon

Our final task is to try to manage a second order transition at zero density with temperature yet a first order transition at zero temperature with density. We have not achieved this within the elliptic dilaton profile. However, we can seek to break the $\rho - L$ symmetry elsewhere in the construction and in particular in the background geometry. Again were we to backreact the D7 branes such a breaking in the geometry would occur but as with the dilaton we shall allow ourselves phenomenological freedom in introducing that breaking.

In particular we introduce our explicit $L-\rho$ symmetry breaking parameter $\tilde{\alpha}$ now through the blackening factors of the metric and not in the dilaton

$$g_t = \frac{(w^4 - T^4)^2}{w^4(w^4 + T^4)}\,, \qquad g_x = \frac{w^4 + T^4}{w^4}\,, \tag{6.25}$$

with

$$w^4 \to \rho^2 + \frac{1}{\tilde{\alpha}} L^2\,, \quad \tilde{\alpha} > 1. \tag{6.26}$$

The logic for the thermal transition at zero density is the same as in section 6.3.1. The elliptical black hole horizon will cover the spherical area with a raised dilaton profile on the L axis but not the ρ axis encouraging a second order transition. At low temperature and high density this configuration allows us to begin with one of the configurations in section 6.2.1 above that has a first order transition in the full phase plane.

We can indeed find a number of new phase diagrams by exploring in the parameter space. Some new examples are shown in figure 6.8. The second phase diagram achieves our goal of reproducing a chiral transition that is second order with temperature but first order with density.

6.4 Summary

In this chapter we have converted the D3/probe-D7 system, that holographically describes $\mathcal{N} = 4$ super Yang-Mills theory with quenched $\mathcal{N} = 2$ quark multiplets, to a phenomenological description of strongly coupled quark matter. We introduced a simple non-backreacted profile for the dilaton that describes a step of variable height and width in the running coupling of the gauge theory (6.3). This breaks the conformal symmetry of the model and introduces chiral symmetry breaking. We have then studied the temperature and chemical potential phase structure of the model.

The phase diagrams consist of three phases: a chirally symmetric phase at large temperature and density, a chirally broken phase with non-zero quark density at

intermediate values of T and μ, and a chiral symmetry broken phase with zero quark density at low T and μ. Figure 5.1(a) shows these phases and their holographic analogue in the previously studied case where chiral symmetry was broken by an applied magnetic field. Here we showed that a small wide step in the gauge coupling running gives rise to a single first order transition between the chirally symmetric and the broken phase (see figure 6.4). If the step is made larger in height or thinner then the chirally broken phase with non-zero density also plays a role. Here the transitions at low temperature with chemical potential can be second order. These results match known results in top-down models in the presence of magnetic fields to induce the symmetry breaking.

We were interested in reproducing phase diagrams with the structure believed to exist in QCD. To do this we made use of the broken $SO(6)$ symmetry of the gravity dual in the presence of D7 branes. Were the branes backreacted the dilaton and geometry would reflect this symmetry breaking. We introduced two further phenomenological parameters $\alpha, \tilde{\alpha}$ in the dilaton profile and black hole blackening factors respectively. These models allow us to control which volumes of the holographic space have a large dilaton value within, which the D7 branes prefer to avoid. Using these few parameters we were able to generate phase diagrams in which all the transitions were second order (see figure 6.7) and a QCD-like case with a chiral restoration transition that was second order with temperature but first order with density (see figure 6.8).

The ease with which such a variety of phase structures could be obtained is very encouraging for the idea of phenomenologically modelling the QCD phase diagram holographically. Further the phenomenological parameters we introduced are very natural in this context and it seems likely that top-down models with such phase structures should be possible as a result.

Chapter 7

Discussion

In this work we studied generalisations of the AdS/CFT correspondence. We explored aspects of strongly coupled gauge theories with quarks. We focused our interest on chiral symmetry breaking.

In chapters 3 and 5 we explored the phase structure of the $\mathcal{N} = 2$ gauge theory whose dual is the D3/D7 system. In chapter 3 we added a magnetic field B to the system, which favours chiral symmetry breaking. We then studied the temperature-chemical potential (T,μ) (or density d) phase diagram, where finite temperature and chemical potential (or density) both favour a chiral symmetry restoration.

Phase diagrams like those in chapter 3 are of great interest in QCD and more general strongly coupled field theories. Our theory is different from QCD, as it has superpartners of the quarks and the gluons present with a large number of colours N and a small number of flavours N_f (quenched approximation). It has also only degenerate quarks and the gluonic degrees of freedom are deconfined at non-zero temperature. In the holographic theory there is a distinct meson melting transition. The deconfinement transition in QCD differs from the meson melting transition and it is believed that the chiral symmetry breaking transition and the deconfinement transition occur simultaneously in QCD. We find considerable structure in our phase diagram, which captures many aspects of QCD. An additional phase is present in which the mesons in our theory are melted but the vacuum is still

chirally symmetric. The orders of our chiral symmetry breaking transition are reversed to the standard picture of QCD.

We would like to note here that the QCD diagram is not perfectly mapped out, as it is hard to compute on a lattice at finite chemical potential. The phase structure and the order of transition depends on the masses of the quarks and it is theoretically possible that QCD exhibits a phase diagram with the order of transitions similar to our phase diagram. We can not match the diagrams point by point but we are providing an environment in which clear computations of the phase diagram in a strongly coupled field theory are possible. In addition to this, the finding of distinct meson melting and chiral symmetry breaking transitions leads us to speculate, whether there is also the possibility of separate deconfinement and chiral symmetry breaking transitions in QCD.

In chapter 5 we studied how robust the diagram found in chapter 3 is to changes of parameters. We introduced an electric field E parallel to the magnetic field, which favours chiral symmetry restoration and a conducting phase as it loosens the binding in mesons. We found a variety of phase structures and transition types (including an insulator-conductor transition) in the B, T, μ and E volume, due to the competition of the different effects of the parameters. We hope that the results can serve as guide for other gauge theories, at least qualitatively. They certainly suggest that a rich structure of phases will be present in many gauge theories. In the future it would be interesting to find the phase diagrams with backreacted flavour branes. It would also be of interest to include stringy physics which has been neglected in chapter 5. The hope then is to study in more detail how energy is dissipated into the surrounding plasma. We could also use quasinormal modes in order to confirm the order of phase transition, which in chapter 5 we could not do by studying the free energy of the theory.

In chapter 4 we used the same kind of analysis to study the phase diagram of the D3/D5 system with fundamental matter fields on a 2+1 dimensional defect with a 3+1 dimensional gauge theory with finite magnetic field, temperature and chemical potential. We found a phase diagram looking similar to that found in the D3/D7

system in chapter 3. The most prominent difference is that we found BKT scaling of the chiral symmetry breaking transition at T=0. This is potentially of interest for condensed matter systems.

In chapters 2 and 6 we studied chiral symmetry breaking in the $\mathcal{N} = 2$ gauge theory whose dual is the D3/D7 system. We used a simple non-backreacted dilaton profile (running coupling) to break conformal symmetry and introduce chiral symmetry breaking. In chapter 2 we computed parameters of the low energy chiral Lagrangian and their dependence of the running coupling. The integral equations we have found are in spirit very similar to the Pagels-Stokar formula for the pion decay constant and the constituent quark model estimates of the chiral condensate. We believe that from our integral equations we can gain intuition about how these parameters depend on the underlying gauge dynamics. We believe that this toy model can guide those who wish to study fully backreacted systems. It would be very interesting to investigate in the future these integral equations in a backreacted system. We also used our set-up to include walking technicolour in holographic frameworks.

After computing phase diagrams in chapters 3 and 5, we asked in chapter 6 whether holographic models can in principle describe a phase diagram like that of real QCD. The holographic dual of QCD is not known, hence we used a phenomenological bottom-up approach to model the QCD phase diagram. We used a series of non-trivial dilaton profiles in our model, which give a very interesting and complex phase structure. One success is that we modelled the structure of the phase diagram of chapter 3. We also successfully modelled the structure of the chiral phase transition in QCD. This result is very encouraging, as we see no intrinsic problem in mimicking the QCD phase diagram with holographic models. Our system might be phenomenologically useful in the future, as we hope that it can be used to predict other features of QCD like time-dependent dynamics during transitions. For the future it would be interesting to see, whether these phase diagrams are as robust to the implementation of new parameters as the diagram in chapter 3. We therefore suggest introducing an electric field into the set-up. A fully backreacted dilaton would also give more insight into the physics of the theory. It

would be interesting to include a baryonic phase into the phase diagrams by adding a baryon vertex into the set-up. Parts of the Southampton High Energy Group around Nick Evans are currently working on this problem.

We would like to conclude that holography is a good tool to explore strongly coupled physics in a regime where established methods fail. Although the gauge theories studied are not real QCD, we can investigate many properties of QCD-like physics. We believe that we can learn valuable lessons in how to construct a holographic dual of QCD, or at least we can learn about qualitative features of strongly coupled theories such as QCD or condensed matter systems.

Bibliography

[1] C. -N. Yang and R. L. Mills, "Conservation of Isotopic Spin and Isotopic Gauge Invariance," Phys. Rev. **96** 191-195 (1954).

[2] H. Fritzsch, M. Gell-Mann and H. Leutwyler, "Advantages of the Color Octet Gluon Picture," Phys. Lett. **B47** 365-368 (1973).

[3] D. J. Gross and F. Wilczek, "Ultraviolet Behavior of Nonabelian Gauge Theories," Phys. Rev. Lett. **30** 1343-1346 (1973).

[4] H. D. Politzer, "Reliable Perturbative Results for Strong Interactions?," Phys. Rev. Lett. **30** 1346-1349 (1973).

[5] M. E. Peskin and D. V. Schroeder, "An Introduction to quantum field theory," Westview Press (1995).

[6] T.-P. Cheng and L.-F. Li, "Gauge theory of elementary particle physics," Oxford University Press (1984).

[7] C. Davies and P. Lepage, "Lattice QCD meets experiment in hadron physics," AIP Conf. Proc. **717** 615-624 (2004). [hep-ph/0311041].

[8] J. Erdmenger, N. Evans, I. Kirsch and E. Threlfall, "Mesons in Gauge/Gravity Duals - A Review," Eur. Phys. J. A **35** 81 (2008) [arXiv:0711.4467 [hep-th]].

[9] H. Georgi, "Weak Interactions And Modern Particle Theory," Menlo Park, USA: Benjamin/cummings (1984) 165p.

[10] M. A. Stephanov, "QCD phase diagram: An overview," PoS **LAT2006** 024 (2006) [arXiv:hep-lat/0701002].

[11] O. Philipsen, "Towards a determination of the chiral critical surface of QCD," PoS **CPOD2009** 026 (2009) [arXiv:0910.0785 [hep-ph]].

[12] P. W. Higgs, "Spontaneous Symmetry Breakdown without Massless Bosons," Phys. Rev. **145** 1156-1163 (1966).

[13] G. S. Guralnik, C. R. Hagen and T. W. B. Kibble, "Global Conservation Laws and Massless Particles," Phys. Rev. Lett. **13** 585-587 (1964).

[14] K. Lane, "Two lectures on technicolor," arXiv:hep-ph/0202255.

[15] S. Weinberg, "Implications Of Dynamical Symmetry Breaking," Phys. Rev. D **13** 974 (1976).

[16] L. Susskind, "Dynamics Of Spontaneous Symmetry Breaking In The Weinberg-Salam Theory," Phys. Rev. D **20** 2619 (1979).

[17] E. Eichten and K. D. Lane, "Dynamical Breaking of Weak Interaction Symmetries," Phys. Lett. B**90** 125 (1980).

[18] B. Holdom, "Raising The Sideways Scale," Phys. Rev. D **24** 1441 (1981).

[19] T. W. Appelquist, D. Karabali and L. C. R. Wijewardhana, "Chiral Hierarchies and the Flavor Changing Neutral Current Problem in Technicolor," Phys. Rev. Lett. **57** 957 (1986).

[20] C. T. Hill and E. H. Simmons, "Strong dynamics and electroweak symmetry breaking," Phys. Rept. **381** 235 (2003) [Erratum-ibid. **390** 553 (2004)] [arXiv:hep-ph/0203079].

[21] G. 't Hooft, "A Planar Diagram Theory for Strong Interactions," Nucl. Phys. **B72** 461 (1974).

[22] O. Aharony, S. Gubser, J. M. Maldacena, H. Ooguri and Y. Oz, "Large N field theories, string theory and gravity," Phys. Rept. **323** 183 (2000) [arXiv:hep-th/9905111].

[23] J. Polchinski, "String theory. Vol. 1: An introduction to the bosonic string," Cambridge University Press (1998).

[24] M. B. Green, J. H. Schwarz and E. Witten, "Superstring Theory. Vol. 1: Introduction," Cambridge, Uk: Univ. Pr. (1987) (Cambridge Monographs On Mathematical Physics).

[25] J. Polchinski, "Dirichlet Branes and Ramond-Ramond charges," Phys. Rev. Lett. **75** 4724-4727 (1995) [hep-th/9510017].

[26] J. M. Maldacena, "The Large N limit of superconformal field theories and supergravity," Adv. Theor. Math. Phys. **2** 231 (1998) [Int. J. Theor. Phys. **38** 1113 (1999)] [arXiv:hep-th/9711200].

[27] G. T. Horowitz and A. Strominger, "Black strings and P-branes," Nucl. Phys. **B360** 197-209 (1991).

[28] E. Witten, "Anti-de Sitter space and holography," Adv. Theor. Math. Phys. **2** 253 (1998) [arXiv:hep-th/9802150].

[29] S. S. Gubser, I. R. Klebanov and A. M. Polyakov, "Gauge theory correlators from non-critical string theory," Phys. Lett. B **428** 105 (1998) [arXiv:hep-th/9802109].

[30] I. R. Klebanov and E. Witten, "AdS / CFT correspondence and symmetry breaking," Nucl. Phys. B **556** 89 (1999) [hep-th/9905104].

[31] A. Karch and E. Katz, "Adding flavor to AdS/CFT," JHEP **0206** 043 (2002) [arXiv:hep-th/0205236].

[32] M. Kruczenski, D. Mateos, R. C. Myers and D. J. Winters, "Meson spectroscopy in AdS-CFT with flavor," JHEP **0307** 049 (2003) [arXiv:hep-th/0304032].

[33] M. Grana and J. Polchinski, "Gauge-gravity duals with holomorphic dilaton," Phys. Rev. **D65** 126005 (2002) [arXiv: hep-th/0106014].

[34] M. Bertolini, P. Di Vecchia, M. Frau, A. Lerda and R. Marotta, "N = 2 gauge theories on systems of fractional D3/D7 branes," Nucl. Phys. B **621** 157 (2002) [arXiv:hep-th/0107057].

[35] J. Babington, J. Erdmenger, N. J. Evans, Z. Guralnik and I. Kirsch, "Chiral symmetry breaking and pions in non-supersymmetric gauge / gravity duals," Phys. Rev. D **69** 066007 (2004) [arXiv:hep-th/0306018].

[36] K. Ghoroku and M. Yahiro, "Chiral symmetry breaking driven by dilaton," Phys. Lett. B **604** 235 (2004) [arXiv:hep-th/0408040].

[37] M. Kruczenski, D. Mateos, R. C. Myers and D. J. Winters, "Towards a holographic dual of large-N(c) QCD," JHEP **0405** 041 (2004) [arXiv:hep-th/0311270].

[38] V. G. Filev, C. V. Johnson, R. C. Rashkov and K. S. Viswanathan, "Flavoured large N gauge theory in an external magnetic field," JHEP **0710** 019 (2007) [arXiv:hep-th/0701001].

[39] J. M. Maldacena, "Wilson loops in large N field theories," Phys. Rev. Lett. **80** 4859 (1998) [arXiv:hep-th/9803002].

[40] S. J. Rey and J. T. Yee, "Macroscopic strings as heavy quarks in large N gauge theory and anti-de Sitter supergravity," Eur. Phys. J. C **22** 379 (2001) [arXiv:hep-th/9803001].

[41] D. Mateos, R. C. Myers and R. M. Thomson, "Thermodynamics of the brane," JHEP **0705** 067 (2007) [arXiv:hep-th/0701132].

[42] D. T. Son and A. O. Starinets, "Viscosity, Black Holes, and Quantum Field Theory," Ann. Rev. Nucl. Part. Sci. **57** 95 (2007) [arXiv:0704.0240 [hep-th]].

[43] S. S. Gubser and A. Karch, "From gauge-string duality to strong interactions: A Pedestrian's Guide," Ann. Rev. Nucl. Part. Sci. **59** 145-168 (2009) [arXiv:0901.0935 [hep-th]].

[44] H. Pagels and S. Stokar, "The Pion Decay Constant, Electromagnetic Form-Factor And Quark Electromagnetic Selfenergy In QCD," Phys. Rev. D **20** 2947 (1979).

[45] B. Holdom, J. Terning and K. Verbeek, "Chiral lagrangian from quarks with dynamical mass," Phys. Lett. B **245** 612 (1990).

[46] T. Sakai and S. Sugimoto, "Low energy hadron physics in holographic QCD," Prog. Theor. Phys. **113** 843 (2005) [arXiv:hep-th/0412141].

[47] S. R. Coleman, J. Wess and B. Zumino, "Structure of phenomenological Lagrangians. 1," Phys. Rev. **177** 2239 (1969).

[48] T. Appelquist, A. Avakian, R. Babich, R. C. Brower, M. Cheng, M. A. Clark, S. D. Cohen, G. T. Fleming *et al.*, "Toward TeV Conformality," Phys. Rev. Lett. **104** 071601 (2010) [arXiv:0910.2224 [hep-ph]].

[49] I. Kirsch and D. Vaman, "The D3/D7 background and flavor dependence of Regge trajectories," Phys. Rev. D **72** 026007 (2005) [arXiv:hep-th/0505164].

[50] A. Karch and L. Randall, "Open and closed string interpretation of SUSY CFT's on branes with boundaries," JHEP **0106** 063 (2001) [arXiv:hep-th/0105132].

[51] K. Rajagopal and F. Wilczek, "The Condensed matter physics of QCD," In *Shifman, M. (ed.): At the frontier of particle physics, vol. 3* 2061-2151 [hep-ph/0011333].

[52] S. Kobayashi, D. Mateos, S. Matsuura, R. C. Myers and R. M. Thomson, "Holographic phase transitions at finite baryon density," JHEP **0702** 016 (2007) [arXiv:hep-th/0611099].

[53] D. Mateos, S. Matsuura, R. C. Myers and R. M. Thomson, "Holographic phase transitions at finite chemical potential," JHEP **0711** 085 (2007) [arXiv:0709.1225 [hep-th]].

[54] A. Karch and A. O'Bannon, "Holographic Thermodynamics at Finite Baryon Density: Some Exact Results," JHEP **0711** 074 (2007) [arXiv:0709.0570 [hep-th]].

[55] S. Nakamura, Y. Seo, S. J. Sin and K. P. Yogendran, "A new phase at finite quark density from AdS/CFT," J. Korean Phys. Soc. **52** 1734 (2008) [arXiv:hep-th/0611021].

[56] S. Nakamura, Y. Seo, S. J. Sin and K. P. Yogendran, "Baryon-charge Chemical Potential in AdS/CFT," Prog. Theor. Phys. **120** 51 (2008) [arXiv:0708.2818 [hep-th]].

[57] K. Ghoroku, M. Ishihara and A. Nakamura, "D3/D7 holographic Gauge theory and Chemical potential," Phys. Rev. D **76** 124006 (2007) [arXiv:0708.3706 [hep-th]].

[58] K. Peeters, J. Sonnenschein and M. Zamaklar, "Holographic melting and related properties of mesons in a quark gluon plasma," Phys. Rev. D **74** 106008 (2006) [arXiv:hep-th/0606195].

[59] C. Hoyos-Badajoz, K. Landsteiner and S. Montero, "Holographic Meson Melting," JHEP **0704** 031 (2007) [arXiv:hep-th/0612169].

[60] J. Erdmenger, M. Kaminski and F. Rust, "Holographic vector mesons from spectral functions at finite baryon or isospin density," Phys. Rev. D **77** 046005 (2008) [arXiv:0710.0334 [hep-th]].

[61] J. Erdmenger, C. Greubel, M. Kaminski, P. Kerner, K. Landsteiner and F. Pena-Benitez, "Quasinormal modes of massive charged flavor branes," JHEP **1003** 117 (2010) [arXiv:0911.3544 [hep-th]].

[62] V. G. Filev, "Criticality, Scaling and Chiral Symmetry Breaking in External Magnetic Field," JHEP **0804** 088 (2008) [arXiv:0706.3811 [hep-th]].

[63] T. Albash, V. G. Filev, C. V. Johnson and A. Kundu, "Finite Temperature Large N Gauge Theory with Quarks in an External Magnetic Field," JHEP **0807** 080 (2008) [arXiv:0709.1547 [hep-th]].

[64] J. Erdmenger, R. Meyer and J. P. Shock, "AdS/CFT with Flavour in Electric and Magnetic Kalb-Ramond Fields," JHEP **0712** 091 (2007) [arXiv:0709.1551 [hep-th]].

[65] A. V. Zayakin, "QCD Vacuum Properties in a Magnetic Field from AdS/CFT: Chiral Condensate and Goldstone Mass," JHEP **0807** 116 (2008) [arXiv:0807.2917 [hep-th]].

[66] V. G. Filev, C. V. Johnson and J. P. Shock, "Universal Holographic Chiral Dynamics in an External Magnetic Field," JHEP **0908** 013 (2009) [arXiv:0903.5345 [hep-th]].

[67] V. G. Filev, "Hot Defect Superconformal Field Theory in an External Magnetic Field," JHEP **0911** 123 (2009) [arXiv:0910.0554 [hep-th]].

[68] K. Y. Kim, S. J. Sin and I. Zahed, "Dense hadronic matter in holographic QCD," arXiv:hep-th/0608046.

[69] K. Y. Kim, S. J. Sin and I. Zahed, "The Chiral Model of Sakai-Sugimoto at Finite Baryon Density," JHEP **0801** 002 (2008) [arXiv:0708.1469 [hep-th]].

[70] R. Apreda, J. Erdmenger, N. Evans and Z. Guralnik, "Strong coupling effective Higgs potential and a first order thermal phase transition from AdS/CFT duality," Phys. Rev. D **71** 126002 (2005) [arXiv:hep-th/0504151].

[71] T. Albash, V. G. Filev, C. V. Johnson and A. Kundu, "A topology-changing phase transition and the dynamics of flavour," Phys. Rev. D **77** 066004 (2008) [arXiv:hep-th/0605088].

[72] D. Mateos, R. C. Myers and R. M. Thomson, "Holographic phase transitions with fundamental matter," Phys. Rev. Lett. **97** 091601 (2006) [arXiv:hep-th/0605046].

[73] S. Nakamura, "Comments on Chemical Potentials in AdS/CFT," Prog. Theor. Phys. **119** 839 (2008) [arXiv:0711.1601 [hep-th]].

[74] Y. Seo, J. P. Shock, S. J. Sin and D. Zoakos, "Holographic Hadrons in a Confining Finite Density Medium," JHEP **1003** 115 (2010) [arXiv:0912.4013 [hep-th]].

[75] P. de Forcrand and O. Philipsen, "The chiral critical point of Nf=3 QCD at finite density to the order $(mu/T)^4$," JHEP **0811** 012 (2008) [arXiv:0808.1096 [hep-lat]].

[76] P. de Forcrand and O. Philipsen, "The chiral critical line of $N_f = 2 + 1$ QCD at zero and non-zero baryon density," JHEP **0701** 077 (2007)

[arXiv:hep-lat/0607017].

[77] J. Langelage and O. Philipsen, "The deconfinement transition of finite density QCD with heavy quarks from strong coupling series," JHEP **1001** 089 (2010) [arXiv:0911.2577 [hep-lat]].

[78] S. Kim, Ph. de Forcrand, S. Kratochvila and T. Takaishi, "The 3-state Potts model as a heavy quark finite density laboratory," PoS **LAT2005** 166 (2006) [arXiv:hep-lat/0510069].

[79] O. DeWolfe, D. Z. Freedman and H. Ooguri, "Holography and defect conformal field theories," Phys. Rev. D **66** 025009 (2002) [arXiv:hep-th/0111135].

[80] J. Erdmenger, Z. Guralnik and I. Kirsch, "Four-Dimensional Superconformal Theories with Interacting Boundaries or Defects," Phys. Rev. D **66** 025020 (2002) [arXiv:hep-th/0203020].

[81] R. C. Myers and M. C. Wapler, "Transport Properties of Holographic Defects," JHEP **0812** 115 (2008) [arXiv:0811.0480 [hep-th]].

[82] M. C. Wapler, "Holographic Experiments on Defects," Int. J. Mod. Phys. A **25**. 4397 (2010) [arXiv:0909.1698 [hep-th]].

[83] M. C. Wapler, "Thermodynamics of Holographic Defects," JHEP **1001** 056 (2010) [arXiv:0911.2943 [hep-th]].

[84] M. C. Wapler, "Massive Quantum Liquids from Holographic Angel's Trumpets," JHEP **1005** 019 (2010) [arXiv:1002.0336 [hep-th]].

[85] K. Jensen, A. Karch, D. T. Son and E. G. Thompson, "Holographic Berezinskii-Kosterlitz-Thouless Transitions," Phys. Rev. Lett. **105** 041601 (2010) [arXiv:1002.3159 [hep-th]].

[86] V. L. Berezinskii, "Destruction of long-range order in one-dimensional and two-dimensional systems having a continuous symmetry group I. Classical systems," Zh. Eksp. Theo. Fiz **59** 907 (1970) [Sov. Phys. JETP **32**, 493 (1971)].

[87] J. M. Kosterlitz and D. J. Thouless, "Ordering, metastability and phase transitions in two-dimensional systems," J. Phys. C **6** 1181 (1973).

[88] D. B. Kaplan, J. W. Lee, D. T. Son and M. A. Stephanov, "Conformality Lost," Phys. Rev. D **80** 125005 (2009) [arXiv:0905.4752 [hep-th]].

[89] N. Iqbal, H. Liu, M. Mezei and Q. Si, "Quantum phase transitions in holographic models of magnetism and superconductors," Phys. Rev. **D82** 045002 (2010) [arXiv:1003.0010 [hep-th]].

[90] K. Y. Kim and J. Liao, "On the Baryonic Density and Susceptibilities in a Holographic Model of QCD," Nucl. Phys. B **822** 201 (2009) [arXiv:0906.2978 [hep-th]].

[91] K. Jensen, A. Karch and E. G. Thompson, "A Holographic Quantum Critical Point at Finite Magnetic Field and Finite Density," JHEP **1005** 015 (2010) [arXiv:1002.2447 [hep-th]].

[92] A. Karch and A. O'Bannon, "Metallic AdS/CFT," JHEP **0709** 024 (2007) [arXiv:0705.3870 [hep-th]].

[93] A. O'Bannon, "Hall Conductivity of Flavor Fields from AdS/CFT," Phys. Rev. D **76** 086007 (2007) [arXiv:0708.1994 [hep-th]].

[94] T. Albash, V. G. Filev, C. V. Johnson and A. Kundu, "Quarks in an External Electric Field in Finite Temperature Large N Gauge Theory," JHEP **0808** 092 (2008) [arXiv:0709.1554 [hep-th]].

[95] A. Karch, A. O'Bannon and E. Thompson, "The Stress-Energy Tensor of Flavor Fields from AdS/CFT," JHEP **0904** 021 (2009) [arXiv:0812.3629 [hep-th]].

[96] J. Mas, J. P. Shock and J. Tarrio, "Holographic Spectral Functions in Metallic AdS/CFT," JHEP **0909** 032 (2009) [arXiv:0904.3905 [hep-th]].

[97] M. Ammon, T. H. Ngo and A. O'Bannon, "Holographic Flavor Transport in Arbitrary Constant Background Fields," JHEP **0910** 027 (2009) [arXiv:0908.2625 [hep-th]].

[98] K. Y. Kim, J. P. Shock and J. Tarrio, "The open string membrane paradigm with external electromagnetic fields," JHEP **1106** 017 (2011) [arXiv:1103.4581

[hep-th]].

[99] K. -Y. Kim, S. -J. Sin and I. Zahed, "Dense and Hot Holographic QCD: Finite Baryonic E Field," JHEP **0807** 096 (2008). [arXiv:0803.0318 [hep-th]].

[100] A. Davody, "Noncritical Holographic QCD in External Electric Field," [arXiv:1102.4509 [hep-th]].

[101] N. Evans, K. Y. Kim and J. P. Shock, "Chiral phase transitions and quantum critical points of the D3/D7(D5) system with mutually perpendicular E and B fields at finite temperature and density," JHEP **1109** 021 (2011) [arXiv:1107.5053 [hep-th]].

[102] D. E. Kharzeev and H. U. Yee, "Chiral helix in AdS/CFT with flavor," arXiv:1109.0533 [hep-th].

[103] J. Erlich, E. Katz, D. T. Son and M. A. Stephanov, "QCD and a holographic model of hadrons," Phys. Rev. Lett. **95** 261602 (2005) [arXiv:hep-ph/0501128].

[104] L. Da Rold and A. Pomarol, "Chiral symmetry breaking from five dimensional spaces," Nucl. Phys. B **721** 79 (2005) [arXiv:hep-ph/0501218].

[105] B. Gwak, M. Kim, B.-H. Lee, Y. Seo and S.-J. Sin, "Phases of a holographic QCD with gluon condensation at finite Temperature and Density,", arXiv:1105.2872 [hep-th].

[106] K. Ghoroku, T. Sakaguchi, N. Uekusa and M. Yahiro, "Flavor quark at high temperature from a holographic model," Phys. Rev. D **71** 106002 (2005) [arXiv:hep-th/0502088].